

**Integration of Catalytic Cracking and Hydrotreating Technology for Triglyceride  
Deoxygenation**

by

Hui Wang

Doctor of Philosophy (Ph.D.), East China University of Science and Technology, 2011

A Dissertation Submitted in Partial Fulfillment  
of the Requirements for the Degree of

**Doctor of Philosophy**

in the Graduate Academic Unit of Chemical Engineering

Supervisor: Ying Zheng, Ph.D, Chemical Engineering

Co-supervisor: Kecheng Li, Ph.D., Chemical Engineering

Examining Board: Rickey Dubay, Ph.D., Mechanical Engineering

Laura Romero-Zeron, Ph.D., Chemical Engineering

William Cook, Ph.D., Chemical Engineering

External Examiner: Natalia Semagina, Ph.D., Department of Chemical and Materials  
Engineering, University of Alberta

This thesis is accepted by the  
Dean of Graduate Studies

THE UNIVERSITY OF NEW BRUNSWICK

August, 2015

©Hui Wang, 2016

## ABSTRACT

Waste cooking oil (WCO) blended in dodecane was hydrotreated over a sulfided CoMo (CoMoS) supported catalyst. Hydrogenation, hydrodeoxygenation (HDO), and hydrodecarbonoxide (HDC) were the dominant reactions at low temperatures (275-325°C), whereas cracking, cyclization, and aromatization were dominant at high temperatures (365 °C). The HDO reaction pathway was more dominant than the HDC at all investigated conditions. The optimal conditions for deoxygenation (DO) and hydrogenation included a relatively low temperature (275 °C), a low pressure (500 psi), a low volume ratio of H<sub>2</sub>/oil (H/O, 100 ml/ml), a low blend ratio (20 wt%), and a low liquid hourly space velocity (LHSV, 2 h<sup>-1</sup>). Hydrogenation activity was strongly improved by the introduction of catalyst support and an increase in temperature. Compared to unsupported CoMoS, supported CoMoS not only exhibits higher hydrogenation and HDO abilities at low temperatures, but also exhibits higher dehydrogenation activity at high temperatures. The deactivation of the CoMoS catalyst started with a decrease in hydrogenation capability followed by HDO capability; however, there were no impacts on the cracking, polymerization, and HDC activities. The main factors contributing to catalyst deactivation are coke deposition, byproduct water, and the loss of sulfur. Coke formation significantly increased due to a high operating temperature (365 °C). By-product water could be partially eliminated by in-situ drying. Loss of sulfur occurred due to the loss of MoS<sub>2</sub> layers.

In catalytic cracking, high oxygen removal rates (>97.7 %) were obtained by using CaO, MgO, and titania. Even though this rate was 73.0 %, the light oil yield was the highest obtained by using alumina for all investigated metal oxide upgrading liquid products. The aromatic contents were lower than 4 % in all liquid products. Decarbonylation (DC) was the major DO reaction among all catalysts. Decarbonylation (DCO) was the primarily DO mechanism for the acidic catalysts, whereas decarboxylation (DCO<sub>2</sub>) for the alkaline catalysts. Higher catalyst acidity was beneficial towards DO but secondary cracking as well. The CaO catalyst exhibited a higher dehydrogenation capability. Acid treated kaolin (ATK) was very effective in the DO of WCO, contributing to the liquid production of high yield and high quality. Both kaolin-based and petroleum commercial catalysts (CC) eliminated more oxygen by dehydration than by DC; DCO was favoured over DCO<sub>2</sub>.

The catalytic cracking/hydrotreating integrated technology presented in this work was successfully applied for the DO of triglycerides: the result was with a high oxygen removal rate, high liquid yield, and low levels of hydrogen consumption.

## ACKNOWLEDGEMENTS

First of all, I would like to express my deepest gratitude to my supervisor, Dr. Ying Zheng, for her persistent guidance and continuous encouragement throughout my Ph.D. study. Her demonstration of a strong enthusiasm for research and a strict scientific attitude will benefit me for my entire life. I also want to give a great thank to Dr. Kecheng Li, my co-supervisor, for his support. This thesis could not have been completed without their guidance, assistance and encouragement.

I would also like to show my sincere appreciation to Dr. Hongfei Lin. He has always warmly and generously provided me with assistance, valuable advice, and endless encouragement during the past four years, not only in my research but also in my life. My special thanks go to Dr. Qikai Zhang for his encouragement of my research and his great help in experimental design. My gratitude also extends to all faculty and staff in the Chemical Engineering department of UNB.

Moreover, I want to thank my best friend, Haiping Zhang, who has always stood by my side, helping and supporting me. I'm grateful for my colleagues Yun Wang, Lin Zhang, Guoliang Li, Kyle Rogers, Weizhi Wang, Xue Han, Peng Feng, Josh Liu, and all of the other research group members, and for my good friends Jianbo Zheng, Miaomiao Xiao, Qiaozhi An, Hao Wang, Peng Lu, and Ming Li. Their acts of companionship, support, and friendship mean the world to me. It has been such a pleasure working with all of them.

I gratefully thank the Natural Sciences and Engineering Research Council of Canada, the Canada Foundation for Innovation, and the New Brunswick Innovation Foundation for the financial assistance.

Last but certainly not least, I want to show my deepest thanks to my husband, Xinli Wu, who has always been there supporting me whenever I need him. Thank you for your love, understanding, and many useful comments on my writing, all of which have made the completion of this thesis possible. I also want to thank my parents, parents in law, brother, and brother in law for their continued patience and support.

## Table of Contents

ABSTRACT .....	ii
ACKNOWLEDGEMENTS .....	iv
Table of Contents .....	vi
List of Tables .....	x
List of Figures .....	xii
List of Abbreviations .....	xiv
Chapter 1 Introduction .....	1
1.1 Background .....	1
1.2 Objectives and thesis outline.....	3
Chapter 2 Literature review .....	8
2.1 Development of biofuels .....	8
2.1.1 The current state and development trend of petroleum consumption .....	8
2.1.2 Increasingly stringent emission standards .....	9
2.1.3 Development of biofuels .....	12
2.2 Upgrading technologies for second-generation biofuels.....	14
2.2.1 Properties and compositions of plant oils.....	14
2.2.2 Comparison of plant oils to petroleum .....	15
2.2.3 Comparison of technologies for biofuel upgrading .....	17
2.2.4 Development of FCC technology and the catalysts.....	18
2.2.5 Application of catalytic cracking technology in biofuel upgrading .....	19
2.2.6 Chemical reactions during plant oils catalytic cracking upgrading.....	19
2.2.7 Effects of catalysts and operational parameters .....	20
2.3 Research objectives .....	25
2.3.1 Investigation of hydrotreating technology.....	26
2.3.2 Development of cracking catalysts.....	32
2.3.3 Development of integration technology .....	35
Chapter 3 Analytical procedures for catalyst characterization and reaction performance evaluation 36	
3.1 Reaction systems .....	36
3.1.1 Fixed-bed reactor for evaluation of hydrotreating process.....	36

3.1.2 Batch reactor for evaluation of hydrotreating process.....	38
3.1.3 Fixed-bed micro reactor for cracking catalyst evaluation .....	38
3.1.4 FCC reactor for cracking catalyst evaluation .....	39
3.1.5 Batch micro reactor for evaluation of hydrotreating process .....	42
3.2 Feeds.....	43
3.3 Catalysts .....	45
3.3.1 Supported CoMoS hydrotreating catalysts.....	45
3.3.2 Unsupported CoMoS hydrotreating catalysts.....	47
3.3.3 Metal oxide cracking catalysts .....	47
3.3.4 Kaolin-based cracking catalysts .....	48
3.4 Product analysis.....	49
3.4.1 Gas products .....	49
3.4.2 Liquid products.....	50
3.4.3 Solid products.....	53
3.5 Catalyst characterization .....	53
3.6 Calculations.....	56
3.6.1 DO (C-O or C-CO cracking) .....	56
3.6.2 Hydrogenation or dehydrogenation .....	57
3.6.3 Valuable products yields .....	57
3.6.4 Oxygen conversion.....	57
3.6.5 Density of acids on catalyst surface .....	57
3.6.6 Produced water in FCC process .....	58
3.7 Experimental programs .....	58
3.7.1 Uniform design (UD) experimental method applied in Chapter 4.....	58
3.7.2 Experimental programs in Chapter 5.....	60
3.7.3 Experimental programs applied in Chapter 6.....	60
3.7.4 Experimental programs applied in Chapter 7.....	60
3.7.5 Experimental programs employed in Chapter 8.....	61
3.7.6 Experimental programs in Chapter 9.....	61
Chapter 4 Hydrotreating of triglycerides over a CoMoS supported catalyst: effects of operational parameters .....	62
4.1 Introduction .....	62

4.2 Experimental .....	63
4.3 Results and discussion.....	63
4.3.1 Operational window of the process .....	63
4.3.2 Verification of the effects of temperature.....	66
4.3.3 Further investigation of operational parameters.....	72
4.4 Conclusions .....	86
Chapter 5 Hydrotreating of triglycerides over CoMoS catalysts: Roles of catalyst support and reaction temperature.....	89
5.1 Introduction .....	89
5.2 Experimental .....	89
5.3 Results and discussion.....	90
5.3.1 Activity studies .....	90
5.3.2 Catalyst characterization studies .....	94
5.3.3 Reaction route discussion .....	98
5.4 Conclusions .....	115
Chapter 6 Hydrotreating of triglycerides over CoMoS supported catalyst: Deactivation mechanisms of the catalyst .....	116
6.1 Introduction .....	116
6.2 Experimental .....	117
6.3 Results .....	117
6.3.1 Variation of the properties, functional groups, and compositions of products with time-on-stream.....	117
6.3.2 Activity variation.....	119
6.3.3 Characterization of fresh sulfided catalyst and spent catalyst.....	127
6.4 Discussion .....	138
6.4.1 Causes for deactivation of catalyst.....	139
6.4.2 Oxygenate deactivation .....	140
6.5 Conclusions .....	144
Chapter 7 Catalytic cracking of oleic acid to fuels and chemicals: roles of catalyst acidity and basicity on product distribution and reaction pathways .....	145
7.1 Introduction .....	145
7.2 Experimental .....	145
7.3 Results and discussion.....	146

7.3.1 Catalyst thermal treatment.....	146
7.3.2 Catalysts characterization.....	148
7.3.3 Reaction pathways.....	163
7.4 Conclusions.....	171
Chapter 8 High deoxygenation and low aromatization performance of kaolin-based cracking catalysts for WCO upgrading.....	173
8.1 Introduction.....	173
8.2 Experimental.....	173
8.3 Results.....	174
8.3.1 Kaolin treatments.....	174
8.3.2 Catalyst characterization.....	176
8.3.3 Product distribution and oxygen removal rate.....	178
8.3.4 Product analysis.....	179
8.4 Discussion.....	182
8.4.1 Non-DO reactions.....	182
8.4.2 DO reactions.....	191
8.5 Conclusions.....	197
Chapter 9 Integration of catalytic cracking and hydrotreating for triglyceride deoxygenation.....	199
9.1 Introduction.....	199
9.2 Experimental.....	199
9.3 Results and discussion.....	200
9.4 Conclusions.....	210
Chapter 10 Conclusions and recommendations.....	211
10.1 Conclusions.....	211
10.1.1 Hydrotreating of triglycerides.....	211
10.1.2 Development of novel cracking catalyst.....	213
10.1.3 Development of integration technology.....	214
10.2 Recommendations.....	215
Bibliography.....	217
Curriculum Vitae	

## List of Tables

Table 2-1 Sulfur content changes in European motor fuel specifications [25].....	10
Table 2-2 Sulfur content changes in Canadian fuel specifications [25] .....	10
Table 2-3 International comparison of sulfur content in gasoline .....	11
Table 2-4 Typical fatty acids compositions of plant oils [29, 30] .....	15
Table 2-5 Comparison of plant oils to petroleum [6, 11] .....	16
Table 2-6 Comparison of biofuels upgrading technologies [5, 6, 11] .....	17
Table 2-7 Triglycerides and VGO cracking products [36] .....	21
Table 3-1 Properties and compositions of feed oils.....	44
Table 4-1 Experimental programs by uniform design method .....	63
Table 4-2 Group compositions of UD results.....	64
Table 4-3 The boiling point distribution of the products.....	65
Table 4-4 Further experimental programs .....	66
Table 4-5 Group compositions.....	70
Table 5-1 Basic properties of CoMoS catalysts.....	95
Table 5-2 The amount of active sites on supported and unsupported catalysts <sup>a</sup> .....	97
Table 6-1 Density and TAN variation with time-on-stream.....	117
Table 6-2 The amount and strength of active sites on the fresh and spent catalysts .....	127
Table 6-3 Type and amount of the coke deposition on the spent catalyst .....	132
Table 6-4 Basic properties of the fresh sulfided and spent catalysts .....	136
Table 6-5 Elemental compositions of the fresh sulfided and spent catalysts .....	138
Table 6-6 The effect of water condensation on catalyst activities.....	141
Table 6-7 Thermodynamic data for reactions of sulfur exchanged by oxygenates .....	143
Table 7-1 Activity evaluation parameters of metal oxide catalysts .....	145
Table 7-2 Surface areas and pore volume of metal oxide catalysts .....	148
Table 7-3 Amount of active sites on metal oxide catalysts .....	149
Table 7-4 Product distributions.....	151
Table 7-5 Oxygen removal rate and valuable product distributions.....	153
Table 7-6 Inorganic gas and coke contents.....	154
Table 7-7 Organic gas product compositions .....	155

Table 7-8 Liquid product elemental compositions .....	156
Table 7-9 Oxygenate compositions .....	160
Table 7-10 Molarity compositions of DO products .....	164
Table 8-1 Acid properties of kaolin-based catalysts and CC.....	176
Table 8-2 Physical properties of kaolin-based catalysts and CC.....	178
Table 8-3 Product distribution and oxygen removal rate.....	179
Table 8-4 Organic gas concentrations.....	180
Table 8-5 Molarity compositions of DO products <sup>1</sup> .....	192
Table 9-1 Product distribution and oxygen removal rate of catalytic cracking process .	208
Table 9-2 Product distribution of hydrotreating process .....	208

## List of Figures

Figure 2-1 Projected world liquid fuels demand and supply [24] .....	8
Figure 3-1 Process flow diagram of hydrotreating reaction system .....	36
Figure 3-2 Catalyst loading.....	37
Figure 3-3 Fixed-bed micro reactor for cracking catalyst evaluation.....	39
Figure 3-4 The flow sheet of the FCC reactor .....	41
Figure 3-5 Molecular structure of feed .....	45
Figure 4-1 Structures of liquid products under different operational parameters.....	67
Figure 4-2 The effect of temperature on selectivity.....	77
Figure 4-3 Catalyst reaction capabilities.....	79
Figure 4-4 The effect of H/O on selectivity.....	79
Figure 4-5 The effect of the blend ratio of WCO on selectivity .....	81
Figure 4-6 The effect of the blend ratio of CLO on selectivity .....	82
Figure 4-7 The effect of LHSV on selectivity .....	84
Figure 5-1 Product fraction distributions of supported and unsupported catalysts .....	91
Figure 5-2 Structures of liquid products at different reaction temperature .....	92
Figure 5-3 TEM images of supported and unsupported catalysts.....	94
Figure 5-4 BJH pore size distribution of supported and unsupported catalysts .....	96
Figure 5-5 TPR spectra of supported and unsupported catalysts.....	97
Figure 5-6 Oxygenates distribution in liquid products .....	101
Figure 5-7 The oxygen conversion and mass ratio of C18/C17 hydrocarbons.....	104
Figure 5-8 Cracking and polymerization over supported and unsupported catalysts.....	105
Figure 5-9 Carbon No. distributions of hydrocarbons in liquid product .....	108
Figure 5-10 Alkane selectivity and ratio of hydrogen to carbon of liquid products.....	110
Figure 5-11 Aromatics ring No. distributions over supported catalyst at 365°C.....	114
Figure 6-1 Variation of functional groups with time-on-stream.....	119
Figure 6-2 Selectivity of Alkanes, alkenes, and oxygenates with time-on-stream.....	120
Figure 6-3 Distributions of different type olefins .....	122
Figure 6-4 Variation of DO capabilities with time-on-stream.....	124

Figure 6-5 Variation of oxygenates in liquid products with time-on-stream.....	125
Figure 6-6 Variation of cracking and polymerization capabilities with time-on-stream	126
Figure 6-7 The strength and amount of active sites on the sulfided and spent catalysts	128
Figure 6-8 TPO result of the spent catalyst .....	131
Figure 6-9 XRD spectra of the fresh and spent catalysts.....	133
Figure 6-10 TEM images of the fresh sulfided and spent catalysts .....	136
Figure 6-11 Variation of pore size distributions .....	137
Figure 7-1 Thermal treatment of metal oxide catalysts .....	147
Figure 7-2 Pore size distributions of metal oxide catalysts .....	149
Figure 7-3 Py-FTIR spectra of acidic metal oxide catalysts.....	150
Figure 7-4 Chemical compositions of liquid products.....	156
Figure 7-5 Carbon No. distributions .....	158
Figure 7-6 Structures and carbon No. distributions of oxygenates in liquid products ...	159
Figure 7-7 TPO results of spent catalysts .....	162
Figure 7-8 Weight loss of spent catalysts .....	163
Figure 8-1 Thermal treatment of kaolin.....	174
Figure 8-2 XRD patterns.....	175
Figure 8-3 Hydrocarbon selectivity and mass ratios of elements .....	181
Figure 8-4 Carbon No. distributions of OLPs.....	187
Figure 8-5 Compositions of chain hydrocarbons in liquid products.....	189
Figure 8-6 Distribution of ring hydrocarbons .....	190
Figure 8-7 Carbon No. distributions of oxygenates.....	195
Figure 8-8 Types of oxygenates.....	196
Figure 9-1 The compositions of ATK-HDO upgrading products.....	201
Figure 9-2 The oxygenate structures of ATK-HDO upgrading products .....	204
Figure 9-3 Chemical compositions of liquid products under optimal conditions.....	206
Figure 9-4 Chemical compositions of directly hydrotreating WCO.....	207
Figure 9-5 Hydrogen consumptions during hydrotreating process.....	209

## List of Abbreviations

Alumina-HDO: Catalytic cracking over alumina integrated with hydrotreating

ATK: Acid treated kaolin

ATK-HDO: Catalytic cracking over ATK integrated with hydrotreating

BAU: Business-as-usual

B acids: Bronsted acids

BET: Brunauer-Emmet-Teller

BJH: Barrett-Joyner-Halenda

BTK: Base treated kaolin

CC: Commercial petroleum cracking catalyst

CC-HDO: Catalytic cracking over CC integrated with hydrotreating

CLO: Camelina oil

CoMoS: Sulphided CoMo

CPO: Crude palm oil

DC: Decarbonoxide

DCO: Decarbonylation

DCO<sub>2</sub>: Decarboxylation

DCO<sub>x</sub>: Deoxygenation as form of CO or CO<sub>2</sub>

DMDS: Dimethyl disulfide

DO: Deoxygenation

EDX: Energy Dispersive X-Ray Analysis

EIA: Energy Information Administration

EMPA: Electron Microprobe analyzer

EOR: Enhanced Oil Recovery

FAME: Fatty acid methyl esters

FCC: Fluid catalytic cracking

FTIR: Fourier transform infrared spectroscopy

GC/FID: Gas chromatography with flame ionization detector

GC/MS: Gas chromatography and mass spectrometry

GC/RGA: Gas chromatography with residue gas analyzer

H/O: Volume ratio of H<sub>2</sub> to oil

HDC: Hydrodecarbonoxide

HDO: Hydrodeoxygenation

L acids: Lewis acids

LCO: Light cycle oil

LHSV: Liquid hourly space velocity

LPG: Liquid petroleum gas

MON: Motor octane number

NMR: Nuclear magnetic resonance

NS-9000: Nitrogen/sulfur analyzer

OLP: Organic liquid products

ORR: Oxygen removal rate

PG: Pressure gauges

PTK: Pretreated kaolin

RGA: Residue gas analyzer

RON: Research octane number

RSO: Rapeseed oil

SBO: Soybean oil

TAN: Total acid value

TEM: Transmission electron microscopy

TGA: Thermo gravimetric analysis

TPD: Temperature program desorption

TPO: Temperature program oxidation

TPR: Temperature program reduction

TSRFCC: Two-stage riser fluid catalytic cracker

UD: Uniform design

UPO: Used palm oil

USY: Ultra stable zeolite Y

VGO: Vacuum gas oil

WCO: Waste cooking oil

WWFC: World-wide fuel charter

XRD: X-ray diffraction

# Chapter 1 Introduction

## 1.1 Background

Reliance on petroleum oil raises two issues: insecurity of energy supply and high greenhouse gas (GHG) emissions. Global demand for oil continues to rise, but there are those who fear that oil production could peak within the next 10-20 years, dropping significantly thereafter. The combustion of petroleum products accounts for one-third of total carbon dioxide emissions in the world, which significantly contributes to global climate change. Canada has just announced its aim to reduce GHG emissions by 30 % by the year 2030 (from levels in 2005) [1]; it had already established a renewable source content of 5 % in gasoline and 2 % in diesel and heating oil since 2012 [2, 3]. It is clear that focus is turning towards improving the utilization of renewable energy resources [4].

First-generation biofuels are made from sugars and vegetable oils; the main types of these commercial fuels are biodiesel and bioethanol. In the past, the development of first-generation biofuels has been hindered because the feedstock required to produce them are also essential food supplies. As a result, second-generation biofuels have been developed, which can be divided into two types: non-edible plant oil and biomass derived oil. Generally, plant oils are triglycerides that mainly consist of three fatty acids: palmitic acid, oleic acid, and linoleic acid. Upgrading biofuels result in drop-in green diesel/gasoline fuels, which contain no oxygen – these are considered as the second-generation biofuels. They are virtually the same as petroleum derived diesel/gasoline and

are fully compatible with petrol. “Drop-in” green fuels eliminate the short shelf-life problem that both ethanol and biodiesel have, and offer a net zero carbon emission. Research on how to remove oxygen from plant oil to produce “drop-in” green fuels has been documented [5].

Up until now, two technologies have become popular for refining second-generation biofuels: catalytic cracking without hydrogen and catalytic hydrotreating with hydrogen. The hydrotreating of plant oils to produce paraffin has been extensively studied and has been implemented for commercial purposes. Plant oil usually contains high amounts of oxygen (8-15 wt%) that need to be removed; if hydrogen is used for hydrotreating, very large amounts are likewise needed which leads to high costs. Traditional sulfided catalysts are easily deactivated due to a loss of sulfur and the existence of byproduct water during the hydrotreating process [6-10]. The products obtained from the hydrotreating of triglycerides are generally long-chain paraffin with high condensation points – this can easily lead to blockage in the reaction system. For all these reasons, it is a challenge to implement the direct hydrotreating of plant oils on a commercial scale [6, 11].

In oil refineries, catalytic cracking is the most widely used process for turning the heavy fraction of crude oil into gasoline and other hydrocarbons. Studies have shown that catalytic cracking can effectively degrade large molecules in fatty acids into smaller compounds which fall mostly in the gasoline boiling range [12]; oxygen can be removed

in the forms of CO, CO<sub>2</sub> or H<sub>2</sub>O [13]. Previous research concerning the use of petrol-intended catalysts in the fluid catalytic cracking (FCC) of plant oils has shown undesirable results: extensive coking (even at lower reaction temperatures), low liquid yields with high contents of aromatics and olefins [14], and irreversible catalyst deactivation were also observed [15-20]. In addition, while catalytic cracking can partially eliminate oxygen from plant oils, there are still massive amounts of unsaturated compounds and relatively small amounts of oxygenates that remain in the products – the result is that the upgraded liquid products still cannot be used directly as fuel.

Previously reported studies focus on either hydrotreating or catalytic cracking plant oil but rarely both [12, 21, 22]. We intended to address the challenge of upgrading plant oils by combining catalytic cracking and hydrotreating technologies, and by developing a novel catalyst for DO. In our proposed process, the majority of oxygen in plant oil is removed by catalytic cracking, and the liquid product is then hydrotreated to eliminate residual oxygen and to saturate the hydrocarbons.

## **1.2 Objectives and thesis outline**

The ultimate objective is to develop an integrated catalytic-cracking/hydrotreating process along with appropriate catalysts, in order to increase the liquid yield, reduce the hydrogen consumption, and enhance the product quality of the plant oil upgrading process. Emphasis was given on the development of a novel DO cracking catalyst. The specific objectives of the study are described as follows:

- (1) Investigate the effect of operational parameters on the DO of triglyceride hydrotreating, conducted over a CoMoS supported catalyst in a fixed-bed reactor.
- (2) Study the effects of catalyst support for the CoMoS catalyst on DO during the triglyceride hydrotreating process.
- (3) Determine the deactivation mechanism of the CoMoS supported catalyst during the triglyceride hydrotreating process.
- (4) Compare the DOs of the oleic acid mechanism, when oil is placed over acidic ( $\text{Al}_2\text{O}_3$  and  $\text{TiO}_2$ ), neutral (quartz), and alkaline (MgO and CaO) catalysts in a fixed-bed micro reactor.
- (5) Develop novel kaolin-based catalysts for the DO and cracking of WCO;
- (6) Compare the combined catalytic-cracking/hydrotreating technology to pure hydrotreating technology.

Overall, this study is mainly presented in three parts: the investigation of the feasibility of triglyceride hydrotreating, the development of a novel cracking catalyst, and the evaluation of the integrated catalytic-cracking/hydrotreating technology in comparison with direct hydrotreating technology. This last part is used to confirm the effectiveness of the novel cracking catalyst, acid treated kaolin.

Chapter 2 summarizes the history of biofuel development, focusing on the second-generation biofuels. A detailed introduction on the technology for upgrading second-generation biofuel is also presented.

Chapter 3 gives information about the performance evaluation systems used to assess catalyst reaction activity, the catalysts and feeds, the catalyst characterization and product analysis methods, and the relevant calculations and experimental programs.

Chapter 4 investigates the effect of operational parameters on DO during triglyceride hydrotreating. Using the uniform design method (UD) with different operational parameters, the reaction routes of this process were identified. The liquid products of triglyceride hydrotreating yielded undesirable results – they contained no paraffin but contained unprecedentedly high concentrations of aromatics and oxygenates. Further experiments were conducted to determine the parameters strongly affect the reaction routes and composition of the products. Then WCO and camelina oil (CLO) were treated under optimal conditions in order to investigate the effect of process parameters on the upgrading process.

Chapter 5 compares the effects of unsupported and supported CoMoS on the DO performance of WCO and also identifies how product distributions and compositions are affected by catalyst support and reaction temperature.

Chapter 6 outlines the variation of catalyst activities and demonstrates how oxygenates influence catalyst activity during the triglyceride upgrading process (reacted over CoMoS supported catalysts). The deactivation mechanism of the spent catalysts and methods to recover them are also discussed.

Chapter 7 investigates the roles of catalyst acidity and basicity (Acid:  $\text{Al}_2\text{O}_3$  and  $\text{TiO}_2$ , alkaline:  $\text{CaO}$  and  $\text{MgO}$ , and Neutral:  $\text{SiO}_2$ ) in the catalytic conversion of oleic acid; this was conducted in a fixed-bed micro-reactor at atmospheric pressure and at temperature of  $470\text{ }^\circ\text{C}$ . The reaction pathways of different catalysts are also discussed.

Chapter 8 presents inexpensive catalysts that can upgrade WCO to organic liquid products (OLP) with high DO and low aromatization. Focus is given on the treatment of kaolin for catalytic DO; a commercial catalyst (CC) for catalytic cracking of petroleum is used as a reference.

Chapter 9 explains the proposed catalytic-cracking/hydrotreating technology, an energy-economic route for upgrading triglycerides into drop-in biofuels. Focus is given to the comparison of the catalytic-cracking/hydrotreating technology to direct hydrotreating technology. The successful application of the catalytic cracking over ATK paired with subsequent hydrotreating (ATK-HDO) is explained; the DO of triglycerides occurred and the final products had a high liquid yield and a suitable liquid product composition. Additionally, this was completed at low levels of hydrogen consumption.

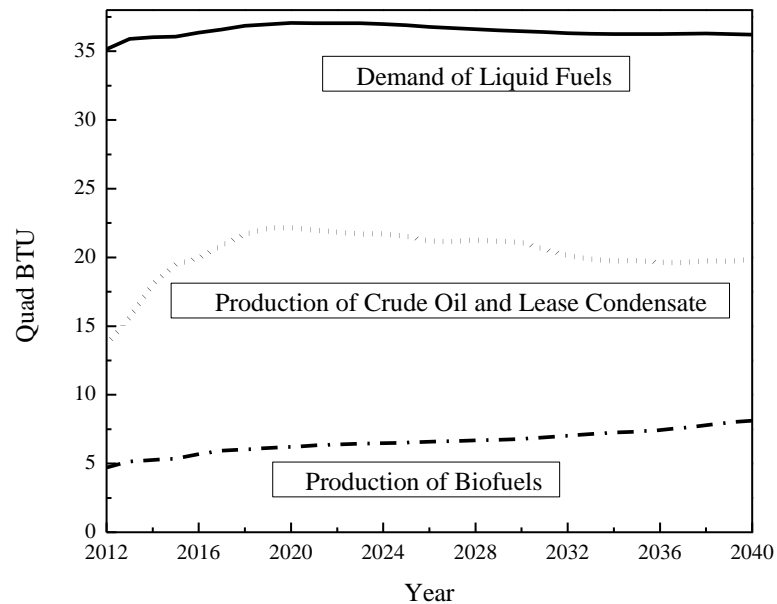
Chapter 10 summarizes the main conclusions of this work and gives recommendations for future work.

## Chapter 2 Literature review

### 2.1 Development of biofuels

#### 2.1.1 The current state and development trend of petroleum consumption

Since the first instance of industrialization, fossil fuels have been at the center of trade and have been vital to the growth of economies worldwide [23]. Figure 2-1 shows the projected supply and demand of world liquid fuels [24].



British thermal unit (BTU)

Lease condensate: mostly pentanes and heavier hydrocarbons in liquid form recovered from lease separators\* or field facilities at associated and non-associated natural gas wells.

Figure 2-1 Projected world liquid fuels demand and supply [24]

\*Lease separator: applies to the area of energy can be defined as ' A facility installed at the surface for the purpose of separating the full well stream volume into two or three parts at the temperature and pressure conditions set by the separator. For oil wells, these parts include produced crude oil, natural gas, and water. For gas wells, these parts include produced natural gas, lease condensate, and water'.

A quad is a unit of energy equal to 10<sup>15</sup> (a short-scale quadrillion) BTU, or 1.055 × 10<sup>18</sup> joules. According to Figure 2-1, conventional oil production rates, dependent upon the production of crude oil and lease condensate, are projected to increase first until 2020 and then decrease from 2020; while the demand of liquid fuel barely changes during the period of 2012 to 2040. Therefore, the production amount of other sources will have to be increased to meet the demand of liquid fuels.

### **2.1.2 Increasingly stringent emission standards**

Due to advancements in environmental policy, the requirements for heteroatom content in oil products are becoming increasingly stricter. In 1970s, it was gradually realized that emissions produced by human activities were conflicting with interests related to environmental protection. It is now very clear that these emissions, especially those produced by petroleum refineries and transportation fuels, have a strong impact on the environment. The main measure that was taken by European countries in order to reduce pollution was to try to remove sulfur from gasoline and diesel fuels [25]. The sulfur contents in European unleaded gasoline and diesel standards, as shown in Table 2-1, were respectively 1000 ppm and 2000 ppm in 1994, 150 ppm and 350 ppm in 2000, and 10

ppm and 10 ppm in 2011. These standards show a significant decrease in the amount of sulfur that was contained in oil products over this time period.

Table 2-1 Sulfur content changes in European motor fuel specifications [25]

Fuel (ppm)	1994	1995	1996	2000	2005
Unleaded gasoline 95/85, EN 228	1000	500	500	150	10
Diesel oil (standard grade), EN 590	2000	2000	500	350	10

Like Europe, Canada has also been experiencing decreasing sulfur contents in its oil products. According to Table 2-2, from 2000 to 2006 the restraints on sulfur content in Canadian gasoline and diesel decreased to their current standings of a maximum of 30 ppm and 15 ppm, respectively.

Table 2-2 Sulfur content changes in Canadian fuel specifications [25]

Fuel (ppm)	2000	2003	2004	2006
Gasoline	1000	150	30	30
Diesel oil	500	500	500	15

Table 2-3 shows the regulations on gasoline sulfur content of several countries or regions. Internationally, sulfur content in gasoline is currently tending towards 10 ppm in order to reduce air contaminant emissions and to improve vehicle fuel quality. California, the EU, Australia, and Japan have already enforced this regulation [26].

Table 2-3 International comparison of sulfur content in gasoline

Countries/regions	China	Canada	California	EU	Australia	Japan	WWFC
Sulfur content (ppm)	50	30	15	10	10	10	10

WWFC: world-wide fuel charter

Similar to sulfur, CO<sub>2</sub> emission is another critical problem. In the 1990s, it was recognized that GHG emissions, such as CO<sub>2</sub>, were one of the main causes of climate change. Worldwide, 21.0 % of CO<sub>2</sub> emission comes from the transportation industry and 8.0 % comes from the oil and gas industry [25]. The Intergovernmental Panel on Climate Change (established by the United Nations) reports that in the 20<sup>th</sup> century, GHG emission had led to an increase in global temperatures and will continue to contribute to climate change well into the 21<sup>st</sup> century [25].

In the past century, major emphasis has been given to the development of fossil feedstocks, which are used to produce multiple products such as fuel, chemicals, lubricants, solvent, waxes, coke, and asphalt. Fossil resources are not sustainable and are also questionable from an ecological and environmental point of view. Biofuels are organic resources that are renewable and also abundant. Furthermore, they are environmental friendly, producing no additional CO<sub>2</sub>, very little sulfur, and lessened nitrogen emissions. Needless to say, biofuels are recognized as one of the most promising potential alternative energy sources.

### **2.1.3 Development of biofuels**

In the near future, sources of petroleum supply will be confronted with rising demand and increasing restrictions due to environmental policy. To meet this additional demand, ways to utilize unconventional resources should be developed [23]. In 2010, global biofuel production reached 105 billion liters (28 billion gallons in the US), which was a 17.0 % increase of biofuel production from 2009. In the same year, biofuels (largely ethanol and biodiesel) made up 2.7 % of the world's fuel for road transport. Global ethanol fuel production also reached 86 billion liters (23 billion gallons in the US) in 2010 [26]. As of 2011, mandates for blending biofuels have existed in 31 countries and in 29 states or provinces, and the International Energy Agency has set a goal to have biofuels meet more than a quarter of world demand for transportation fuels by 2050 [26]. In December 2006, the Government of Canada announced its intention of developing regulations requiring an average of 2.0 % renewable fuel content in diesel fuel and heating oil by 2012. As of July 1, 2011, Environment Canada's *Regulations Amending the Renewable Fuels Regulations* has come into force, establishing a minimum average annual renewable fuel content of at least 2.0 % for producers and importers of diesel fuel and heating distillate oils (5 % renewable content in gasoline by 2010) [2, 3, 25]. These recent events indicate that an era of biofuel is coming.

#### **2.1.3.1 First-generation biofuels**

First generation biofuels are made from sugars and vegetable oils, which can be extracted easily using conventional technology. The main types of first generation biofuels used commercially are biodiesel and ethanol.

Biodiesel mainly consists of fatty acid methyl esters (FAME) and is produced from oils or fats by transesterification. Feedstocks for biodiesel include animal fats, vegetable oils, soy, rapeseed, sunflower, and palm oil. Biodiesel can be used in any diesel engine, either mixed with mineral diesel or used as a full substitute; it is also safe to handle because it has a high flash point compared to petroleum diesel fuel. However, biodiesel is an oxygenated fuel, meaning it is more acidic and has higher oxygen content than fossil diesel. There are also some unsaturated hydrocarbons in biodiesel, which means that biodiesel is air sensitive. Biodiesel may become more viscous at lower temperatures, so it should be handled carefully in cold regions.

Bioethanol is an alcohol made by fermentation, and is derived mostly from carbohydrates produced in sugar or starch crops such as corn or sugarcane [26]. Ethanol can be used as fuel, but it is usually used in gasoline as an additive to increase octane. Ethanol has a smaller energy density than gasoline. It therefore takes more ethanol than fossil fuel to produce the same amount of work.

A study from the International Center for Trade and Sustainable Development shows that the market driven expansion of ethanol in the US increased corn prices by 21.0 % from 2004 to 2009 [26]. This increase in food price has prompted researchers to develop biofuel crops and technologies that can reduce the impact of the growing biofuel industry

on the cost of food. Second-generation biofuels, which do not significantly affect the food economy, are being developed for this very purpose.

### **2.1.3.2 Second-generation (advanced) biofuels**

Second generation biofuels, also known as advanced biofuels, can be produced sustainably by using mainly two types of biomass. The first type is plant oil, such as jatropha oil; this type also includes wastes, such as waste cooking oil. The second type is biomass derived oil, which includes the residual non-food parts of crops such as stems, leaves, and husks; this type also includes inedible crops such as switchgrass, and industry waste such as woodchips [27]. Algae are a source of biofuel that could potentially make use of unprofitable land and wastewater. This research was conducted using WCO (representing triglycerides-based plant oils) as a general feedstock, using CLO as a reference for comparing, and oleic acid as model compound.

## **2.2 Upgrading technologies for second-generation biofuels**

### **2.2.1 Properties and compositions of plant oils**

The compositions of plant oils are listed in Table 2-4. The presence of olefins in catalytic cracking feeds can significantly affect the product distribution, as these species are often involved in hydrogen-transfer reactions that lead to the formation of aromatics [28].

Table 2-4 Typical fatty acids compositions of plant oils [29, 30]

Feedstock (%)	Fatty acids							
	14:0*	16:0	16:1	18:0	18:1	18:2	18:3	Others
Crude palm oil	1	40-45	-	4-6	36-39	9-10	<1	1
Used palm oil	-	23	8	13	28	15	2	11
Rapeseed oil	-	5	-	1	61	21	12	-
Jatropha oil	-	15	-	4-10	34-46	29-44	-	-
Canola oil	-	4	-	2	61	21	11	1
Cottonseed oil	-	23	-	2	17	55	<1	2
Soybean	-	11	-	4	23	54	8	-
Sunflower	-	7	-	5	16	71	1	-

\*n:m – “n” means the number of carbon in fatty acids, “m” means the number of C=C bonds in the fatty acids, for example, 14:0 means there are 14 carbons and no double carbon bonds in the fatty acids.

### 2.2.2 Comparison of plant oils to petroleum

Petroleum refineries have already been built, and therefore the infrastructure for a biofuel refinery needs little capital investment (they use similar processes). This research focuses on upgrading waste cooking oil by using existing petroleum refinery methods. The compositional differences between triglycerides and petroleum are listed in Table 2-5.

Table 2-5 Comparison of plant oils to petroleum [6, 11]

Properties and Composition		Plant oils	Petroleum
Elemental Composition (wt%)	Carbon	75-82	83-86
	Hydrogen	10-12	11-14
	Sulfur	-	<4
	Nitrogen	-	<1
	Oxygen	8-15	<1
Chemical composition		Triglycerides, acids	Paraffin, naphthenic, aromatic hydrocarbon

Most elemental compositions (i.e. carbon, hydrogen, nitrogen, and sulfur contents) are lower in plant oils than in petroleum. The oxygen content, however, is significantly higher in plant oils than in petroleum; this is the reason that plant oils have a lower gross heating value (with low energy density), have a higher acidity and viscosity. Petroleum mainly consists of hydrocarbons, such as paraffins, naphthenics, and aromatics, whereas plant oil consists mainly of triglycerides, such as C18 triglycerides. Furthermore, there are some unsaturated hydrocarbons in plant oils. Because of these factors, plant oil cannot be used directly as fuel – it should be upgraded first. This upgrading process must include oxygen removal.

There are currently two main routes proposed for upgrading plant oil, both of which are already present in today's refinery systems: catalytic hydrotreating with hydrogen and catalytic cracking without hydrogen.

### 2.2.3 Comparison of technologies for biofuel upgrading

There are two options available for converting biofuels into oil products/chemicals using petroleum refineries: catalytic cracking and hydrotreating. The comparison of these two technologies in regards to biofuel upgrading is presented in Table 2-6.

Table 2-6 Comparison of biofuels upgrading technologies [5, 6, 11]

Comparison	Catalytic cracking	Hydrotreating
Pressure	Atmosphere	High pressure
Hydrogen	No	Yes
Catalysts	Zeolites	Co(Ni)MoS <sub>2</sub> /Al <sub>2</sub> O <sub>3</sub>
Lifetime of catalysts	Several seconds	Not more than 200 hours

Catalytic cracking and hydrotreating are very different. A catalytic cracking reaction takes place without hydrogen under normal atmospheric pressure, whereas a hydrotreating reaction happens with hydrogen under high pressure. The catalysts employed for cracking are mainly zeolites, and their deactivation time is several seconds. Hydrotreating is conducted using conventional hydrotreating catalysts, such as CoMo/Al<sub>2</sub>O<sub>3</sub>, which have deactivation times of no more than 200 hours. Presently, petroleum industrial catalytic cracking catalysts become deactivated within several seconds of use, but industrial hydrotreating catalysts can last up to 2-3 years. This

indicates that hydrotreating catalysts undergo short activation times, which make them expensive (use hydrogen) and dangerous (operate under high pressures). Catalytic cracking is the most important conversion process in petroleum refineries; over 50 % of the refineries' heavy petroleum goes through the FCC process. The principal aim of catalytic cracking is to convert high molecular weight hydrocarbons into more valuable products (mainly gasoline), and to deoxygenate the feedstock.

#### **2.2.4 Development of FCC technology and the catalysts**

Since the mid-20<sup>th</sup> century, catalysis has developed remarkably both in terms of fundamental knowledge and applications. In the beginning of the 21<sup>st</sup> century, approximately 80-90 % of the products used daily had “seen” a catalyst at some point in their manufacturing process [25]. Catalytic cracking is one of the oldest processes in catalysis, and is also one of the most important in refining. The FCC process was first used at the end of the 1930s. The yield of desired products obtained from catalytic cracking is greatly dependent on operating variables, such as the type of catalyst, reaction temperature, catalyst-to-oil ratio, residence time, and reactor design. In the beginning of the 1960s, zeolite Y containing rare earth catalyst was used, which greatly increased gasoline yield. In the 1980s, gains in octane number were obtained using the new ultra stable zeolite Y (USY). Nowadays, virtually all catalysts are made from USY due to its high thermal and hydrothermal stability. Most cracking catalysts currently use zeolite Y as the active component and ZSM-5 as a catalyst additive to boost the gasoline octane number and to increase the yield of light olefins in the matrix of silica–alumina [25].

### **2.2.5 Application of catalytic cracking technology in biofuel upgrading**

Several researchers have provided information related to the catalytic cracking of triglycerides. The work by Ong and Bhatia [29] includes the proposal of a kinetic scheme for the catalytic cracking of vegetable oil but does not provide any equations or kinetic parameters. Mustafa et al. [30] evaluated in detail the effects of operational conditions and catalysts on the product qualities and quantities of renewable oil processing, when using existing FCC technology. They also organized and discussed the works related to the processing of different types of biofuels.

### **2.2.6 Chemical reactions during plant oils catalytic cracking upgrading**

The reaction mechanisms that occur during plant oil catalytic upgrading are described by Tani et al [31]. Triglycerides are first hydrolyzed into glycerin and three fatty acid molecules. Then, the glycerin is dehydrated to form water and gaseous hydrocarbons. As for the fatty acids, they can undergo either decarbonylation/dehydration reactions to form CO and water, or decarboxylation reactions to produce CO<sub>2</sub> and hydrocarbons (paraffins and olefins). According to Dupain et al. [32] dehydration reactions are the most productive. Tani et al. [31], however, found decarboxylation to be the most productive. The reason for this discrepancy could be the fact that Tani et al. [31] used an agitated flow system with longer reaction times (in the order of hours) and MgO catalysts, which can promote decarboxylation and water-gas shift reactions, while Dupain et al. [32] used conventional FCC catalysts and a micro-riser reactor with more realistic FCC reaction times (in the order of seconds).

Another reaction pathway for the catalytic cracking of palm oil over HZSM-5 was proposed. Palm oil first underwent thermal and catalytic cracking on the external surface of catalysts to produce heavy hydrocarbons and oxygenates. However, initial fragmentation could occur on the external surface of catalysts followed by diffusion into the pores [33]. These products were further cracked into light alkenes and alkanes, water, carbon dioxide, and carbon monoxide, which were assumed to be the primary cracking that occurred within the internal pore structure of zeolite catalysts. Light alkenes could also undergo oligomerization to produce a mixture of heavier alkenes and alkanes that fall under the gasoline, diesel, and kerosene fractions. The aromatic hydrocarbons were produced by the aromatization, alkylation, and isomerization of heavier olefins and paraffins. Coke was produced by the direct condensation of palm oil and the polymerization of aromatics. Ooi et al. [34] and Bhatia et al. reported on the kinetic model of catalytic cracking using palm oil (UPO) and a palm oil-based fatty acid mixture [35]. The kinetic model was based on three lumps: gaseous products, coke, and OLP. The OLP were further separated into another three lumps according to chemical function: the gasoline fraction (60–120 °C), the kerosene fraction (120–180 °C), and the diesel fraction (180–200 °C). This kinetic model agreed well with experimental data.

### **2.2.7 Effects of catalysts and operational parameters**

Watkins et al. [36] performed catalytic cracking pilot runs, using pure rapeseed oil (RSO) over FCC equilibrium catalysts. They were able to obtain higher conversions using RSO, crude palm oil (CPO), and soybean oil (SBO) compared to using conventional FCC feedstocks, such as vacuum gas oil (VGO). This result is shown in Table 2-7.

Table 2-7 Triglycerides and VGO cracking products [36]

Feedstock	RSO	SBO	CPO	VGO
Conversion (wt%)	81.0	79.0	80.0	66.0
Hydrogen (wt%)	0.1	0.1	0.1	0.2
C1-C2 (wt%)	2.3	2.6	2.4	1.3
C3-C4 (wt%)	14.5	13.1	15.2	13.5
Gasoline (wt%)	47.3	44.8	44.3	49.5
Light cycle oil (wt%)	16.1	17.9	16.7	15.5
Heavy cycle oil (wt%)	1.9	2.0	2.1	14.4
Bottoms (wt%)	3.2	3.0	3.4	18.4
Coke (wt%)	2.6	2.9	2.6	1.1
MON	81.2	81.3	79.5	80.4
RON	93.0	93.4	91.7	92.8

The reaction temperature and the catalyst/oil ratio were at 538 °C and 2, respectively.

On the other hand, less gasoline was produced by using RSO, SBO, and CPO (40-50 wt%) as feedstock than by using conventional feeds (60 wt%). For instance, during the catalytic cracking of CPO, the gasoline yield could only reach up to 40-50 wt% using either a commercial equilibrium catalyst or a nanocrystalline zeolite beta catalyst – these results are reported by Melero et al. [37] and Taufiqurrahmi et al. [38], respectively. Despite the low gasoline yields however, it has been reported that vegetable oil derived gasoline have a higher octane number than conventional gasoline, because there are more aromatics in the product pool. A hydrocarbon distribution analysis of 430 °C catalytically cracked CPO (Tani et al.) [31], showed that C15 hydrocarbons were the predominant species in

the final liquid product; these C15 hydrocarbons came from the acid group of the triglyceride molecule. The same results were obtained using both carbon and MgO-on-carbon catalysts. Other hydrocarbons, ranging from C7 to C20, were observed in small quantities.

Temperature is an important factor in the catalytic cracking of plant oils. He et al. [39] reported that when the reaction temperature was increased from 400 to 450 °C, the vapor product yield also increased from 35.0 to 40.0 wt%. Increasing the reaction temperature up to 500 °C further led to an increase in vegetable oil conversion [40, 41]: the amount of gaseous products increased significantly, but this happened at the expense of the liquid yield [38]. Li et al. observed that the degree of cracking increased when the reaction temperature, reaction time, or catalyst/oil ratio were increased [42]. Bielsky et al. [43] reported that more hydrocarbon gases were produced by using vegetable oils, such as RSO, SBO, and CPO than by using VGO. With regards to the vapor product, vegetable oils gave higher C1-C2 and propylene yields than conventional petroleum feedstocks under similar conditions, as reported by Watkins et al. [36]. As for oxygenates, the amount of water formed during the cracking of palm oil (using an equilibrium catalyst) was about 10.0 wt% – almost twice that of CO and CO<sub>2</sub> combined (5.0 wt%) [44]. Tani et al. [31] observed that during the cracking of CPO, the amount of CO<sub>2</sub> generated was greater than the amount of water generated. This could be attributed to the reaction system and the MgO-supported catalysts that promoted the decarboxylation of fatty acids.

Under the same conditions, higher catalytic cracking conversion can be obtained by using plant oils than by using VGO. This can be attributed to the low thermal stability and high diffusion rates of catalyst pores on the fatty acids in plant oils. Plant oil derived gasoline has a higher research octane number (RON), motor octane number (MON), and lower amounts of sulfur/nitrogen than petroleum gasoline.

While the use of WCO provides a number of advantages from an energy and environmental perspective, the catalytic cracking of WCO has not been explored much in published studies. Melero et al. [45] investigated the co-processing of WCO and VGO using a micro active testing unit with an industrial FCC equilibrium catalyst. It was observed that gasoline, light cycle oil (LCO), and decant oil yields in the final product decreased when the WCO content in the feed was increased. Specifically, there was a decrease of 47.0 to 40.0 wt% in the gasoline yield, 20.0 to 12.0 wt% in the LCO yield, and 9.0 to 3.0 wt% in the decant oil yield, when the fraction of WCO content was increased from 0 to 100% in the feed. However, there was also a slight increase in liquid petroleum gas (LPG), a decrease in the amount of total liquid products, and an increase in aromatic content. Most of the aromatics ended up in the gasoline fraction, resulting in a higher gasoline octane number. As indicated by Melero et al., water content also increased – there was almost 5.0 wt% water that formed from the co-processing of 30.0 wt% WCO in VGO, but there was 11.0 wt% water that formed from cracking pure WCO.

In oil refineries, catalytic cracking is the most widely used process for cracking the heavy fraction of crude oil to gasoline and other hydrocarbons. Studies have shown that catalytic cracking can effectively degrade large fatty acid molecules into smaller compounds falling mostly in the gasoline boiling range. Oxygen can also be removed as CO, CO<sub>2</sub>, or H<sub>2</sub>O through the following reaction:  $C_6O_6H_{12} = aC_xH_{2x} + 2O_y + bCO_2 + cH_2O + dCO + eC$  [13]. There are several problems, however, that arise when upgrading biofuels by the FCC process. For example, substantial amounts of char and coke are formed during FCC biofuel upgrading, even at lower reaction temperatures. Poor hydrocarbon yields and subpar fuel quality (high aromatic content) are also observed; these are drawbacks that need to be overcome. Different methods have been developed in order to solve these problems.

Sharma and Bakhshi [46] developed a dual-reactor system, wherein two catalytic reactors worked in series at different temperatures. Using this method, it was possible to nearly double the amount of organic distillate products and aromatic hydrocarbon yields, while also reducing the coke/char formation (10.0 wt% lower than in the single reactor). Tian et al. [47] used a two-stage riser fluid catalytic cracker (TSRFCC) to crack CPO and animal fats; the catalyst they used was a Co-Rh catalyst, containing USY and LTB-2 (ZSM-5 was used as the active component). The result was a high yield of LPG (45.0 wt%) and a gasoline yield reaching 21.0 wt%. When the secondary cracking reaction of the TSRFCC reactor was terminated early, however, a high olefin yield (47.0 wt%) was observed. This result indicates that a high aromatic concentration happens due to large amounts of

hydrogen-transfer, cyclization, and aromatization reactions. These new dual reactors can effectively solve the coke problem and lower the aromatic content in products. However, to implement them requires building new plants (and therefore high capital investments).

Graca et al. [14] suggested upgrading biofuels in combination with conventional feedstocks in dedicated units. Many published studies [13, 48-50] have compared co-processed products to petroleum products, in order to assess the suitability of using biofuels as potential feedstocks [45]. The results of these studies indicate that co-processing, to some extent, can only partially alleviate the coke problem.

### **2.3 Research objectives**

Although, by itself, catalytic cracking can partially eliminate oxygen from plant oils, the products still contain high amounts of unsaturated compounds and significant amounts of oxygenates. The hydrotreating process can also eliminate oxygen, but it requires large amounts of hydrogen to do so. Therefore, in this study a new technology is used for triglyceride upgrading: the catalytic cracking/hydrotreating combined technology. First, catalytic cracking is used to eliminate oxygen from the triglycerides. This process reduces the hydrogen consumption that would be needed if only hydrotreating was utilized. This process acts the upgrading of the long-chain wax-like normal paraffins through cracking, isomerization, and cyclization, leading to a better quality feedstock for the hydrotreating process. The products of the catalytic cracking are then hydrotreated. This not only leads to the saturation of unsaturated compounds, but can also further remove any oxygen that was left over from catalytic cracking products.

Currently, several problems need to be overcome before triglycerides can be efficiently upgraded through the integration of catalytic cracking and hydrotreating technology. This study focuses mainly on three areas of research: investigating the feasibility of hydrotreating triglycerides, the development of a novel cracking catalyst, and comparing the combined FCC/hydrotreating technology to direct hydrotreating technology.

### **2.3.1 Investigation of hydrotreating technology**

During hydrotreating triglyceride section, three points were investigated: the effects of hydrotreating parameters on triglyceride deoxygenation, the effects of catalyst support on triglyceride deoxygenation, and the deactivation mechanism and the activity recovery of supported sulfided CoMo catalysts during the triglyceride hydrotreating process.

#### **2.3.1.1 Effects of hydrotreating parameters on triglyceride deoxygenation**

Commonly, the catalysts used for the hydrotreating of triglycerides are: NiMo, CoMo, and noble metal catalysts such as Pt or Pt-Re [51-56]. This thesis focuses on the use of the supported CoMoS catalyst for hydrotreating of triglycerides [56]. Sankaranarayanan et al. [54] proposed that using supported CoMoS catalysts results in better products by increasing the reaction pressure (30-60 bars) and by decreasing the weight hourly space velocity. They speculated that at a temperature range of 320-350 °C, a 95.5 % conversion rate was possible under these conditions, using a blend of sunflower oil (20 % and 40 %) and gas oil (diesel range) as feed. Bezergianni et al. [51, 57-59] reported that lower temperatures (330-398 °C), pressures (8.27-9.65 MPa), LHSVs (0.5, 1.0, and 1.5 h<sup>-1</sup>), and

H/Os (543-890 m<sup>3</sup>/m<sup>3</sup>) were more conducive for diesel production [51, 58], and that high temperatures favored isomerization reactions [59]. They also investigated the hydrotreating of heavy gas oil mixed with WCO, and suggested that heteroatom removal is favored by an increase in temperature (310 to 350 °C), whereas better conversion is favored by lower amounts of WCO in the feedstock (<30 %) [60].

CLO is a relatively new vegetable oil to the North American Market. The hydrotreating of CLO has not been reported yet, so an exploratory study was performed on the hydrotreating of CLO in order to compare it with WCO. Of great interest from these experiments were the effects of temperature, pressure, LHSV, H/O volume ratio, and oil concentration (for both WCO and CLO) on the hydrotreating process.

### **2.3.1.2 Roles of catalyst support on triglyceride deoxygenation**

During triglyceride hydrotreating, DO depends significantly on the catalyst used; the two important parts of the catalyst are the active component and the catalyst support. MoS<sub>2</sub>, a very popular catalyst for petroleum hydrodesulfurization and hydrodenitrogenation, is also regarded as an effective catalyst for DO during triglyceride hydrotreating [51, 53-56]. Laurenti et al. [61] investigated the promotional effects of cobalt on the hydrotreating of guaiacol (2-methoxyphenol), a model compound used to represent ligno-cellulosic biomass pyrolysis oil. They reported that DO was strongly improved after the catalyst was promoted with cobalt. These results agreed with our previous research, which studied the impact of different promoters (Ni and Co) on the DO performance of unsupported MoS<sub>2</sub>. This study revealed that different oxygen removal reaction pathways exist when

working with different promoters [62]. Abundant sulfur vacancies were generated by MoS<sub>2</sub> that were promoted by Ni; Ni improved the hydrogenation ability of the catalyst. Those sulfur vacancies also showed a higher selectivity for HDO over HDC. Comparatively, Co-promoted catalysts exhibited saturated edge sites in a hydrogen atmosphere, favoring cracking by C-C hydrogenolysis; Co-promoted catalysts also showed a higher selectivity for HDC over HDO. The enhancement of HDO due to Ni was primarily suggested by the synergy effect of Mo and Ni on the unsaturated sites of metal edges. On the contrary, the HDC reaction was enhanced due to Co-promoted MoS<sub>2</sub>, through the adsorption of carbon atoms on the sulfur edge adjacent to Co.

Different catalyst supports [63] (even those only differing in morphology, orientation, or composition [64-67]) had a significant effect on the hydrotreating process. Laurenti et al. studied the effects of different catalyst supports including zirconia, titania, alumina, and no support on DO during hydrotreating. They concluded that zirconia supports can very efficiently help to convert guaiacol into deoxygenated hydrocarbons [61, 68]. The catalytic system CoMoS/ZrO<sub>2</sub> was found to be very selective towards C<sub>aromatics</sub>-O hydrogenolysis, as demethoxylation and direct DO were the main pathways observed. This was probably a result of the combined effect between CoMoS phases, wherein a close interaction with support enabled the activation of oxygenated molecules. With alumina supporting the CoMoS, methylation reactions occurred to a large extent, which did not correlate with the DO capability, and the formation of heavier products, (precursors of coke) had been found to also diminish the DO activity. With titania

supporting the CoMoS, hydrogenation reactions occurred primarily at a lower rate. Centeno et al. found that more acidic CoMoS catalyst supports (alumina, carbon, and silica) could enhance decarbonylation and deesterification reactions of carboxyl groups (on diethylsebacate). They also reported that there were no direct decarboxylation active sites on both alumina supported and unsupported catalysts, and that the active sites for decarbonylation could correspond to metal sulfides bound to the alumina support [69].

To compare the oxygen removal of aromatic and aliphatic reactants, Ryymin et al. studied the DO of phenol and methyl heptanoate individually and also mixed together. These experiments were conducted over a sulphided NiMo catalyst. They found that conversion, the fractions of completely deoxygenated products and intermediates, and the reaction pathways were changed when the reactants were mixed, compared to being separated [70]. This indicated that there was a distinction between the model compound and the real oil when they were used as reactants.

### **2.3.1.3 Deactivation mechanism and activity recovery of supported CoMoS catalyst**

Traditional sulfided CoMo or NiMo catalysts have been studied extensively for their potential use in the triglyceride hydrotreating process. A major problem is that these catalysts are quickly deactivated during reaction. Therefore, it has been heavily debated whether sulfided hydrotreating catalysts can be economically employed for the DO of triglycerides. One reason for the deactivation of these catalysts is that they produce water as a by-product [8-10, 71, 72]. Vogelzang et al. reported that the water formed was an inhibitor of 1-naphthol HDO for sulfided NiMo/Al<sub>2</sub>O<sub>3</sub> catalysts [72]. Krause et al. also

observed that the increasing amounts of water decreased the conversions of methyl heptanoate and ethyl heptanoate [9]. Some researchers found that increasing the partial vapor pressure (within a certain range) during hydrotreating process played no role in deactivating catalyst HDO. Badawi et al. [8] found that deactivation of the CoMoS catalyst was fully reversible, even after the presence of water at 340 °C caused additional deactivation. Laurent and Delmon [73, 74] discovered that additional water up to 3-4 % only caused a slight inhibition of the HDO of 4-methylacetophenone, diethyldecanedioate, guaiacol, 4-methylphenol, 2-ethylphenol, and dibenzofuran using NiMo/Al<sub>2</sub>O<sub>3</sub> and CoMo/Al<sub>2</sub>O<sub>3</sub> catalysts. A partial pressure of water of 2.5 MPa under 7 MPa total pressure should have been responsible for the loss of two-thirds of initial HDO activity, when using a NiMo/Al<sub>2</sub>O<sub>3</sub> catalyst to treat a mixture of substituted phenols for 60 hours [10]. However, Lavopa and Satterfield [71] observed that water could actually enhance the HDO of dibenzofuran over a NiMo/Al<sub>2</sub>O<sub>3</sub> catalyst. Due to all these conflicting results, it was necessary to clarify the effects of water on catalyst activity and deactivation, as well as whether deactivation is reversible or not.

Loss of sulfur is another root cause of catalyst deactivation during the HDO process [7, 9, 73, 75, 76]. Adding H<sub>2</sub>S or a sulfiding agent to the feed is a proposed solution to this problem – it would help to maintain the sulfided active sites and HDO activities of the catalysts during reaction. Laurent et al. [74] found that the hydrogenation activity of 4-methylphenol HDO (over conventional CoMo catalysts but below NiMo catalysts) was slightly promoted by H<sub>2</sub>S. Krause et al. [9, 77] observed that the presence of H<sub>2</sub>S could

effectively improve the HDO activity of methyl heptanoate/ethyl heptanoate, when CoMo/Al<sub>2</sub>O<sub>3</sub> and NiMo/Al<sub>2</sub>O<sub>3</sub> were used as catalysts. This could have even been enough to compensate for the HDO inhibition caused by water. Kubicka et al. [7] reported that the presence of H<sub>2</sub>S could not only partially restore catalyst DO performance, but could also lower the ratio of HDO to HDC by a considerable amount. Contrarily, Ferrari et al. [75] and Krause et al. [76] concluded that H<sub>2</sub>S acts as an inhibitor for the hydrogenolysis route of HDO, and that the presence of H<sub>2</sub>S changes the occurrences of different reaction pathways. Ferrari et al. [75] drew their conclusions by studying the transformation of a mixture of guaiacol, ethyldecanoate, and 4-methylacetophenone, under the following conditions: a partial H<sub>2</sub>S pressure from 10 to 150 kPa (under a total pressure of 7 MPa) and temperatures of 270 and 200 °C. They found [75] that decarboxylation and alcohol dehydration reactions occurred due to the existence of H<sub>2</sub>S, and that the average degree of reduction decreased due to an increase in H<sub>2</sub>S concentration. Krause et al. [76] observed that the presence of H<sub>2</sub>S strongly decreased the HDO activity of phenol/anisole during hydrotreating using a sulfided CoMo/Al<sub>2</sub>O<sub>3</sub> catalyst. Etienne Laurent et al. [73] discovered that the HDO activity of 4-methylacetophenone was reduced by H<sub>2</sub>S when using an NiMo catalyst, but not when using a CoMo catalyst. They also observed that the conversion of diethyldecanedioate was enhanced through the promotion of the decarboxylation reaction.

Other reasons for catalyst deactivation were also reported in the literature – coke formation was significant among them. Due to high concentrations of phospholipids in

trap grease [7] or high molecular weight reaction products, coke can be formed from oxygen-containing compounds during phenol and anisole HDO [76]; during this process, alkalis can also be deposited on active sites because of their high concentration in waste rapeseed oil [7].

### **2.3.2 Development of cracking catalysts**

During the catalytic cracking process, the problems that need to be considered include: poor hydrocarbon yields, extensive coking, and poor qualities [15-20]. When cracking biofuels, feedstock conversion, product yields, product compositions and distributions, and coke produced are all highly dependent upon the catalysts used. Until now, HZSM-5 has been regarded as an effective catalyst for upgrading bio-oil into organic distillates, overall hydrocarbons, and aromatics. As the FCC unit operates in continuous reaction/regeneration cycles, the behavior of HZSM-5 was studied when upgrading bio-oil during these cycles. It was observed that the continued regeneration of the HZSM-5 leads to an irreversible deactivation of the catalyst. To improve hydrothermal stability, HZSM-5 was modified to have higher Si/Al ratios and to be impregnated with Ni [78]. These modified zeolites were tested, and it was found that they could only maintain their kinetic behavior for 10 reaction/regeneration cycles. Other published reports have studied the FCC of plant oil, using existing FCC catalysts designed for petrol [13, 21, 22, 29]. Few novel cracking catalysts for upgrading bio-oils have been developed, even though there is a wide range of possibilities to explore with catalysts.

### 2.3.2.1 Development of metal oxide catalysts

The structures, active (acidic or basic) sites, and the bonds between metal and oxygen all influence the ability of catalysts to adsorb reactants on their active sites – these are the primary factors when considering catalyst utilization [79]. The use of acidic and basic cracking catalysts for biofuel upgrading started in 1980s [80]. Dosanjos et al. investigated the decomposition of oleic acid by  $\text{Al}_2\text{O}_3$  and  $\text{MgO}$  in a glass tubular reactor at 300~500 °C. They found that oleic acid could yield a mixture of oxygen containing products and hydrocarbons with a low mean molecular weight [81]. Activated alumina was used for deoxygenating fatty acids into chain alkenes and some alkanes (at atmospheric pressures and at 450 °C) [82, 83]. Idem et al. studied the various roles that catalyst basicity played in the process and product distribution of canola oil conversion. They used calcium oxide and magnesium oxide catalysts in a fixed-bed microreactor at an atmospheric pressure of argon. The temperatures were 400 °C and 500 °C, respectively [84]. They observed that the basic sites in the catalysts strongly inhibited secondary cracking, which resulted in high residual oil yields and low gas yields. Researchers have compared the various impact of oxygenates to the upgrading process both by acid and base catalysts [85-88]. Xu et al. found that when using base catalysts (such as  $\text{Na}_2\text{CO}_3$  and  $\text{K}_2\text{CO}_3$ ) the amounts of carboxylic acids and aldehydes, as well as the high acid value found in the products, were significantly decreased. These results were obtained by using base catalysts (such as  $\text{CaO}$ ) and were described in comparison to the results obtained by using  $\text{Al}_2\text{O}_3$  catalyst. At low temperatures, the base catalyst products also showed good solubility in diesel, good cold flow properties, and had high heat values [86-88].

### **2.3.2.1 Development of kaolin-based catalysts**

Furthermore, the characteristics of catalysts such as strength, type, amount of acidic sites, and pore structure are very important and all of them affect triglyceride cracking reaction pathways. Small variations in these characteristics can influence the OLP yield, composition, and fraction distribution [80]. With respect to the OLP yield, when comparing zeolite to amorphous silica-alumina or MCM-41 [89, 90], the increase in the concentrations and strengths of acidic sites could cause over-cracking, which could lead to a decrease in OLP yield. With respect to the OLP composition, ZSM-5 catalyst favors the formation of benzene and toluene (80-95 wt% of OLP) because of its strong acidity and unique pore dimensions and architecture. On the other hand, mildly acidic amorphous silica-alumina could produce significant concentrations of aliphatic hydrocarbons (10-30wt% of OLP) [89]. Considering the fractional distribution, the highest yield of gasoline fraction was achieved over HZSM-5/MCM-41 composite catalysts (containing 10-30 wt% of mesoporous phase) compared to HZSM-5 when upgrading a fatty acid mixture, crude palm oil, and was to palm oil. This was due to a good balance between initial and secondary cracking in the mesoporous material, as well as to aromatization in the micropores of HZSM-5 [90-92]. These catalysts were made according to the same theory that created the petroleum cracking catalyst matrix – they include a 30-50 wt% substrate, whose function is to provide active sites for the primary cracking of large molecules on the mesopores (the products are then transferred into the micropores).

Treated kaolin was extensively used as a catalyst to improve coke selectivity and yield distribution [93], significantly to reduce sulfur content [94], and to enhance metal tolerance performance [95, 96] during petroleum upgrading process. If kaolin-based catalysts can work well with the WCO upgrading process, irreversible catalyst deactivation should no longer be a problem. The reason is that kaolin has been proven to work well even under severe petroleum catalytic cracking conditions [15-20].

### **2.3.3 Development of integration technology**

The developed cracking catalysts were evaluated in the FCC reactor and the resulting cracking liquid products were then hydrotreated in a batch reactor over a commercial supported CoMoS catalyst. The products of this new integrated technology were compared with the products of direct hydrotreating.

## Chapter 3 Analytical procedures for catalyst characterization and reaction performance evaluation

### 3.1 Reaction systems

#### 3.1.1 Fixed-bed reactor for evaluation of hydrotreating process

An autoclave engineers BTRS-JR-PC fixed-bed micro-reactor was used for the hydrotreating process (over a supported CoMoS catalyst) outlined in Chapters 4 to 6.

Figure 3-1 shows the process flow diagram.

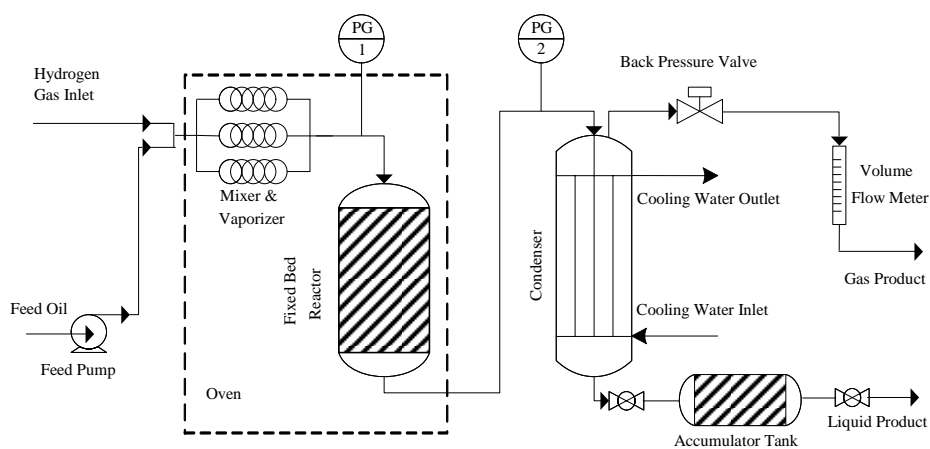


Figure 3-1 Process flow diagram of hydrotreating reaction system

At the start of the reaction, the oil and hydrogen gas are preheated and then the mixture flows downwards through the catalyst bed. The pressure drop across the reactor was measured using pressure gauges (PG) 1 and 2. The reaction products are condensed and the liquid products and gas products were separated at the bottom and the top of

condenser, respectively. The liquid products were collected from the bottom of the condenser by an accumulator tank, while the gas products were released after flowing through a volume flow meter connected to the top of the condenser.

Figure 3-2 describes how the catalyst was loaded into the reactor (the diameter of the reactor was 1.3 cm). A 200 mesh screen was placed in the bottom of the reactor to prevent any solids from falling through while fluids were flowing. Glass wool was placed at the top and bottom of the reactor to hold the catalyst bed. Glass beads (GB) were used to position the catalyst in the center of the reactor and help provide greater heat transfer.

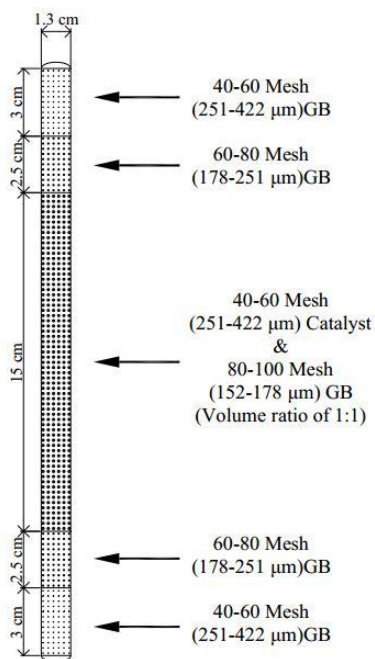


Figure 3-2 Catalyst loading

The mass balance of all runs conducted using this fixed-bed reactor was higher than 95 %.

### **3.1.2 Batch reactor for evaluation of hydrotreating process**

The reaction performance evaluation of the unsupported CoMoS catalyst (Chapter 5) was carried out in a 1000ml batch reactor (Parker Autoclave Engineers Inc.) under a pressure of 9 MPa hydrogen (99.99 %) and at temperatures of 300, 340, and 375 °C. Hydrogen was supplemented into the system whenever the pressure dropped below 8.6 MPa. The mass ratio of catalyst to feed was 1:200 and the reaction time was 8 hours.

### **3.1.3 Fixed-bed micro reactor for cracking catalyst evaluation**

A fixed-bed micro reactor was used as the system to evaluate the metal oxide catalytic cracking performance (under atmospheric pressure with nitrogen at 470 °C) (Chapter 7). This reaction system is shown in Figure 3-3; it consists of a quartz tube reactor (inner diameter: 10 mm, length: 100 mm), a nitrogen gas feed system, a liquid feeding syringe, a heater and temperature control system, a condenser, an iced ethanol/saturated salt mixture cooling system, and a liquid and gas product collection system.

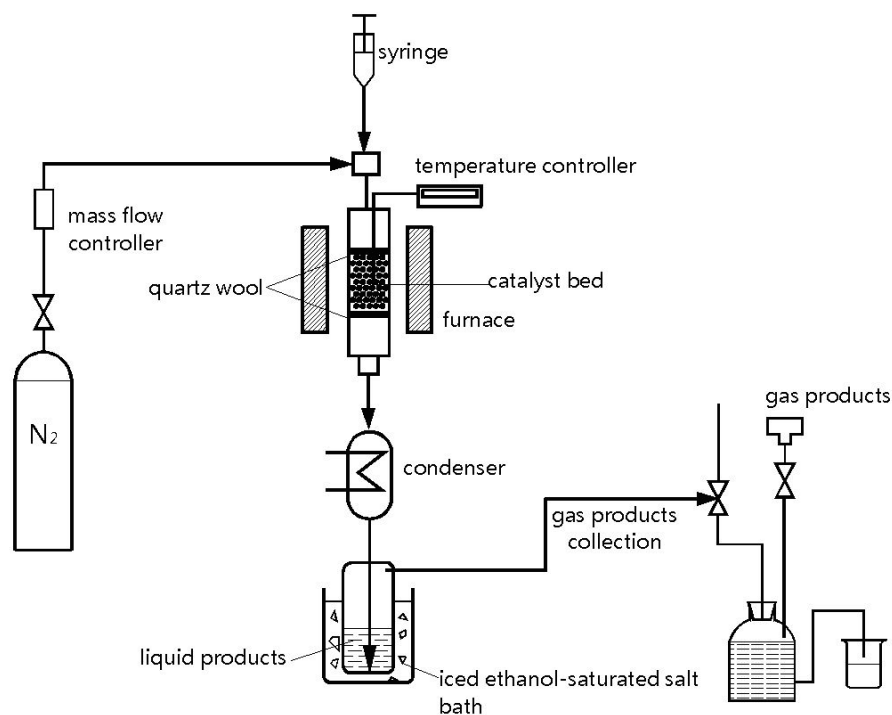


Figure 3-3 Fixed-bed micro reactor for cracking catalyst evaluation

### 3.1.4 FCC reactor for cracking catalyst evaluation

A FCC reactor was used to evaluate the cracking performance of kaolin-based catalysts as discussed in Chapters 8 and 9.

#### 3.1.4.1 Fluid state calculation

The fluid state was calculated first according to Equation 3-1, Equation 3-2, and Equation 3-3. The same water flow rate (3 ml/min) was used for each catalyst because the composition of each catalyst matrix was the same: 80 wt% kaolin-based or commercial catalyst as the main component, and 20 wt% binder.

$$u_{mf} = [0.0078d_p^2(\rho_p - \rho_f)g]/\mu_f \quad \text{Equation 3-1}$$

$$u_t = gd_p^2(\rho_p - \rho_f)/(18\mu_f) \quad \text{Equation 3-2}$$

$$d_{p,av} = \frac{1}{\Sigma(x_i/d_{p,i})} \quad \text{Equation 3-3}$$

where,

$u_{mf}/u_t$  is the minimum or terminal fluidized velocity, in cm/s;

$d_p$  is the diameter of catalyst particles, in cm;

$\rho_p/\rho_f$  is the density of catalyst particles or fluidized gases, in g/cm<sup>3</sup>;

$g$  is the acceleration due to gravity, which equals 981 cm/s<sup>2</sup>;

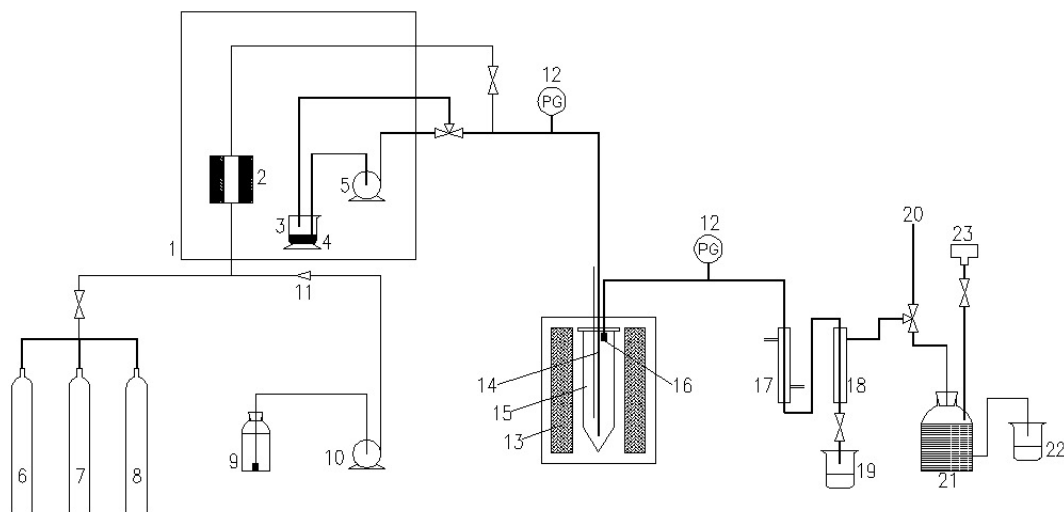
$\mu_f$  is the viscosity of fluidized gases, in Pa s; and

$x_i$  is the mass fraction of  $d_{p,i}$  particle diameter in all particles, in cm.

### 3.1.4.2 Catalyst performance evaluation

In order to get relatively stable catalyst activities, all fresh catalysts were prepared to the hydrothermal treatment in steam at 700 °C for 5 hours (the flow rate of water was set to 0.95 ml/min, calculated according to ASTM D 4463). Without this treatment, the lifetime of the catalysts would be very short.

The flow sheet of the FCC reactor is shown in Figure 3-4.



1-Preheat oven (80°C); 2-Steam generator; 3-Feedstock; 4-Electric balance; 5-Oil pump; 6-Hydrogen cylinder; 7-Nitrogen cylinder; 8-Oxygen cylinder; 9-Water tank; 10-Water pump; 11-One way valve; 12- Pressure gauge; 13-Reactor furnace; 14-Thermocouple; 15-Reactor; 16-Filter; 17-Condenser; 18-Gas/liquid separator; 19-Liquid product; 20-Gas vent; 21-Saturated salt water; 22-Water collecting tank; 23-Gas sample

Figure 3-4 The flow sheet of the FCC reactor

At first, the catalysts and nitrogen were introduced into the system to make the catalysts fluidize and to purge air out of the system. The system was powered on, and the hydrothermal treatment of the catalysts began. When the temperature rose to the set point, distilled water was pumped into the steam generator to be converted into steam, and the nitrogen cylinder could then be closed. After the hydrothermal treatment had finished, the temperature was set back to the reaction temperature. When the temperature reached the set point, the oil pump was opened. The oil inlet system was located in the oven (80 °C)

to maintain mobility of the feed oil. Carried by steam, this oil was introduced into the system and was allowed to preheat before being fed into the reactor. The cracking process started once the feedstock vapors came into contact with the hot catalysts in the reactor. The vapors then travelled up along the reactor until they separated from the catalysts. The product vapors were released from the top of the reactor and introduced into a condenser so that the gas/liquid products could be collected from the separator. The liquid products were retrieved from the bottom of the separator, while the gas products were retrieved after being displaced by salty water. The water phase was separated from the OLP phase before being analyzed. The spent catalysts were either left in the reactor for regeneration (done by burning coke off the surface of the catalysts at 650 °C) or were taken out of the reactor for analysis. Oxygen and steam were used in the regeneration process: steam was primarily used to remove entrained hydrocarbons from the catalysts and to benefit heat transfer, whereas oxygen was introduced for the combustion of coke. The use of steam in the catalyst regeneration process requires that the catalyst must be hydrothermally stable.

### **3.1.5 Batch micro reactor for evaluation of hydrotreating process**

A 25 ml batch micro reactor was used to evaluate the performance of the combined catalytic-cracking/hydrotreating technology, conducted over a CoMoS supported catalyst at 275-325 °C and under 250-500 psi. This is outlined in Chapter 9. The total mass received from the process could reach 100±5 wt%.

### 3.2 Feeds

Oleic acid (purchased from Fisher Scientific) was only used as a model compound for the reaction mechanism investigation presented in Chapter 7.

CLO (purchased from Canpressco Products Inc.) was only used as a comparison feed during the triglyceride hydrotreating process outlined in Chapter 5.

WCO (purchased from McCain Foods Limited) was used as the general feed for experiments in this thesis; it is relevant in Chapters 4, 5, 6, 8, and 9. Dodecane (a mixture of isomers, CAS number: 93685-81-5) was used as a solvent for dispersing the oil and for preventing the gumming up of oil inside the catalyst bed, in all hydrotreating processes excluding those outlined in Chapters 7 and 8.

Table 3-1 shows the properties and compositions of WCO and CLO. The density and TAN are very similar for both oils, at  $0.9177 \text{ g/cm}^3$  (WCO) and  $0.9194 \text{ g/cm}^3$  (LCO), and  $0.86 \text{ g KOH/g oil}$  (WCO) and  $0.67 \text{ g KOH/g oil}$  (LCO), respectively. The carbon element content of WCO is 2.8 % lower than that of CLO, whereas the oxygen element content of WCO is 2.9 %, higher than that of CLO. After the feed oils underwent hydrolysis and esterification according to the literature [97], their fatty acid compositions were determined by gas chromatography and mass spectrometry (GC/MS). The fractions of

C18 were 91.0 % in WCO and 68.6 % in CLO. The amounts of unsaturated acids were 90.1 % in WCO and 88.8 % in CLO.

Table 3-1 Properties and compositions of feed oils

Items		WCO	CLO
Properties	Density (g/cm <sup>3</sup> )	0.9177	0.9194
	TAN (mg KOH/g oil)	0.86	0.67
Element compositions (wt%)	Carbon	77.9	80.6
	Hydrogen	11.5	11.6
	Oxygen	10.6	7.7
Fatty acids compositions (wt%) ((n:m(o))*)	16:0*	7.5	7.4
	16:1	0.5	0.0
	18:0	2.5	3.7
	18:1(9)	71.3	53.8
	18:2(9, 12)	17.2	11.1
	20:1	0.0	19.1
	20:2	0.7	0.0
	20:3	0.0	0.5
	22:1	0.0	2.0
	22:2	0.4	2.0
24:1	0.0	0.3	

\* n: m (o), n is the number of carbon atoms in fatty acids; m is the number of C=C double bonds in fatty acids; o is the number of carbon double bond position, only WCO was tested. For example, 18:2(9, 12) is a fatty acid with 18 carbon atoms, 2-carbon double bond, and the carbon double bonds are at No. 9 and No. 12 carbon, as shown in Figure 3-5 .

In WCO only, the position of the carbon double bond was determined by tandem Mass Spectrometry after Paterno–Buchi reaction, according to the literature [98], at Purdue University. This information was important for the investigation of the catalytic cracking mechanism.

The molecular structure of feed is drawn in Figure 3-5 according to the compositions results shown in Table 3-1.

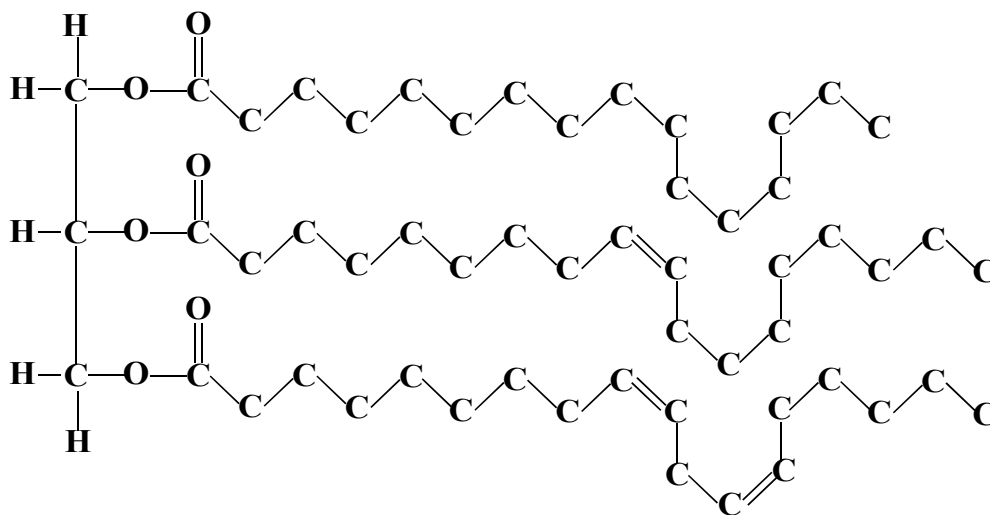


Figure 3-5 Molecular structure of feed

### 3.3 Catalysts

#### 3.3.1 Supported CoMoS hydrotreating catalysts

The catalyst used in Chapters 4 to 6 was a commercial supported CoMoS catalyst, whose supports were alumina, silica, and titania. Glass beads (40-100 mesh) were used to

position the catalyst (40-60 mesh) in the center of the reactor and to provide greater heat transfer. Prior to the experiment, the catalyst underwent in-situ drying, pre-sulfiding, conditioning, and stabilization. In-situ drying was first performed with a nitrogen flow rate of 80 ml/min and 200 psi, at an ambient temperature for 30 minutes; the temperature was then increased to 200 °C and drying continued for 4 hours. Pre-sulfiding was performed using the pre-sulfiding feed 3.7 wt% dimethyl disulfide (DMDS) in dodecane, at a LHSV of 2.0 h<sup>-1</sup>, a hydrogen flow rate of 100 ml/min, and a pressure of 120 psi. The following temperature program was used: 150 °C (rate: 20 °C/min, 2 hours), 230 °C (rate: 20 °C/min; 2 hours), 280 °C (rate: 10 °C/min; 2 hours), 320 °C (rate: 5 °C/min; 4 hours), and 350 °C (rate: 1 °C/min; 3 hours). Then the catalysts underwent conditioning at 350°C for 8 hours with a conditioning feed of 20 wt% light gas oil/dodecane, at a LHSV of 1.0 h<sup>-1</sup>, a hydrogen flow rate of 100 ml/min, and a pressure of 600 psi. Afterwards, the temperature was reduced to 300 °C and the catalyst stabilization was performed for 3 days with a feed of 2 wt% WCO in dodecane, at a LHSV of 2.0 h<sup>-1</sup>, a hydrogen flow rate of 60 ml/min, and a pressure of 800 psi.

The catalyst used for the hydrotreating process outlined in Chapter 9 was the same supported CoMoS commercial catalyst. Before the experiment, the catalyst underwent drying and pre-sulfiding. Drying was performed at 300 °C in a muffle oven for 4 hours. Pre-sulfiding was performed using a mass ratio of catalyst to DMDS at 1:10, under a pressure of 200 psi. The following temperature program was used: 220 °C (rate: 20 °C/min), 280 °C (rate: 1 °C/min; 2 hours), and 320 °C (rate: 1 °C/min; 2 hours).

### **3.3.2 Unsupported CoMoS hydrotreating catalysts**

An unsupported CoMoS hydrotreating catalyst was used to investigate the impact of support on WCO DO (Chapter 5). The unsupported CoMoS catalyst was synthesized from the compounds  $\text{MoO}_3$ ,  $\text{Na}_2\text{S} \cdot 9\text{H}_2\text{O}$ ,  $\text{HCl}$ , and  $\text{Co}(\text{NO}_3)_2 \cdot 6\text{H}_2\text{O}$  using a hydrothermal method. These compounds were purchased from STEM Scientific and Fisher Scientific, and were used exactly as received. The hydrothermal synthesized reaction conditions were: a temperature of  $320\text{ }^\circ\text{C}$  and a stirring speed of 500 rpm, for 2 hours. Before evaluation, the unsupported catalysts were also sulfided for 2 hours: this was done at  $280\text{ }^\circ\text{C}$  under a pressure of 220 psi and with a hydrogen flow rate of 80 ml/min, as well as a 0.1 ml/min flow of dodecane solution containing 2 % DMDS.

### **3.3.3 Metal oxide cracking catalysts**

The roles of catalyst acidity and basicity (Acid:  $\text{Al}_2\text{O}_3$  and  $\text{TiO}_2$ , Alkaline:  $\text{CaO}$  and  $\text{MgO}$ , and Neutral: quartz) in the conversion of oleic acid were studied in a fixed-bed quartz micro reactor at atmospheric pressure.

Alumina was prepared from boehmite. Boehmite was dissolved in deionized water and then  $\text{HCl}$  was added in drops. Then, the mixture was placed into a water bath at  $60\text{-}65\text{ }^\circ\text{C}$ ; the pH value of this mixture was adjusted with  $\text{HCl}$  to 3-4, and colloidal substances were produced. The solution was then dried in an oven at  $105\text{ }^\circ\text{C}$  for 5 hours. Finally, the dried sample was calcined in a muffle oven at  $700\text{ }^\circ\text{C}$  for 2 hours [99].

TiO<sub>2</sub> and quartz were used as received.

CaO and MgO underwent in-situ drying with nitrogen at 800 °C, in order to remove metal hydroxide and metal carbonate.

### **3.3.4 Kaolin-based cracking catalysts**

Kaolin-based catalytic cracking catalysts were used to investigate the DO of waste cooking oil. Catalyst preparation included two parts: kaolin treatment and catalyst matrix preparation.

#### **3.3.4.1 Kaolin treatment**

Kaolin was purchased from Fisher Scientific. ATK was prepared from natural kaolin and an HCl solution [95]. One hundred grams of natural kaolin, calcined at 800 °C for 1h, was added to a 300ml solution containing 21.9 g HCl. The reaction took place at 92 °C and continued for 12 h. The mixture was then washed with distilled water to remove Cl<sup>-</sup> (tested with an AgNO<sub>3</sub> solution) and dried overnight in an oven at 120 °C.

Base treated kaolin (BTK) was prepared from natural kaolin and an NaOH solution [95]. One hundred grams of natural kaolin, calcined at 1000 °C for 1h, was added to a 300 ml solution containing 50 g NaOH. The reaction took place at 95 °C and continued for 2 h. The mixture was then washed (until the pH value was at 7), filtrated, and dried.

Pretreated kaolin (PTK) was dried overnight in an oven at 105 °C and was thermally but not chemically treated during the matrix preparation process in section 3.3.4.2.

### **3.3.4.2 Catalyst matrix preparation**

For catalyst matrix preparation, 40 g of binder was dissolved in 80 g of concentrated HNO<sub>3</sub>. Then the catalysts (either kaolin, treated kaolin, or CC) were added into the solution and stirred until distributed evenly. Next, the mixture was introduced into an extruding machine to shape the catalysts that were then dried at room temperature overnight and further dried at 120 °C for 2 hours. The dried catalysts were subsequently calcined at 550 °C for 2 hours. Finally, the calcined catalysts were crushed and sieved through 40-80 mesh sieves.

## **3.4 Product analysis**

### **3.4.1 Gas products**

The compositions of inorganic gases, such as CO, CO<sub>2</sub>, and H<sub>2</sub>, were tested by a combination of a GC (Varian GC-3400) equipped with an Agilent HP-PLOT Q column (19095P-QO4, 30 m×0.53 mm×40 μm), and a Residue Gas Analyzer (GC/RGA). Helium was used as a carrier gas, and the flow rate of helium was 15 ml/min. The quality analysis of CO, CO<sub>2</sub>, and H<sub>2</sub> in the gas products was determined from the signals of the mass/charge (m/z) ratios: 12, 44, and 2; and the quantity analysis was determined by external standard method.

Composition of hydrocarbons in the gas products was determined by gas chromatography with a Flame Ionization Detector (GC/FID, GC-17A), which was equipped with a middle range polarity column (19095P-S25, 50 m\*0.53 mm\*15  $\mu$ m DF). The temperature program was: 35 °C for 2 min, 190 °C with 10 °C/min, and 190 °C for 20 min. The injection temperature and detector temperature were 60 °C and 210 °C, respectively. The quality analysis was conducted by standard gas and the quantity analysis was conducted by external standard method.

### **3.4.2 Liquid products**

For the feeds/liquid products, the water content and the total acid value (TAN) were respectively determined according to ASTM D 4377 and ASTM D 664. The equipment that was used was a 701 KF Titration (Metrohm AG, Switzerland) and a ZD-2 potentiometric titrator (Shanghai Ai Yi Qi Shi Ye Co. Ltd., China).

The functional groups and structures of the feeds and liquid products were recognized by Fourier transform infrared spectroscopy (FTIR) and Nuclear magnetic resonance (NMR). A Nicolet FTIR-6700 (Thermo Fisher Scientific Inc., USA) with 100 mg potassium bromide (KBr) pellets was used to analyze functional groups. The scanning was performed at a resolution of 4  $\text{cm}^{-1}$  in a range of 4000-400  $\text{cm}^{-1}$ . H-NMR analysis was conducted on a Varian UNITY INOVA 300 MHz spectrometer (Agilent Technologies, Inc., USA) in order to determine the presence and relative intensity of hydrogen containing functional groups. A 5 wt% liquid sample in chloroform-D was used in the analysis.

The contents of carbon, hydrogen, and oxygen in the feeds and liquid products were tested by a LECO CHN-932 elemental analyzer (LECO Corporation, MI, US) according to ASTM D 5291. Liquid samples were combusted in an oxygen atmosphere at 1150 °C. The responses to the contents of carbon and hydrogen were calibrated by the standards, whereas the contents of oxygen were calculated by the differences.

The boiling point distribution of the liquid products was determined using a gas chromatograph (Shimadzu GC-2010) coupled with an FID, equipped with an Agilent Technologies DB-2887 column (100 % dimethyl polysiloxane, 10 m×0.53 mm×3.0 µm). The temperature program was: 35 °C→340 °C (20 °C/min, hold for 5 min). The injection and detector temperatures were at 325 °C and 360 °C, respectively. The liquid samples were measured by the internal standard method according to ASTM D2887.

The qualitative chemical compositions of the liquid products were analyzed by gas chromatography (SHIMADZU GC-17A) coupled with mass spectrometry (SHIMADZU MS-QP5000) (GC/MS, Shimadzu Scientific Instruments, Japan), equipped with an Agilent HP-5MS column. The temperature program was: 60 °C (held for 5 min), 180 °C (rate: 10 °C/min, held for 5 min), 240 °C (rate: 8 °C/min, held for 5 min), and 300 °C (rate: 20 °C/min, held for 4.5 min). The injection and interface temperatures were at 305 °C and 320 °C, respectively. Full-scan mass spectra were acquired from 50 to 500 m/z at a scan speed of 1000.

The quantitative testing of hydrocarbons in the liquid samples was determined by external standard method using a Varian 450 gas chromatography coupled with an FID, equipped with a non-polar capillary column (Agilent J&WVF-1ms). The temperature program was: 60 °C (held for 5 min), 230 °C (rate: 7 °C/min), and 300 °C (rate: 10 °C/min, held for 5 min). The injection and interface temperatures were at 305 °C and 320 °C, respectively.

The quantitative testing of oxygenates in the liquid products was complicated; this testing is discussed in Chapter 5. The total oxygen contents in the feed and hydrotreated products were calculated by the differences of carbon and hydrogen contents, examined by a CHN-932 elemental analyzer (LECO Corporation, MI, US) according to ASTM D 5291. The free fatty acids were analyzed by both gas chromatography (Shimadzu GC-17A) and titration (ZD-2A Automatic potentiometric titrator, Saegmoter Company, Shanghai, China) according to ASTM D 664. The contents of alcohols and aldehydes were calculated from GC/MS results by the peak area and response factors of 1.3 and 1.4 [100]. The oxygen balance can also show the content of unreacted glycerides in the liquid products.

### **3.4.3 Solid products**

The coke contents of the spent catalysts were determined by thermo gravimetric analysis (TGA, TGA-Q500). The pre-treatment procedures and analyzing programs used were the same as those of the temperature program oxidation (TPO) testing in Section 2.5.

### **3.5 Catalyst characterization**

The specific surface area, pore volume, and pore size distribution of catalysts were determined by N<sub>2</sub> adsorption at -77K on an Autosorb1-C (Quantachrome Instruments, USA). Prior to measurement, the sample (50-500 mg) was degassed at 300 °C until the 1-minute vacuum pressure was lower than 20 micron. The surface area of the catalysts was calculated using the Brunauer-Emmet-Teller (BET) method. The total pore volume was the volume of nitrogen that was adsorbed under the relative pressure  $p/p_0$  at 0.995. The pore size distribution of catalysts was calculated using the Barrett-Joyner-Halenda (BJH) method.

The strength and amount of acidic/alkaline sites on the surface of catalysts was determined by NH<sub>3</sub>/CO<sub>2</sub> temperature program desorption (TPD) using a Quantachrome Autosorb 1-C and a Residue Gas Analyzer (RGA-200, Stanford Research Systems Inc., USA). A 100-1000 mg catalyst sample was loaded into a U-shaped quartz tube, which was then installed in a furnace. The catalyst was treated in-situ at 120 °C for 1 hour in helium and then was vacuumed (lower than 3000 micron) for 30 minutes. Next, the catalyst underwent NH<sub>3</sub> or CO<sub>2</sub> adsorption at 120 °C for 1 hour, and then physio-desorption at 120 °C by helium purging. Finally, the catalyst was heated up to 900 °C (at

a rate of 10 °C per minute) for chemi-desorption. The weak, medium, and strong active sites of the catalyst were assigned to the peak areas of the NH<sub>3</sub>-TPD curves lower than 350 °C, between 350 and 500 °C, and above 500 °C.

The amount and strength of the hydrogenating active sites on the catalysts, as well as the type and amount of coke on the spent catalysts, was determined by temperature program reduction (TPR) and TPO, using a Quantachrome Autosorb 1-C and an RGA-200. A 100-200 mg sample of catalyst was loaded in a U-shaped quartz tube and installed in a furnace. The catalyst was exposed to a flow of helium (50 ml/min), and heated to 120 °C at a rate of 10 °C/min, remaining at 120 °C for 1 hour. Any physisorbed water in the catalyst sample was removed. Subsequently, the catalyst was heated up to 900 °C at a rate of 10 °C/min and under a flowing gas mixture of 2 %vol hydrogen or oxygen (1 ml/min) in helium (49 ml/min).

The types and strengths of acids on the surfaces of catalysts were tested by Pyridine-FTIR. A catalyst sample of 2-15 mg was pressed to form wafers (1cm in diameter) and installed on the support located in a cell. The cell included two KBr windows through which IR could be transmitted. The IR cell was degassed at 450 °C by an N<sub>2</sub>/He flow for 1 hour. When the cell's temperature cooled down to 100/150 °C, the pressure of the system was evacuated to 100 micron by a high vacuum pump. Pyridine was then introduced for adsorption. The excess or physisorbed pyridine was purged by N<sub>2</sub>/He. Infrared spectra were recorded on a Nicolet FTIR-6700 at temperatures of 100/150, 250,

350, and 450°C. Data obtained from the spectrometer was analyzed by Omnic 8 software. The characteristic bands at 1450 cm<sup>-1</sup> and 1550 cm<sup>-1</sup> were respectively assigned to Lewis (L) and Bronsted (B) acid sites [101]. The ratio of L acids to B acids was calculated by the method used in the literature [102]. With this ratio, and the total acidity obtained from the NH<sub>3</sub>-TPD experiment, the densities of L and B acids were calculated.

Transmission Electron Microscopy (TEM, JEOL 2011 Scanning Transmission Electron Microscope, JEOL Ltd., Japan) was used to determine and compare the morphology of active metals on the sulfided catalysts. An Energy Dispersive X-Ray Analysis (EDX, Genesis 4000 spectrometer) was applied to estimate the elements and their approximate compositions on the catalyst. Image analysis software was used to measure the slab length and layer number of the CoMoS catalyst. The average slab length and layer number were calculated from 100+ slabs on different particles.

X-ray diffraction (XRD) was conducted in the range of 5-75 °, at 2θ with a step of 0.02 °, for 1.0 seconds on a Bruker D8 Advance spectrometer (Bruker Corporation, Germany); the operating conditions were 40 kV and 30 mA.

The thermal treatment of kaolin and metal oxide catalysts was analyzed by a TGA (TGA-Q500) connected to an RGA (RGA-200). A sample of 25 mg of natural kaolin was loaded into a platinum pan, which was then heated up to 1000 °C at a rate of 10 °C/min

under a flow of helium (rate: 50 ml/min) – the released gases were recorded by the RGA-200.

The compositions of active metal components in supported catalysts were determined by a JEOL JXA-733 Electron Microprobe Analyzer (EMPA, JEOL Ltd., Japan) and the compositions of active metal components in unsupported catalysts were determined by a TEM/EDX.

The total sulfur contents in supported sulfided catalysts were determined by an Antek Nitrogen/Sulfur Analyzer (NS-9000, ANTEK INSTRUMENTS, Inc., US) and the total sulfur contents in unsupported sulfided catalysts were determined by a CHN-932 elemental analyzer.

### **3.6 Calculations**

#### **3.6.1 DO (C-O or C-CO cracking)**

In WCO, the fatty acids are the acids that only have an even number of carbon atoms. C18 fatty acids are the primary fatty acids in WCO, with a concentration of more than 91 wt%. The degree of DO carried out by either C-O or C-CO cracking (HDO or HDC) are therefore determined by the ratio of C18 to C17 hydrocarbons that are generated in the final products (Equation 3-4):

$$C_{18} / C_{17} \text{ ratio} = \frac{\text{Mass of } C_{18} \text{ hydrocarbons}}{\text{Mass of } C_{17} \text{ hydrocarbons}} \quad \text{Equation 3-4}$$

### 3.6.2 Hydrogenation or dehydrogenation

Hydrogenation activity is reflected by alkane selectivity (Equation 3-5):

$$\text{Alkane selectivity} = \frac{\text{Mass of Alkanes}}{\text{Mass of (Alkanes + Alkenes)}} \quad \text{Equation 3-5}$$

### 3.6.3 Valuable products yields

$$Y_V = Y_{LO} * Y_O / 100 + Y_{HC(3+)} \quad \text{Equation 3-6}$$

where,

$Y_V$  is the yield of the valuable products;

$Y_{LO}$  is the yield of the <350 °C fraction, determined from simulated distillation results;

$Y_O$  is the yield of oil; and

$Y_{HC(3+)}$  is the yield of C3+ gas hydrocarbons, determined by GC-FID results.

### 3.6.4 Oxygen conversion

$$\text{ORR} = (M_{OF} - M_{OO}) / M_{OF} * 100\% \quad \text{Equation 3-7}$$

where,

ORR is the oxygen removal rate, in %;

$M_{OF}$  is the mass of oxygen in the feed, in grams; and

$M_{OO}$  is the mass of oxygen in the oil products, in grams.

### 3.6.5 Density of acids on catalyst surface

The density of acids is calculated by Equation 3-8:

$$\text{Density of acids} = \text{Acidity/Surface area}$$

Equation 3-8

### 3.6.6 Produced water in FCC process

The amount of produced water products is calculated from the difference between the oxygen content in the feed and the oxygen content in all non-water compounds in the products (Equation 3-9):

$$M_{H_2O} = M_{OD}/16 \cdot 18 = (M_{OF} - M_{OCO} - M_{OOLP})/16 \cdot 18$$

Equation 3-9

where,

$M_{H_2O}$  is the mass of produced water, in grams;

$M_{OD}$  is the mass of oxygen in the produced water calculated by difference, in grams;

$M_{OF}$  is the mass of oxygen in the feed, in grams;

$M_{OCO}$  is the mass of oxygen in the CO and CO<sub>2</sub>, in grams; and

$M_{OOLP}$  is the mass of oxygen in the OLP, in grams.

## 3.7 Experimental programs

### 3.7.1 Uniform design (UD) experimental method applied in Chapter 4

Compared to orthogonal design, the number of experiments that need to be conducted by the UD method is significantly less. The UD method has the following advantages [103, 104]: the experimental points are highly representative of the studied experimental domain; it is very robust for determining an unknown model, even among all experimental design methods; the number of levels that can be analyzed for each factor is larger than in other experimental methods. For these reasons, UD is an appropriate

method for identifying the factors of a chemical process that affect the reaction products, as well as the specific effects of these factors, using a minimal number of experiments. For the experiments conducted in this thesis, UD was particularly useful for identifying reaction routes that were unknown; it was also useful for investigating the triglyceride hydrotreating process, a method that involves many continuously changing parameters. In this research, UD was applied for the first time to study the triglyceride hydrotreating process and its reaction routes.

Pressure, LHSV, H/O, and temperature are regarded as the dominant parameters in the triglyceride hydrotreating process [51, 54, 57-59]. A higher pressure, higher H/O, and lower LHSV benefit hydrogenation and HDO reactions. However, higher pressures and H/O ratios lead to higher costs, and lower LHSVs lead to a reduction in products obtained.

According to the literature, pressure less than 1400 psi [51], LHSV in the range of 1-4 h<sup>-1</sup> [54], and H/O at 500 ml/ml [54] are conditions that can yield desirable results. A high temperature can also benefit the hydrogenation and oxygen removal rates, but can also lead to over-cracking and lower diesel fractions. Olefins cannot saturate at temperatures below 250 °C. During pre-trials, over-cracking occurred when the temperature was higher than 365 °C. The experiments in this chapter were therefore limited to temperatures in the range 275-365 °C. The experimental programs are listed in Table 4-1.

### **3.7.2 Experimental programs in Chapter 5**

The reaction performance evaluation of the supported CoMoS catalysts was conducted at temperatures of 250, 275, and 365 °C, at a pressure of 500 psi hydrogen, LHSV of 4 h<sup>-1</sup>, and an H/O ratio of 500 ml/ml.

The reaction performance evaluation of the unsupported, sulfided CoMo catalysts was conducted in a 1000 ml batch reactor (Parker Autoclave Engineers Inc.), under pressure of 9 MPa hydrogen (99.99 %), and at temperatures of 300, 340, and 375 °C. Hydrogen was supplemented into the system whenever the pressure dropped below 8.6 MPa. The mass ratio of catalyst to feed was 1:200; the reaction time was 8 hours.

### **3.7.3 Experimental programs applied in Chapter 6**

The reaction conditions for the supported, sulfided CoMo catalysts were: a temperature of 275 °C, a pressure of 1100 psi, an LHSV at 3 h<sup>-1</sup>, and an H/O ratio at 50 ml/ml. The reaction time was 220 hours. Samples were taken at the 77<sup>th</sup>, 107<sup>th</sup>, 138<sup>th</sup>, 177<sup>th</sup>, and 213<sup>th</sup> hours. The five samples were given the tags “R<sub>i</sub>”, where i denote the numbers 1 to 5 (respective to chronological order).

### **3.7.4 Experimental programs applied in Chapter 7**

For the performance evaluation of the catalytic cracking of metal oxides, a fixed-bed quartz reactor was used as the reaction system (under an atmospheric pressure of nitrogen and at temperature of 470 °C). The operational parameters of this performance evaluation are listed in Table 7-1.

### **3.7.5 Experimental programs employed in Chapter 8**

The performance evaluation of the novel catalysts was carried out under these conditions: a water inlet flow rate of 3 ml/min, a temperature of  $470 \pm 3$  °C, a mass ratio of catalyst to feed of  $3.3 \pm 0.3$ , and a weight hourly space velocity of  $10.5 \pm 1.2$  h<sup>-1</sup>.

### **3.7.6 Experimental programs in Chapter 9**

ATK was evaluated in the FCC reactor at 470 °C and under atmospheric pressure, and steam was used as the carrier gas. After undergoing catalytic cracking with ATK, the product was hydrotreated in a batch reactor (at 275-325 °C and 250-500 psi). This integrated process was named ATK-HDO. The products from ATK-HDO were compared with those obtained from: catalytic cracking with alumina followed by hydrotreating (Alumina-HDO, at 325 °C and 500 psi), catalytic cracking with CC followed by hydrotreating (CC-HDO, at 325 °C and 500 psi), and using hydrotreating only (at 325 °C and 500/1000 psi).

## **Chapter 4 Hydrotreating of triglycerides over a CoMoS supported catalyst: effects of operational parameters**

### **4.1 Introduction**

The previous studies focused individually on single factors, and the researchers reported the reactions that occurred during hydrotreating, including the saturation of carbon double bonds, the oxygen removal, the hydrocracking of fatty acid chains of triglyceride, the cyclization, the aromatization, and the isomerization [57, 58, 60, 105]. In this present study, a mix of WCO (10 wt%) and dodecane was hydrotreated over a supported CoMoS catalyst in a fixed-bed reactor. The operational window was investigated by using the uniform design method. The desired products of the triglyceride hydrotreating process are chain hydrocarbons without oxygenates – cyclization and aromatization should therefore be minimized whereas DO should be maximized. The product hydrocarbons should also fall in the diesel range, so cracking reactions must be carefully controlled. The operational window should therefore be optimized to limit the composition of products. In order to do this, parameters affecting the triglyceride hydrotreating process were investigated using the results from uniform design. The main objectives of the study performed in this chapter were listed as follows:

1. to determine the reaction routes,
2. to identify the product distributions and compositions,

3. and to provide a basis for industrial production for the triglyceride hydrotreating process.

## 4.2 Experimental

The experimental programs are listed in Table 4-1.

Table 4-1 Experimental programs by uniform design method

Run No.	Temperature ( °C)	Pressure (psi)	LHSV (h <sup>-1</sup> )	H/O (ml/ml)
R1*	275	1100	3	50
R2	300	800	1	300
R3	325	1400	2	100
R4	365	500	4	500

\*R stands for run, for example, R1 means run 1.

Four trials were conducted, and the previously mentioned parameters were separated into four factors each having four levels. The optimal outcome was to obtain products in the diesel fraction with low oxygen contents.

## 4.3 Results and discussion

### 4.3.1 Operational window of the process

Group compositions of the samples R1 to R4 are summarized in Table 4-2, according to GC/MS results.

Table 4-2 Group compositions of UD results

Composition (wt%)	Alkane	Oxygenate	Others*
WCO	0.0	100.0	0.0
R1	100.0	0.0	0.0
R2	100.0	0.0	0.0
R3	99.7	0.0	0.3
R4	7.8	17.5	74.7

\* Others includes olefins, cycloalkanes, cycloolefins, and aromatics

As shown in Table 4-2, the compositions of R1, R2, and R3 were simple and favorable – the alkane contents were as high as 100.0 %, 100.0 %, and 99.7 %. Specifically, oxygen in WCO was completely removed and unsaturated hydrocarbons were completely saturated, when the conditions fell into the following ranges: a temperature of 275 °C to 325 °C, a pressure of 800 psi to 1400 psi, an LHSV of 1 h<sup>-1</sup> to 3 h<sup>-1</sup>, and an H/O of 50 to 300 ml/ml. These results reveal that the supported CoMoS catalyst is insensitive to changes in parameters that fall in the above operational windows (for DO). The group composition of R4 consisted of many aromatics, oxygenates, olefins, cycloalkanes, but only contained 7.8% alkanes: it differed significantly from the three other samples. This result suggests that, at a temperature of 365 °C, pressure of 500 psi, LHSV of 4 h<sup>-1</sup>, and H/O of 500 ml/ml (the conditions of R4), deoxygenation is not the main reaction while cracking, cyclization, and aromatization reactions are dominant in this process.

Water is a by-product of the triglyceride hydrotreating process. However, in the hydrotreated liquid samples R1, R2, and R3, water was not detected. The water content of the R4 sample was 3.1 %. This difference can be explained by the compositions of the samples: oxygenates are hydrophilic whereas hydrocarbons are hydrophobic, and therefore water was more likely to remain in the oxygenate-heavy R4 sample.

The boiling point distribution of the samples is given in Table 4-3. The boiling point range of hydrocarbons in the diesel fraction is 200 to 350°C [106]. More than 97.4 %, 88.7 % and 74.4 % of R1, R2, and R3 (respectively) had boiling points that fell into this diesel fraction range. The operational parameters that are favorable for producing products in the diesel fraction are therefore: a temperature of 275 °C, a pressure of 1100 psi, an LHSV of 1 h<sup>-1</sup>, and an H/O of 50 ml/ml (parameters of the UD experimental domain).

Table 4-3 The boiling point distribution of the products

Boiling point distribution (wt %)	R1	R2	R3
Gasoline fraction (B.P.<200°C)	2.2	11.0	25.4
Diesel fraction (200-350°C)	97.4	88.7	74.4

As indicated, the primary reaction route changed between R1, R2, R3, and R4, when tested in the UD experimental domain. Lower pressures favored diesel production, whereas higher pressures promoted cracking reactions; increases in the H<sub>2</sub>/oil ratio led to

an increase in diesel production; higher LHSVs also promoted diesel production [51]. R4 was reacted as a higher temperature, lower pressure, higher LHSV, and higher H/O ratio compared to R1, R2, and R3. Therefore, the temperature or H/O ratio should have been responsible for the R4's undesirable composition. After the first four runs, another three experiments (listed in Table 4-4) were carried out to find out which parameter (temperature or H/O ratio) was mainly responsible for the cracking, cyclization, and aromatization reactions that occurred in R4. Table 4-4 shows that R4 and R5 only differed in reaction temperature whereas R6 and R7 had the same reaction temperature as R4.

Table 4-4 Further experimental programs

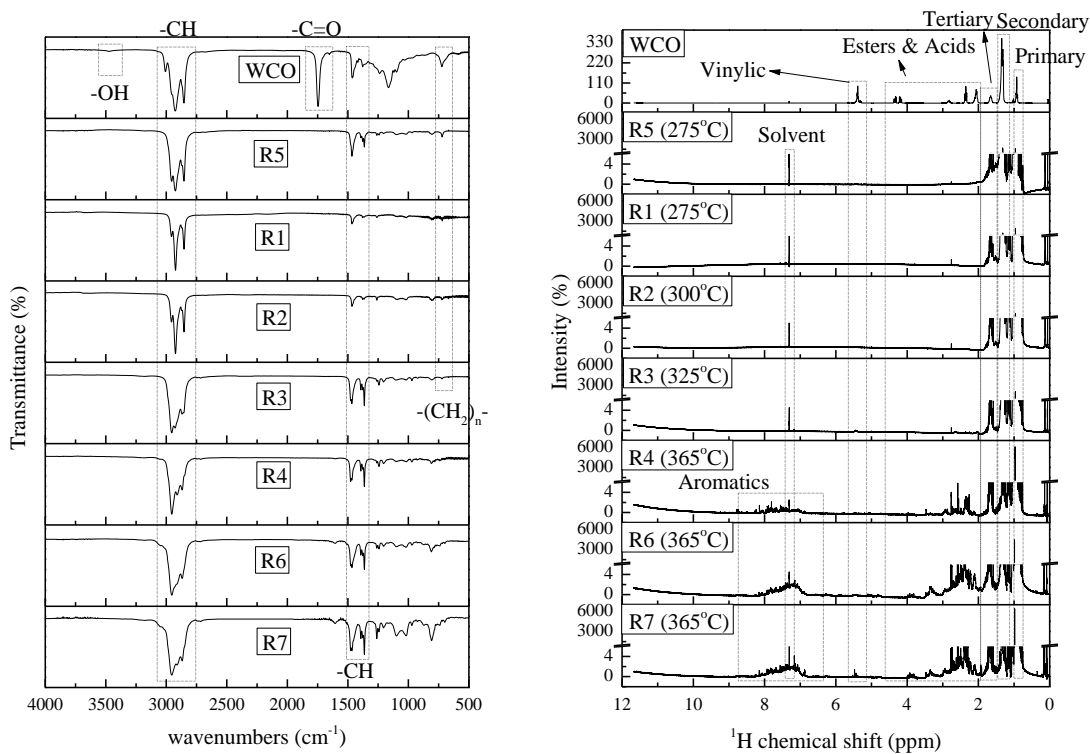
Run No.	Temperature (°C)	Pressure (psi)	LHSV (h <sup>-1</sup> )	H/O (ml/ml)
R5	275	500	4	500
R6	365	500	2	100
R7	365	1100	4	100

### 4.3.2 Verification of the effects of temperature

#### 4.3.2.1 Structures and compositions of liquid products

FTIR analysis was used to detect the presence of significant functional groups in the oil products – these included oxygenated groups, olefin groups, and paraffin groups. H-NMR analysis was used to determine the presence and relative intensity of hydrogen containing functional groups in the oil products. Figure 4-1 (a) and 4-1 (b) portray the FTIR spectra and the H-NMR results for the WCO and hydrotreated products. As expected, FTIR

analysis of the WCO showed a strong presence of esters, free fatty acids, and alkane and alkene groups typical in triglycerides. After hydrotreating, the carboxylic acid and ester functional groups ( $1680\text{-}1770\text{ cm}^{-1}$ ) disappeared. Throughout the FTIR analysis, spectra showed a strong presence of alkane groups in the wavenumber ranges of  $3000\text{-}2850\text{ cm}^{-1}$ ,  $1500\text{-}1400\text{ cm}^{-1}$ , and  $1370\text{-}1350\text{ cm}^{-1}$ . There was also present the specific peak of C-H rock in long chain alkanes (near  $720\text{ cm}^{-1}$ ) [107] in WCO and the samples R1 to R3 and R5, but this peak was absent in all high temperature liquid products.



(a) FTIR spectra

(b)  $^1\text{H-NMR}$  spectra

Figure 4-1 Structures of liquid products under different operational parameters

The H-NMR results mainly confirmed the FTIR results. In the WCO H-NMR spectrum, the relatively small peaks in the ranges of 2.0-4.4 ppm and 5.2-6.0 ppm were attributed to oxygen containing functional groups and carbon double bonds, respectively. In all samples, the H-NMR results consistently showed evidence of a high concentration of primary and secondary hydrogen; this corresponded to the peaks in the range 0.7-1.8 ppm. As seen in Figure 4-1 (b), most of the differences between the samples were in the distribution of peak heights – these differences were especially true between low temperature liquid products (R1 to R3 and R5) and high temperature products (R4, R6, and R7). The amount of primary hydrogen increased, whereas the amount of secondary hydrogen decreased. Another obvious difference was that there were aromatic and oxygenate specific peaks in the high temperature products (distributed in the ranges of 6.5-8.5 ppm and 2.0-4.0 ppm, respectively) that were absent in the low temperature products.

Also from H-NMR analysis, the degree of isomerization that occurred was determined from the differences in primary, secondary, and tertiary hydrogen concentration. Oil with a high degree of isomerization contained more primary and tertiary hydrogen, and contained less secondary hydrogen. A high ratio of primary hydrogen to secondary hydrogen, or tertiary hydrogen to secondary hydrogen, indicated that an oil sample had a high degree of isomerization. The hydrogen peak areas of WCO and the liquid products were compared (Figure 4-1 (b)). All treated products had a higher primary to secondary

hydrogen ratio compared to WCO. This indicates that cracking and isomerization took place, and that considerable amounts of primary and tertiary hydrogen were produced from secondary hydrogen during hydrotreating. Furthermore, the degree of isomerization increased as the temperature was increased.

The group compositions of all samples are summarized in Table 4-5. The compositions of the samples R1 to R3, and R5 were primarily the same (more than 99 % paraffin); the diesel fraction contained in R5 was 96.5 %. The samples R4, R6, and R7 were also very similar to each other. They all included considerable amount of aromatics, olefins, cycloalkanes, cyclo-olefins, and oxygenates, and all contained paraffin contents of less than 10%. The only difference in operational parameters between R4 and R5 was the temperature, and all the high temperatures samples (R4, R6, and R7) gave undesirable results. Therefore, temperature was the main factor affecting the production of undesired products (olefins, cyclo-olefins, aromatics, and oxygenates). This conclusion is supported by Bezergianni et al. [51, 57-59], who obtained the same results.

Table 4-5 Group compositions

Group composition (wt%)		Alkane	Oxygenate	Others*
Low temperature 275-325 (°C)	275(°C, R5)	99.4	0.0	0.7
	275(°C, R1)	100.0	0.0	0.0
	300(°C, R2)	100.0	0.0	0.0
	325(°C, R3)	99.7	0.0	0.3
High temperature 365 (°C)	R4	7.8	17.5	74.7
	R6	5.4	24.7	69.9
	R7	1.5	3.4	95.1

\* Others includes olefins, cycloalkanes, cyclo-olefins, and aromatics

After dodecane was removed via vacuum distillation, all the samples became wax-like and solid. This indicates that the addition of dodecane as a solvent was necessary; otherwise these solids would have caused blockage in the reaction system. And through performing subsequent isomerization or hydrocracking is a method to transfer the wax-like long chain normal paraffin into iso-paraffin or short chain paraffin. An interesting phenomenon occurred wherein the samples R1, R2, R3 and R5 took on a white color, whereas R4, R6, and R7 took on green, clear red, and brown colors. These strong differences can be explained by the coloration caused by the presence of aromatics and oxygenated compounds in the lesser-refined products. For samples reacted under the operational temperature 275-325 °C, only R3 contained cyclo-olefins (0.3 %); all of the low temperature products consisted almost entirely of C18 alkane. Therefore,

hydrogenation and HDO (on CoMo sites) were the main reactions that occurred when WCO was hydrotreated at low temperatures (275-325 °C).

Based on the analysis above, temperature is the dominant factor affecting the composition of products during WCO hydrotreating (at least among the parameters inspected). Alkanes (with no oxygenates) are the favored products. Oxygen can be efficiently removed by hydrotreating at temperatures of 275 to 325 °C, as shown in Table 4-5.

The general aim of WCO hydrotreating is to produce oxygen-free, diesel-fraction oil. High temperatures (365 °C), however, caused the products to have considerable amounts of oxygenated compounds. This was contrary to our expectations. Most of these oxygenated compounds (detected by GC/MS) were alcohols, aldehydes, and epoxies. The high oxygen contents were due to the fact that, at high temperatures, cracking reactions of oxygenated carbon chains occurred faster than HDO and HDC reactions. Therefore, at high temperatures, C-C bond and C-H bond cracking (due to acid catalytic sites) were advantageous during WCO hydrotreating. Despite the high amounts of short chained and highly constituted oxygenates in the products, DO still happened at high temperatures. This was known because alcohols, ketones, and epoxies were found in the high-temperature products. Cracking, cyclization, dehydrogenation (including aromatization and condensation), and DO were all observed in the high temperature reactions (samples

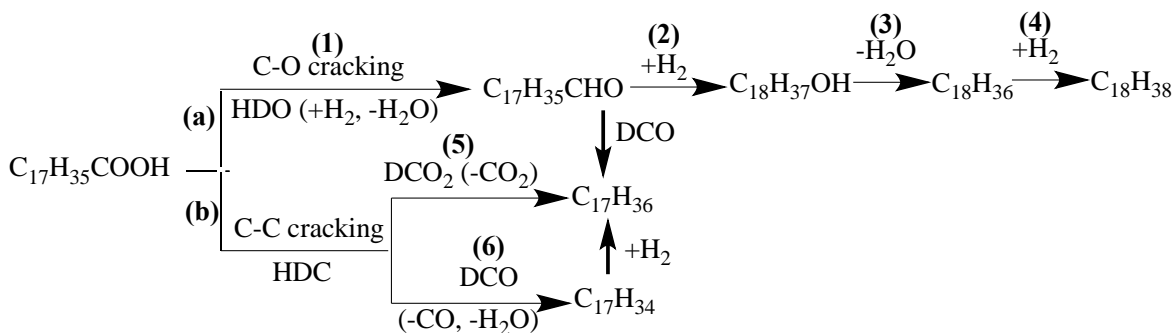
R4, R6, and R7) – there were a minor amounts of paraffin and cycloalkanes, a significant amount of olefins and cyclo-olefins, and a great amount of oxygenates and aromatics in the final products. The lack of paraffinic compounds was primarily attributed to dehydrogenation, cyclization, aromatization, and condensation.

The outcomes well indicate that the saturation ability of WCO hydrotreating weakened at excessively high temperatures. This can be explained by the fact that the hydrogenation of carbon-double bonds was exothermic, and therefore olefins were produced via dehydrogenation at 365 °C [108]. The formation of aromatic compounds occurred due to sequential dehydrogenation reactions. From these results, it can be concluded that dehydrogenation was supported by excessively high temperatures. Experiment R7 had higher aromatic content than R4 – this was because R4 experienced less dehydrogenation due to having a higher supply of hydrogen.

#### **4.3.3 Further investigation of operational parameters**

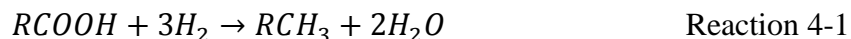
As shown in Table 3-1, over 93 % of the fatty acids in WCO were unsaturated acids. At low temperature hydrotreating, the unsaturated triglycerides underwent hydrogenation making unsaturated carbon-carbon double bonds saturate into carbon-carbon single bonds. Then, carboxylic acids were produced through the breaking down of newly saturated triglycerides into various intermediates – these included carboxylic acids, diglycerides, monoglycerides, and gas hydrocarbon products [52-55, 60, 109]. Finally, paraffin was formed through DO (HDO and HDC: decarbonylation DCO and decarboxylation DCO<sub>2</sub>).

Whether HDO or HDC/cracking reactions dominated the final reaction steps was decided by the parameters of the reaction. Models of the two different routes are described in Scheme 4-1.

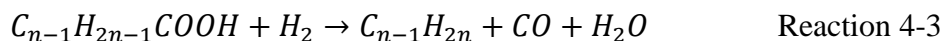
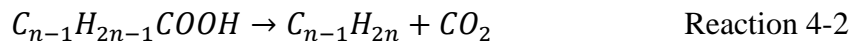


Scheme 4-1 Triglyceride reaction pathways model

In the HDO reaction route, a fatty acid intermediate reacts with hydrogen, forming an aldehyde and water (Scheme 4-1-(a)-1). The aldehyde can then undergo acid catalyzed tautomerism, forming an enol that will readily react with hydrogen to produce an alcohol (Scheme 4-1-(a)-2) [109]. The alcohol can then undergo dehydration (reacts with hydrogen via an acidic site) producing a hydrocarbon and water (Scheme 4-1-(a)-3, Scheme 4-1-(a)-4). Since no carbons from the fatty acids are lost during the HDO process, the resulting hydrocarbons are equivalent in length to the fatty acids present in the original triglycerides. The chemical equation for the HDO reaction is given in Reaction 4-1.



In the HDC/cracking reaction outlined in Scheme 4-1-(b), a hydrocarbon with an n-1 carbon number is produced (where n is the carbon number of the original fatty acid) [54, 56, 109]. Decarboxylation can occur via a hydrogenolysis reaction (Scheme 4-1-(b)-5) – the results are an n-1 hydrocarbon chain and carbon dioxide. Decarbonylation can also occur together with a hydrogenation reaction (Scheme 4-1-(b)-6) followed by a cracking reaction [108] – the results are an n-1 hydrocarbon chain, water, and carbon monoxide. The equations for the decarboxylation and decarbonylation reactions are given by Reactions 4-2 and 4-3.



The selectivity between DCO<sub>2</sub> and DCO is calculated from the ratio of produced CO<sub>2</sub> to CO; methanation (CO or CO<sub>2</sub> reacting with H<sub>2</sub> to form water and methane) and water-gas-shift (CO reacting with water to form H<sub>2</sub> and CO<sub>2</sub>) [109] reactions are neglected. The occurrence ratio of HDO to HDC reactions is obtained by comparing the concentration of even number hydrocarbons to the concentration odd number hydrocarbons [110] in the

final products. WCO and CLO consist of mainly C18 fatty acids (91.0 % and 68.6 %, respectively), so studying the content of C18 and C17 for these oils is sufficient to compare the HDO and HDC reaction pathways. C17 is produced by both HDC pathways, but hydrogen is needed by the DCO pathway whereas no hydrogen is needed by the DCO<sub>2</sub> pathway. The HDO pathway involves converting an oxygenate and hydrogen into an alkane and water. Bi-functional catalysis, including hydrogenation reactions (on CoMo sites) and dehydration reactions (on acid catalytic sites), are therefore involved in the HDO pathway.

The chemical compositions of the low-temperature products consisted predominantly of C17 and C18 paraffins, but also contained some C15, C16, and C15<sup>+</sup> paraffins. The C18 content in WCO was higher than 91.0% and the WCO also did not contain any hydrocarbon that had a carbon number of less than 16 (Table 3-1). The C15<sup>+</sup> detected in the products was therefore attributed to cracking reactions.

More experiments (under optimal UD operational windows) were conducted to further explore the effects of operational parameters on reaction pathways. Glycerol conversion (CG), DO capability (CD), hydrogenation capability (CH), cracking capability (CC), selectivity of HDO to HDC (SHDO/HDC), and selectivity of DCO to DCO<sub>2</sub> (SDCO/DCO<sub>2</sub>) were all studied extensively. These values were calculated according to the Equations 4-1 to 4-6.

CG = 100% - glycerol content in the liquid product      Equation 4-1

CD = hydrocarbon content in the liquid product      Equation 4-2

CH = content of alkane/content of hydrocarbon\* 100%      Equation 4-3

CC = C<sub>15</sub><sup>-</sup> content in liquid product (CC1) or gas hydrocarbon yield (CC2) Equation 4-4

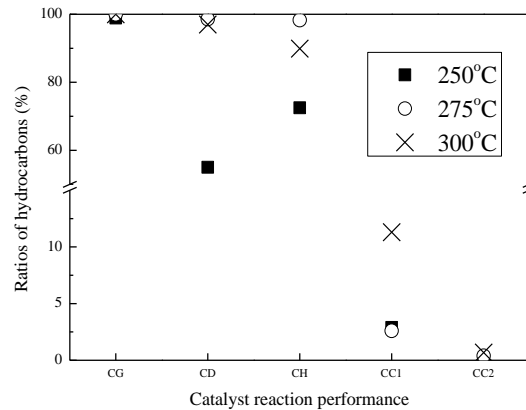
SHDO/HDC = Ratio of paraffin and olefins C18 to C17 in OLPs      Equation 4-5

SDCO/DCO<sub>2</sub> = Ratio of CO to CO<sub>2</sub> in the gas product      Equation 4-6

These values were derived from GC/MS results. In the additional experiments, glyceride conversion could have reached 100 % and no polymerization was observed for almost all reaction conditions (shown in Figure 4-2 to Figure 4-7). The only exception occurred using the following conditions: a temperature of 250 °C, a pressure of 1100 psi, an LHSV of 2 h<sup>-1</sup>, an H/O of 100 ml/ml, and a blend ratio of 10 % WCO to dodecane. In the liquid product that resulted from this trial, 1.1 % of octadecanoic acid, propyl ester was detected. This product can further confirm the first proposed reaction pathway – the hydrogenolysis reaction that is required to break triglycerides down into propane and fatty acids (other intermediates such as monoglycerides).

### 4.2.3.1 Reaction temperature effects

Figure 4-2 describes the effects that temperature had on the reactions that used the following conditions: a pressure of 1100 psi, an LHSV of  $2 \text{ h}^{-1}$ , an H/O of 100 ml/ml, and a blend ratio of 10 % WCO to dodecane. The temperature ranged from 250 to 300 °C. As the temperature increased, the DO capability also increased. The oxygen removal rate reached 100 % when the reaction temperature was higher than 275 °C. Research shows that increases in temperature can make catalysts more reactive [54, 57, 60, 111, 112].



Catalyst reaction capabilities

Figure 4-2 The effect of temperature on selectivity

Increases in temperature can also increase cracking reactions, which produce alkenes. In the experiments, cracking capability remained the same when the temperature was in the range 250 to 275 °C, but increased when the temperature rose from 275 to 300 °C. This reveals that the cracking capability can suddenly be enhanced at temperature 300 °C or higher for the examined catalyst.

The selection that occurred between the HDO and HDC reaction pathways during triglyceride hydrotreating was of great interest. HDO consumes more hydrogen, but HDC requires more thermal energy and results in a loss of carbon. Comparing the amounts of even and odd carbon-numbered paraffins (and olefins) in the products provides an understanding as to which conditions favor HDO over HDC (or vice versa). As discussed in 4.2.3, this comparison can easily be determined by comparing the C18 and C17 paraffin (and olefin) contents in the products, because WCO contains very high concentrations of C18 fatty acids.

#### **4.3.3.2 Hydrogen amount effects**

Figure 4-3 and Figure 4-4 show the effects of changes in the volume ratio of hydrogen to oil (H/O) (50, 100, 300, and 500 ml/ml) on the triglyceride hydrotreating process, for reactions conducted using the following conditions: a temperature of 275 °C, a hydrogen pressure of 1100 psi, an LHSV of 2 h<sup>-1</sup>, and a blend ratio of 10 % WCO and dodecane.

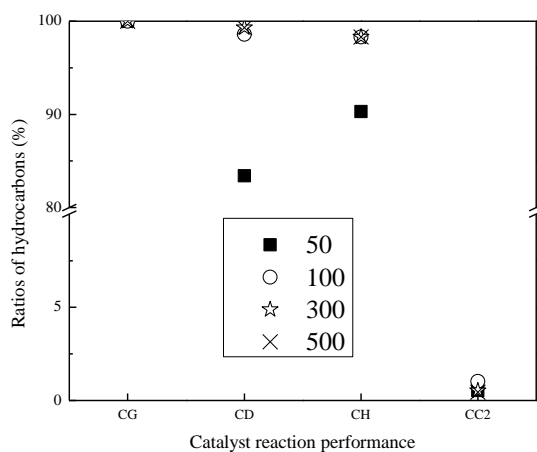


Figure 4-3 Catalyst reaction capabilities

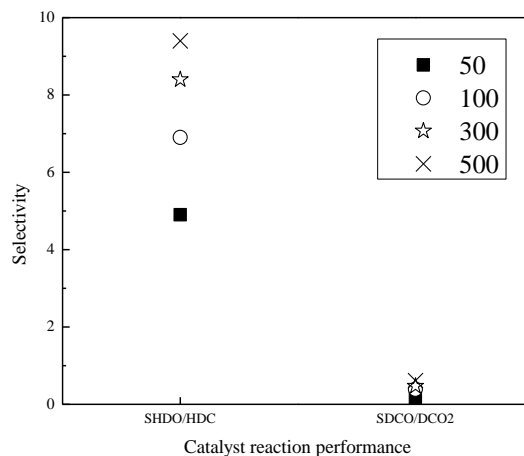


Figure 4-4 The effect of H/O on selectivity

Increases in H/O showed no significant effects on cracking capabilities or selectivity between DCO and DCO<sub>2</sub>. The DO and hydrogenation capabilities increased with the H/O increasing from 50 to 100 ml/ml; however, these capabilities were almost the same for all

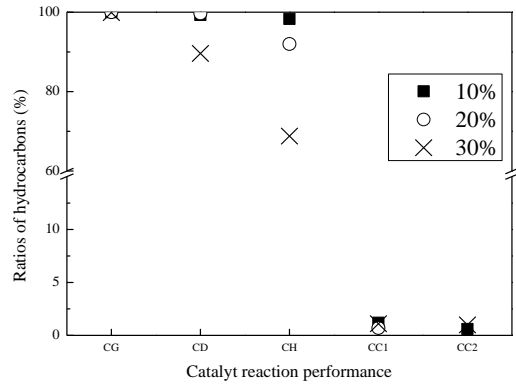
H/Os higher than 100 ml/ml. This indicates that the hydrogen supplying limits DO and hydrogenation reactions at a lower hydrogen concentration (lower than 100 ml/ml), while it is not a key factor for DO and hydrogenation at a higher hydrogen concentration (higher than 100 ml/ml). Therefore, for obtaining a high DO and hydrogenation capabilities, 100 ml/ml is the suitable H/O. As predicted by Le Chatelier's principle, the selectivity of HDO over HDC increased as the H/O increased. For higher H/Os, a higher concentration of reactant (hydrogen) also forced the reaction towards the side of the products, improving the consumption of the limiting reagent (the triglycerides in WCO).

#### **4.3.3.3 Blend ratio effects**

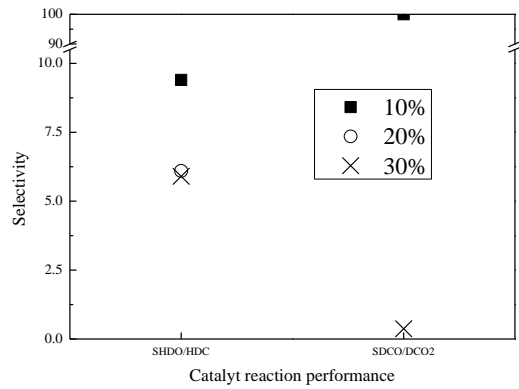
In this study, an introductory investigation was conducted on the hydrotreating of CLO. The results from CLO hydrotreating were compared to the results from WCO hydrotreating (at the same conditions). This comparison was used to determine CLO's viability as a future feedstock. Figure 4-5 and Figure 4-6 demonstrate the effects of WCO (10 %, 20 %, and 30 % concentrations, with the rest being dodecane) and CLO concentrations (10 %, 20 %, and 30 % concentrations, with the rest being dodecane) on the triglyceride hydrotreating process. Reaction conditions included a temperature of 275 °C, a hydrogen pressure of 1100 psi, an LHSV of 2 h<sup>-1</sup>, and an H/O of 500 ml/ml.

As shown in Figure 4-5 and Figure 4-6, the catalyst cracking capabilities did not change when the blend ratios of WCO and CLO increased. The DO and hydrogenation capabilities decreased when the blend ratios of WCO and CLO increased. For WCO, the selectivity of HDO to HDC and DCO to DCO<sub>2</sub> decreased when the concentration was

increased. For CLO, there were no significant changes in selectivity for the different blend ratios.

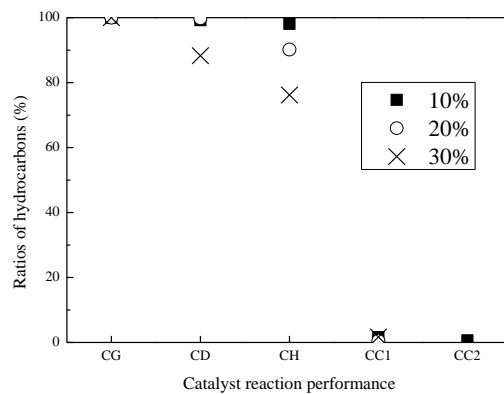


(a) Catalyst reaction capabilities

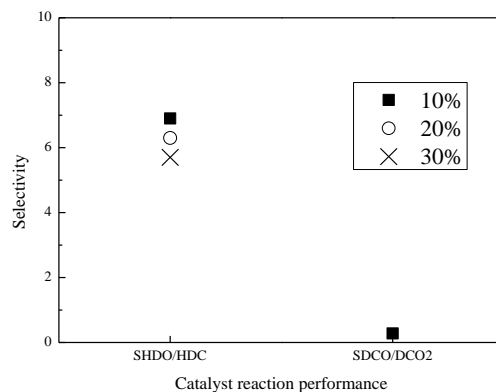


(b) Selectivity

Figure 4-5 The effect of the blend ratio of WCO on selectivity



(a) Catalyst reaction capabilities



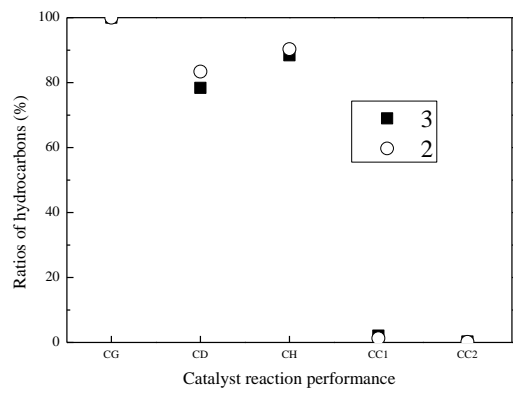
(b) Selectivity

Figure 4-6 The effect of the blend ratio of CLO on selectivity

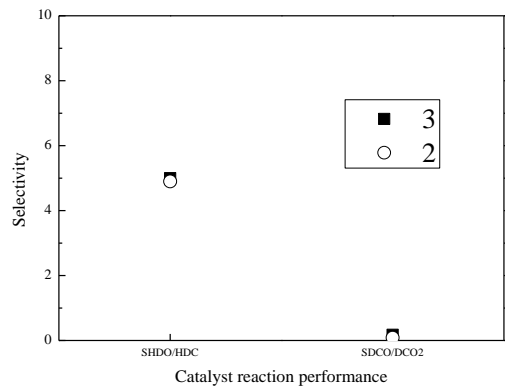
The two experiments that were performed with 30 wt% WCO and 30 wt% CLO resulted in products with similar concentrations of 1-eicosanol. However, the CLO product contained greater concentrations of hexadecanal and 1-dococanol than the WCO product (which contained no 1-dococanol). The reason for this is that CLO generally contains more long-chain fatty acids than WCO (see Table 3-1).

#### 4.3.3.4 Other parameter effects

Figure 4-7 shows the effect of a change in LHSV (2 and 3 h<sup>-1</sup>) on the triglyceride hydrotreating process, for two reactions conducted under the following conditions: a temperature of 275 °C, a hydrogen pressure of 1100 psi, an H/O of 50 ml/ml, and a blend ratio of 10 % WCO to dodecane. There were no significant changes in catalyst cracking capability, HDO/HDC selectivity, or DCO/DCO<sub>2</sub> selectivity when the LHSV was increased from 2 to 3 h<sup>-1</sup>. DO capability decreased by 5.0 % and hydrogenation capability decreased by 1.9 % when the LHSV was increased from 2 to 3 h<sup>-1</sup>. The reason for these changes is that a higher LHSV gives the molecules less time to fully react, resulting in products with higher oxygen contents [60].



(a) Catalyst reaction capabilities



(b) Selectivity

Figure 4-7 The effect of LHSV on selectivity

Other researchers have concluded that HDC is favored over HDO at higher temperatures (significant differences were found above 340 °C), and at lower supplies of hydrogen (lower H<sub>2</sub>/oil ratios and lower hydrogen pressures) [54-56, 105, 112].

Sankaranarayanan, et al. studied the effects of LHSV on the selectivity of HDC over HDO, at conditions of 320 °C, 60 bar (~870 psi), and 500 ml/ml H<sub>2</sub>/oil. They found that the selectivity of DCO<sub>2</sub>/DCO increased by increasing the LHSV and proposed that this increased selectivity occurred because the hydrogenolysis of the C-O bond (Scheme 4-1 (a)-cleavage 1) happened slower than the cracking of the -C(=O)-R bond (Scheme 4-1 (b)-cleavage 1) [54]. The same results were not observed in the experiments presented in this study. It can be deduced that changes in the two reaction rates (for C-O bond hydrogenolysis and -C(=O)-R bond cracking) are dependent on temperature, pressure, and H<sub>2</sub>/oil volume ratio. Therefore, the effects of LHSV on HDO/HDC selectivity is dependent on other reaction conditions.

GC-MS results showed that the most common aldehyde found in the products was octadecanal. Samples upgraded at low temperatures of 250 °C, low H/Os of 50 ml/ml, or high blend ratios of 30 % had octadecanal concentrations in the range of 0.6-1.4 wt%. The most prevalent alcohol in the products was octadecanol, which appeared in samples alongside octadecanal in various concentrations as high as 41.4 wt%. The presence of even-carbon-numbered aldehydes and alcohols confirmed the aldehyde-enol tautomerism step in HDO. Since carboxylic acids and aldehydes were barely found in all products, the rate-determining step for the complete HDO of triglycerides was the removal of the hydroxyl group via dehydration [54, 109]. Significant appearances of octadecanol and octadecanal also help to explain acidity; all samples upgraded at low temperatures of 250 °C, low volumetric ratios of H<sub>2</sub> to feed at 50 ml/ml, or high blend ratios at 30 %, had

TAN values greater than 5 mg KOH/g oil, octadecanol concentrations of 8.4 wt% to 41.4 wt%, and octadecanal concentrations greater than 0.6 wt%. All of the samples that had octadecanol concentrations greater than 8.4 wt% were solid at STP, which is explainable by octadecanol's high melting point of 59 °C. The presence of octadecanol was not the only factor contributing to the formation of wax-like solids, however – the presence of non-isomerized, long-chain hydrocarbons also played an important role. Although it has been proven difficult, in order to produce an acceptable fuel it is vital to remove long-chain alcohols like octadecanol from the products, as they contribute to acidity and the formation of solids.

#### **4.4 Conclusions**

In this section, an extensive study of the hydrotreating of triglycerides (WCO and CLO) was provided. The main topics addressed the determination of the effect of operational windows on establishment of the factors affecting glyceride conversion, DO and hydrogenation capabilities, and the selectivity of HDO to HDC and DCO to DCO<sub>2</sub> under optimal conditions.

The uniform design method was an effective method for determining suitable operational windows and for exploring the reaction routes that occur when WCO is hydrotreated over supported CoMoS catalysts. It was necessary to blend WCO with a solvent for the experiments conducted, because the oil has poor flow ability at room temperature; this solvent helped to disperse the oil and to prevent blockage in the reaction pipeline. Suitable operational windows for producing good quality diesel using hydrotreating with

a supported CoMoS catalyst are as follows: a reaction temperature around 275 °C, an LHSV under 1-4 h<sup>-1</sup>, an H/O range 50-300 ml/ml, and a blend ratio of 10 % WCO to dodecane. Undesired compounds were produced as the temperature became too high; cyclization took place as the temperature rose to 325 °C and aromatization took place as the temperature rose to 365 °C. Hydrogenation and DO were the dominant reactions at temperatures of 275-325 °C, whereas dehydrogenation reactions were the dominant reactions at a temperature of 365 °C.

All the investigated parameters had effects on the DO and hydrogenation capabilities of the catalysts. The DO capability increased when the reaction temperature increased from 250 to 275 °C, and stayed at 100 % when the temperature was higher than 275 °C. Hydrogenation capability increased when the reaction temperature rose from 250 to 275 °C, but decreased when the reaction temperature rose from 275 °C to 300 °C. An increase in H/O also caused increases in the DO and hydrogenation capabilities, but this was true only up to an H/O of 100 ml/ml. When the concentrations of WCO and CLO in the feed increased, the DO and hydrogenation capabilities decreased; the same was true for the LHSV. In all experiments, the only change that significantly increased the cracking capability was an increase in temperature over the range 275 to 300 °C. Higher reaction temperatures and higher concentrations of WCO in the feed favored the occurrence of DCO<sub>2</sub> over DCO. Although hydrotreated CLO contained less olefin than hydrotreated WCO, it also had a higher chance of containing long-chain alcohols.

Among all sets of reaction conditions studied, HDO was overall the most dominant reaction pathway in removing oxygen from WCO and CLO. The selectivity of DCO<sub>2</sub> and DCO can be increased over HDO without significantly decreasing total oxygen removal, however, by decreasing the hydrogen supply (H/O: 50 ml/ml) or by increasing the WCO concentration in the feed.

When hydrotreating triglycerides, the removal of long-chain alcohols is vital. This is because the DO of long-chain alcohols is the rate-determining step for HDO, and long-chain alcohols also contribute significantly to acidity and the formation of solids in the products. To prevent the formation of solids and to improve the desired hydrocarbon fraction in the fuel (determined by boiling point distribution), it is advisable to decrease the concentration of n-paraffins – this can be done with screening catalysts, which perform isomerization or subsequent hydrocracking.

## **Chapter 5 Hydrotreating of triglycerides over CoMoS catalysts: Roles of catalyst support and reaction temperature**

### **5.1 Introduction**

In addition to catalyst type, operational parameters are another important factor affecting the triglyceride hydrotreating process. Reaction temperature is one of the most significant factors – it significantly affects product composition [57, 58, 60, 105]. Comparing the effects of unsupported catalysts to the effects of supported catalysts may make it easier to comprehend how support plays a role on DO. This present work investigated the impact of support by comparing the DO performances of unsupported and supported CoMoS at different reaction temperatures. The main objectives were to explore the reaction routes, to identify the effects of support/temperature on product distributions and compositions, and to provide a basis for industrial production using the triglyceride hydrotreating process.

### **5.2 Experimental**

The reaction performance evaluation of the supported CoMoS catalysts was conducted at temperatures of 250, 275, and 365 °C, at a pressure of 500 psi hydrogen, LHSV of 4 h<sup>-1</sup>, and an H/O ratio of 500 ml/ml. The reaction performance evaluation of the unsupported, sulfided CoMo catalysts was conducted under pressure of 9 MPa hydrogen (99.99 %) and temperatures of 300, 340, and 375 °C. Hydrogen was supplemented into the system whenever the pressure dropped below 8.6 MPa. The mass ratio of catalyst to feed was 1:200; the reaction time was 8 hours.

## **5.3 Results and discussion**

### **5.3.1 Activity studies**

#### **5.3.1.1 Compositions of feed and liquid products**

The WCO feed was primarily composed of triglycerides, which were converted into the corresponding fatty acid methyl esters (determined by GC/MS) [97]. C16 saturated fatty acids (palmitic acid) and C18 unsaturated acids (71.3 wt% oleic acid and 17.2 wt% linoleic acid) were the primary fatty acids in WCO, accounting for 7.5 and 88.5 wt%, respectively. Figure 5-1 shows the product fractions of chemical compounds in the hydrotreated liquid products.

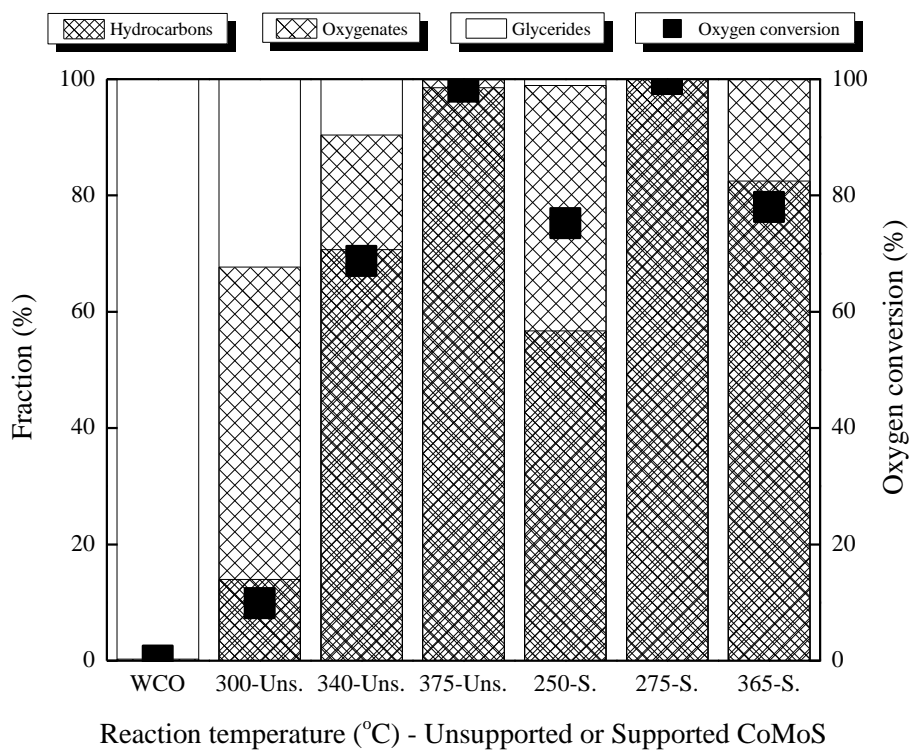
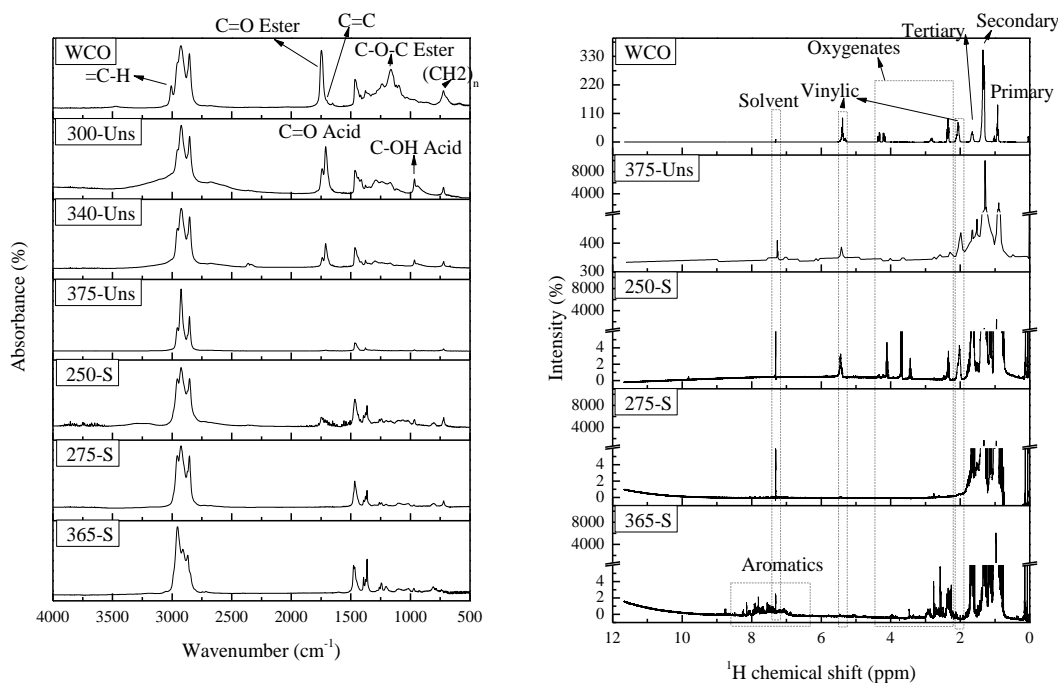


Figure 5-1 Product fraction distributions of supported and unsupported catalysts

For the unsupported catalyst, the hydrocarbon fractions increased when the temperature rose from 300 to 375 °C. For the supported catalyst, the hydrocarbon fractions first increased then subsequently decreased when the temperature rose from 250 to 365 °C. The hydrocarbon fraction was close to 100 % when the temperatures were at 375 °C for the unsupported CoMoS and at 275 °C for the supported CoMoS.

### 5.3.1.2 The functional groups and structures of feed and liquid products

The variations in the feed and hydrotreated liquid products produced by unsupported and supported CoMoS catalysts and at different temperatures were determined by FTIR and NMR (shown in Figure 5-2 (a) and (b)).



(a) FTIR spectra

(b) H-NMR spectra

Figure 5-2 Structures of liquid products at different reaction temperature

\*The number is reaction temperature; Uns and S mean unsupported and supported CoMoS, respectively.

e.g. 275-S: the liquid product is upgraded at 275°C over supported CoMoS

These results agree well with GC/MS results shown in section 5.2.1.1. Throughout the FTIR analysis, the resulting spectra show a strong presence of alkane groups within the

wavenumber ranges of 3000-2850  $\text{cm}^{-1}$ , 1500-1400  $\text{cm}^{-1}$ , and 1370-1350  $\text{cm}^{-1}$ . C=O (1680-1770  $\text{cm}^{-1}$ ) and C-O-C (around 1170  $\text{cm}^{-1}$ ) ester functional groups disappeared from the feed when it was hydrotreated by supported catalyst at 275 and 365 °C, and by unsupported catalyst at 375 °C; there were still C=O acid specific peaks, however, in the products that were upgraded by supported catalyst at 250 °C, and by unsupported catalyst at 340 and 300 °C. Figure 5-2 (a) shows the presence of C-H rock bonds (near 720  $\text{cm}^{-1}$ ) in the feed, in all unsupported catalyst upgraded products, as well as in low temperature (250 and 275 °C) supported catalyst upgraded products. The C-H rock bonds were absent in high temperature (365 °C) supported catalyst upgraded products.

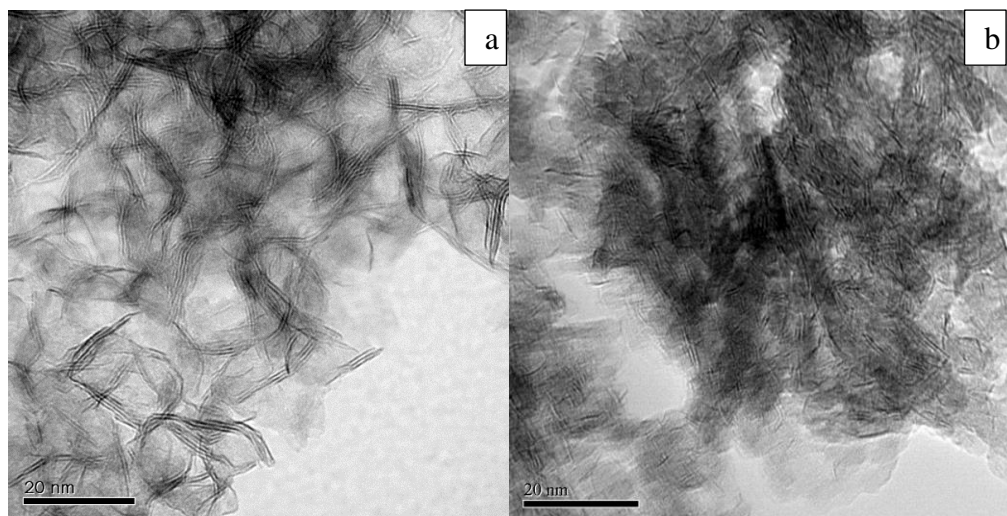
The results indicate that the conversion of glycerides was close to 100 % at 375 °C over the unsupported CoMoS. On the other hand, very high levels of deoxygenation activity were noted when supported CoMoS was used. No obvious glyceride containing structures were observed in the liquid products upgraded by supported CoMoS at temperatures higher than 275 °C. Thus, it is likely that catalyst support strongly enhances the DO capabilities of CoMoS.

The H-NMR results were mainly in accordance with the FTIR results. The H-NMR results consistently showed evidence of a high concentration of primary and secondary hydrogen in all samples, as evidenced by the peaks that were observed in the range 0.7-1.8 ppm. The relatively small peaks in the range of 2.2-4.4 ppm, around 2.1 ppm, and in the range of 5.2-6.0 ppm indicate that there were oxygen containing functional groups

and carbon double bonds in the WCO and the products upgraded at 250 °C by supported CoMoS. There was also evidence of carbon double bonds in the products upgraded at 375 °C by unsupported CoMoS. Aromatic and oxygenate specific peaks, distributed in the ranges of 6.5-8.5 ppm and 2.2-4.0 ppm respectively, were detected in the product upgraded at 365 °C by supported catalyst. From this data, it can be concluded that the optimal temperatures for WCO hydrotreating and DO were 375 °C by unsupported CoMoS and 275 °C by supported CoMoS.

### 5.3.2 Catalyst characterization studies

The crystalline structures of unsupported and supported CoMoS catalysts were determined by TEM imaging (Figure 5-3). In the images, supported CoMoS appears to have shorter slabs (Figure 5-3 (b)) compared to unsupported CoMoS (Figure 5-3(a)). The main properties of each catalyst are listed in Table 5-1.



(a) Unsupported CoMoS

(b) Supported CoMoS

Figure 5-3 TEM images of supported and unsupported catalysts

The average layer number of the unsupported CoMoS was 2.92 nm, whereas the average layer number of the supported CoMoS was 2.34. The average slab length of the unsupported CoMoS was 7.80 nm, whereas the average slab length of the supported CoMoS was 5.84 nm. Using the method described by Calais et al. [113], the ratios of edge metal atoms to edge atoms (including Cobalt and Molybdenum metal atoms as well as sulfur atoms) of these two catalysts were found to be 0.25 (unsupported) and 0.15 (supported). The atomic ratios of Co to total Co+Mo were 0.25 for unsupported CoMoS and 0.31 for supported CoMoS. Supported catalysts had larger surface areas but lower pore volumes than unsupported catalysts.

Table 5-1 Basic properties of CoMoS catalysts

Catalysts	Supported catalyst	Unsupported catalyst
Average slab length (nm)	5.8	7.8
Average layer numbers	2.3	2.9
Fraction of edge metal atoms	0.25	0.15
Surface area (m <sup>2</sup> /g)	150.0	82.2
Pore volume (cm <sup>3</sup> /g)	0.35	0.53
Co/(Co+Mo) (atom ratio)	0.31	0.25

In Figure 5-4, a bimodal pore size distribution with a sharp peak at 2.5 nm and a broad peak at around 12 nm can be observed for the unsupported catalyst; and only one broad peak near to 6 nm, can be observed for the supported catalyst.

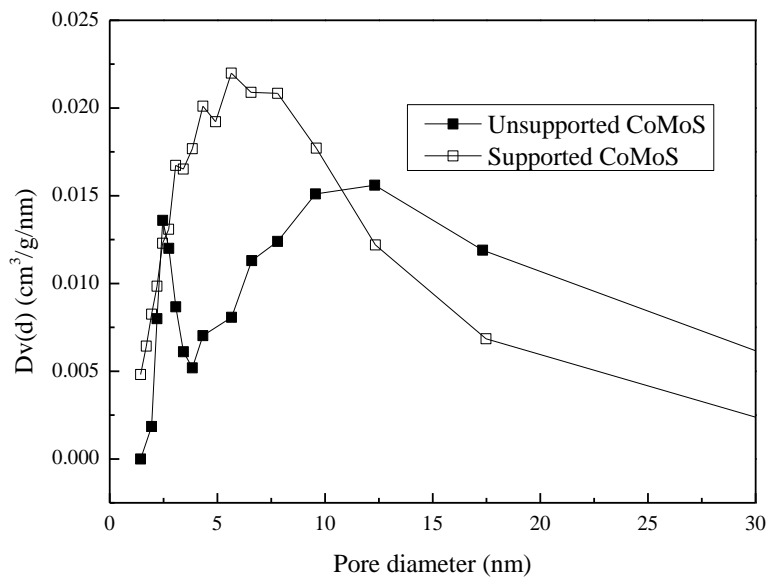


Figure 5-4 BJH pore size distribution of supported and unsupported catalysts

The TPR spectra shown in Figure 5-5 are quantitatively summarized in Table 5-2.

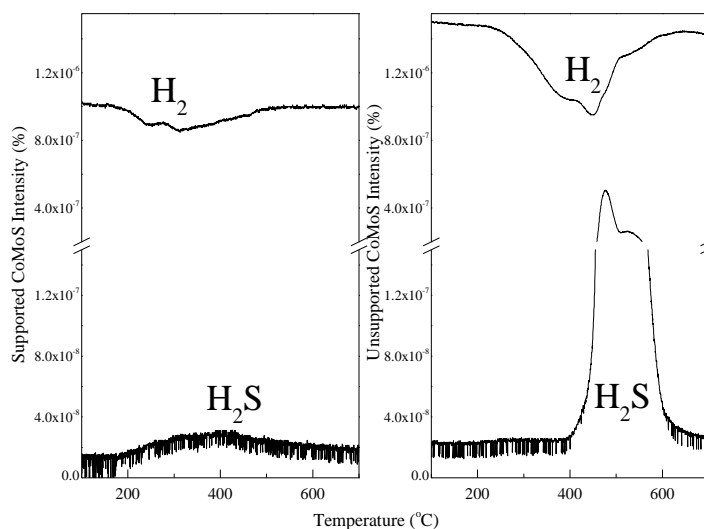


Figure 5-5 TPR spectra of supported and unsupported catalysts

Table 5-2 The amount of active sites on supported and unsupported catalysts <sup>a</sup>

Catalysts	H <sub>2</sub> consumption		H <sub>2</sub> S	
	Peak temperature (°C)	Amount (mmol/g)	Peak temperature (°C)	Amount (mmol/g)
Supported	175-275/430	0.6	175-610	0.1
Unsupported	230-430	2.6	402-510	1.3

<sup>a</sup> Calculation based on the first peak

H<sub>2</sub>S was not generated over the unsupported catalyst until the temperature was higher than 400 °C. The trials with supported catalysts generated different results – H<sub>2</sub>S was detected right when the consumption of H<sub>2</sub> began. The temperature of the supported

catalyst's first H<sub>2</sub> consumption peak (at 175 to 275 °C) was much lower than that of the unsupported catalyst (at around 230 to 430 °C). The amounts of H<sub>2</sub> consumption and H<sub>2</sub>S production were also much lower for the supported catalyst than they were for the unsupported catalyst. These results indicate that the unsupported catalyst contained more active sites than the supported catalyst, but the supported catalyst displayed a higher activity.

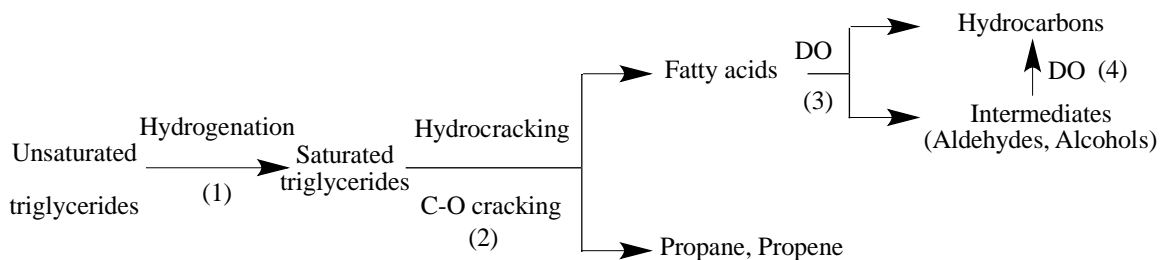
The unsupported catalyst only contained metal active sites, whereas the supported catalyst was a bi-functional catalyst, having both metal and acidic sites. There were no strong acids in the catalyst support, but the amounts of weak and medium acids were 2.26 and 0.23 mmol per gram of catalyst, respectively. It should be noted that only Lewis acids exist on the two supports, alumina and titania.

### **5.3.3 Reaction route discussion**

Considering the significant differences in liquid product composition that were obtained by doing the reactions with supported and unsupported catalysts at different temperatures, the reaction routes were primarily examined from three points of interest: DO (C-O cracking or C-CO cracking), cracking (C-C cracking) / polymerization (C-C chain growth), and hydrogenation (C=C saturation) / dehydrogenation (C-H cracking).

The reaction routes of the hydrotreating of WCO over an unsupported CoMoS catalyst were already investigated previously [114]. The simplified reaction pathways are shown in Scheme 5-1. As discussed in section 4.2.3, unsaturated triglycerides were first

subjected to hydrogenation, which transformed unsaturated carbon-carbon double bonds into saturated carbon-carbon single bonds (Scheme 5-1-1). Then, carboxylic acids were produced through the breaking down of the newly saturated triglycerides into various intermediates (including diglycerides, monoglycerides, carboxylic acids, and gas hydrocarbon products) (Scheme 5-1-2). This process occurred very quickly and was irreversible. The by-product of this process, glycerol, was quickly converted into propane or propene and water by hydrotreating. The fatty acids were then deoxygenated (which produced CO, CO<sub>2</sub>, and H<sub>2</sub>O) into hydrocarbons under different reaction routes (Scheme 5-1-3 and Scheme 5-1-4). The produced hydrocarbons could then undergo further non-oxygen reactions. Focus was given to the DO, as well as to the non-oxygen reactions of the supported and unsupported CoMoS catalysts.



Scheme 5-1 Simplified reaction pathways

### 5.3.3.1 DO (C-O cracking or C-CO cracking)

#### Types of oxygen containing compounds

The general goal of studying the WCO hydrotreating process was to produce oxygen-free biofuels. The oxygenate fraction in the products decreases with the increasing of reaction temperature when using unsupported CoMoS as a catalyst. The oxygen could be totally removed from the products at 275 °C by using supported CoMoS; there were considerable amounts of alcohols in the products obtained from other temperature trials using the supported catalyst (Figure 5-6). Neither too low nor too high reaction temperatures were beneficial for DO. Under high temperatures, the cracking reaction of oxygenated carbon chains could have occurred faster than the HDO and HDC reactions.

The oxygenate intermediates in the liquid products of unsupported CoMoS were fatty acids, whereas the oxygenate intermediates in the products of supported CoMoS were alcohols. Step 3 in Scheme 5-1 corresponds to the reaction-limiting step when using unsupported CoMoS; step 7 in Scheme 4-1-(a)-3 is the reaction-limiting step when using supported CoMoS. This indicates that the catalyst support changed the limiting step by causing an acceleration in the rate that fatty acids were deoxygenated into alcohols by HDO. An explanation for this change is that Lewis acid sites on the support of Al<sub>2</sub>O<sub>3</sub> and TiO<sub>2</sub> might have increased the occurrence of dehydration reactions, which led to an enhancement of the HDO pathway [70].

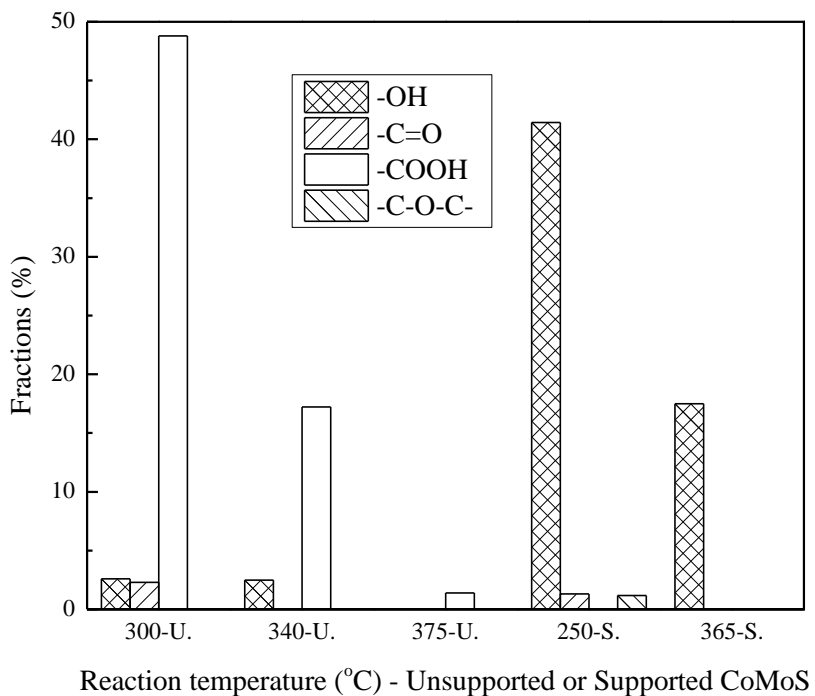


Figure 5-6 Oxygenates distribution in liquid products

### HDO vs. HDC (C18/C17 ratio)

The WCO that was hydrotreated over the supported CoMoS catalyst at 365 °C is not discussed in this section because it experienced severe overcracking (it contained lower than 1.3 wt% C15-C18 hydrocarbons: Figure 5-8).

The two reaction routes that fatty acids undergo for DO were HDO (C-O cracking) and HDC (C-CO cracking), which included DCO and DCO<sub>2</sub>. As discussed in section 4.2.3, stearic acid was used as an example to illustrate these DO routes (see Scheme 4-1).

Differentiating between  $\text{DCO}_2$  and  $\text{DCO}$  was difficult due to the fact that  $\text{CO}_2$  and  $\text{CO}$  could undergo in-situ methanation ( $\text{CO}$  or  $\text{CO}_2$  reacting with  $\text{H}_2$  to form water and methane) or water-gas-shift ( $\text{CO}$  reacting with water to form  $\text{H}_2$  and  $\text{CO}_2$ ) [109]. As a result, most researchers simply divided the  $\text{DO}$  reaction routes into two pathways,  $\text{HDO}$  and  $\text{HDC}$  [110].  $\text{C}_{18}$  and  $\text{C}_{17}$  hydrocarbons were the major components of the hydrotreated liquid product, while fatty acids and alcohols were the main intermediates during the process. Although many alkane  $\text{C}_{17}$  products were obtained through the  $\text{HDC}$  pathways, unsaturated  $\text{C}_{17}$  hydrocarbons were also produced due to fatty acids releasing  $\text{CO}$  and water [115].  $\text{C}_{17}$  olefins could be converted to paraffin, however, when the consumption of hydrogen was involved. The decarboxylation of fatty acids did not require hydrogen and resulted in a by-product of  $\text{CO}_2$  [70, 116]. The decarbonylation of aldehydes required hydrogen and resulted in a by-product of  $\text{CO}$  [117].  $\text{C}_{18}$  hydrocarbons were produced through  $\text{HDO}$  and by-product  $\text{H}_2\text{O}$  was also produced [118, 119] – the oxygen-containing fatty acids reacted with hydrogen to produce alkanes and water. Bi-functional catalysis, hydrogenation reactions ( $\text{CoMo}$  sites), and dehydration reactions (acid catalytic sites) were all involved in  $\text{HDO}$ . Concerning intermediates, alcohols could be formed from the reduction of aldehydes. The ratio of the occurrences of  $\text{HDO}$  reactions to  $\text{HDC}$  reactions was measured by relating the concentration of even number hydrocarbons to odd number hydrocarbons in the products. Based on the composition of the  $\text{WCO}$ , which consisted of a majority of  $\text{C}_{18}$  fatty acids (91 %), this method was suitable for obtaining the  $\text{HDO}/\text{HDC}$  ratio. The results were confirmed by the ratios of  $\text{C}_{16}/\text{C}_{15}$ , because the  $\text{C}_{16}$  content in the  $\text{WCO}$  was 8.0 % (7.5 % saturated

and 0.5 % unsaturated as shown in Table 3-1). The errors were less than 3.0 % between C18/C17 ratios and C16/C15 ratios.

The comparison between the C18/C17 ratios of different products is shown in Figure 5-7. It was noticed that the C18/C17 ratio of the product obtained by using supported CoMoS was much higher than the product obtained by using unsupported CoMoS. This suggests that HDO was the main reaction pathway of the supported CoMoS catalyst (oxygen was removed primarily in the form of H<sub>2</sub>O). On the other hand, this result also suggests that HDC was the main reaction pathway of the unsupported CoMoS (oxygen was removed primarily in the form of CO and/or CO<sub>2</sub>). Support of the CoMoS catalyst obviously heavily influenced the triglyceride deoxygenation process [69, 70] – the reason for this is that Lewis acid sites on the supports increased the hydrogenation and dehydration abilities of the catalyst, strongly enhancing the occurrence of the HDO pathway [70].

The DO mechanisms of the HDO reactions and the HDC reactions (for the CoMoS catalyst) differed greatly from one another. HDO took place on the active sites that were unsaturated and oxygen was removed by the sulfur vacancies residing on the catalyst surfaces. Conversely, HDC took place on the sulfur-saturated sites. Supported CoMoS catalyst preferred the HDO reaction, resulting in mainly of C18 hydrocarbon products; unsupported CoMoS catalyst favored the HDC reaction, resulting in more C17 hydrocarbons products (shown in Figure 5-7 and Figure 5-9). The effects of catalyst support were attributed to differences in supported/unsupported catalyst structures. The

supported catalyst contained abundant amounts of sulfur vacancies, whereas the unsupported catalyst contained none up until the reaction temperature reached 400 °C. This was evidenced by the TPR results shown in Figure 5-5. At the reaction temperature of 250-375 °C, the main active sites of supported catalyst were therefore unsaturated, whereas the unsupported catalyst was dominated by saturated sites. These distinct active sites may be responsible for the different main reaction pathways observed.

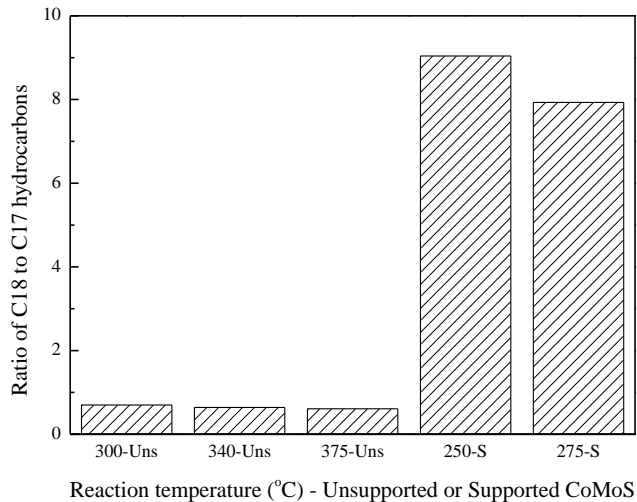


Figure 5-7 The oxygen conversion and mass ratio of C18/C17 hydrocarbons

Ryymän et al. studied the DO of phenol and methyl heptanoate over a sulphided NiMo catalyst, in order to compare the oxygen removals of aromatic and aliphatic reactants. They reported the same conclusions: reduction reactions (including hydrogenation) occur

on coordinately unsaturated sites (CUS) independently, and decarbonylation and acid-catalysed reactions occur on sulfur-saturated sites [70].

For both the supported and unsupported CoMoS, the influence of temperature on the HDO and HDC pathways was similar – HDC was found to be slightly more favorable under higher temperatures.

### 5.3.3.2 Hydrocracking (C-C cracking) and polymerization (C-C chain growth)

In this experimental section, the cracking and polymerization selectivities of unsupported and supported CoMoS catalyst products different temperatures were evaluated and the experiment results are shown in Figure 5-8.

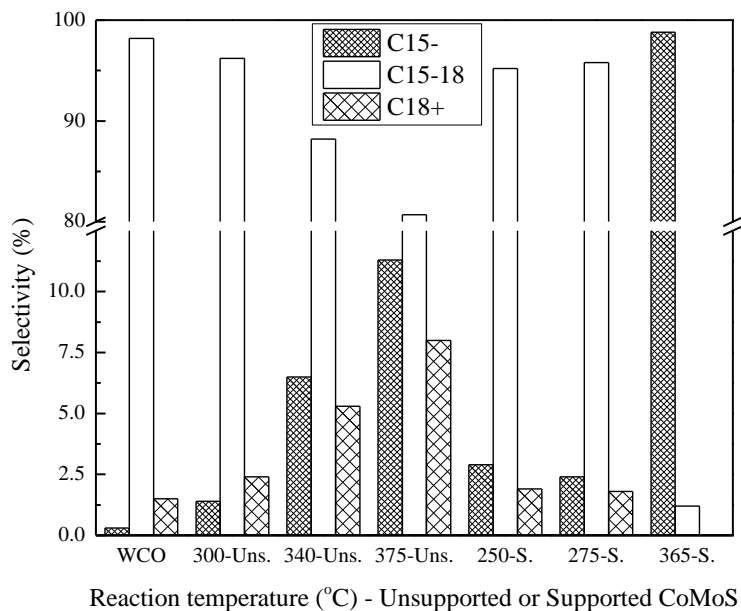


Figure 5-8 Cracking and polymerization over supported and unsupported catalysts

WCO was composed of 99 wt% C16 and C18 fatty acids. The C15 to C18 hydrocarbons were therefore the expected corresponding deoxygenated products if no cracking and/or polymerization occurred [120]. Hydrocarbons with carbon numbers lower than 15 and carbon numbers higher than 18 were thus considered to be the products of hydrocracking and polymerization. In comparison with the feed, the hydrotreated products had a higher C15<sup>-</sup> and a lower C15-18 distribution.

Reaction temperature was a key factor in the cracking/polymerization of WCO hydrotreating using a CoMoS catalyst; Bezergianni et al. [51, 57-59] observed the same phenomena. When the reaction temperature increased from 300 to 375 °C, the product fraction of hydrocarbons lighter than C15 increased from approximately 3.4 wt% to 11.1 wt%, and the product fraction of C15-18 decreased from 94.6 wt% to 81.0 wt% (for the unsupported CoMoS). The same effect also occurred for the supported CoMoS, but to a much higher degree: When the reaction temperature increased from 250 to 365 °C, the C15<sup>-</sup> fraction increased from 2.1 wt% to 98.7 wt% and the C15-18 fraction decreased from 96.1 wt% to 1.3 wt%. For both the unsupported and supported CoMoS, the cracking degree increased with increasing reaction temperature, and was especially high at very high temperatures (365 °C for supported CoMoS and 375 °C for unsupported CoMoS). Except for the liquid product upgraded at the conditions of 365 °C over the supported CoMoS, all liquid products were primarily composed of C15-18. Therefore, the catalyst support could not only significantly enhance the deoxygenation capability of CoMoS, but

could also increase its cracking capability as well (especially at high temperatures). The highest degree of hydrocracking, close to 1, was observed in the product obtained by using the supported CoMoS at 365 °C. This indicates that hydrocracking capability can be significantly improved not only by high temperatures, but also by catalyst support.

For unsupported CoMoS, the following changes were observed when the reaction temperature increased from 300 to 375 °C: 13.6 % of C15-18 was converted into 7.7 % of C15<sup>-</sup> and 5.9 % of C18<sup>+</sup>. The C15<sup>-</sup> was produced because of cracking, whereas the C18<sup>+</sup> was produced due to polymerization. The degree of polymerization increased with increasing reaction temperature. An interesting observation was that only cracking reactions occurred during WCO hydrotreating using the supported CoMoS – polymerization was not observed.

The trial that WCO was upgraded over supported CoMoS at 365°C was an exception to all the other trials in that the primary reaction was cracking instead of deoxygenation – the fraction of C15-18 produced was close to 0 % and most of the products (98.7 %) were C15. This illustrated that high temperatures favored cracking reactions when using the supported catalyst. This trial was omitted from the DO route discussion (5.2.3.1 HDO vs. HDC) because the abundance of cracking influenced the results of DO.

Compared to the supported CoMoS catalyst, the unsupported catalysts caused lower levels of hydrocracking and higher levels of polymerization [14, 29] (shown in Figure 5-8). It has been reported that hydrocracking activity can be facilitated by saturated active sites on sulfur edges. However, it was observed that the C17 fraction of the product upgraded by supported CoMoS at 275 °C was higher than the C17 fraction of the product upgraded by unsupported CoMoS at 300 °C, indicating that supported CoMoS caused higher levels of hydrocracking and HDC activities compared to unsupported CoMoS (shown in Figure 5-9). Lack of acidic support led to lower hydrocracking and higher polymerization capabilities – Lewis acid sites on supports therefore had an important impact on the reaction pathways and final product qualities.

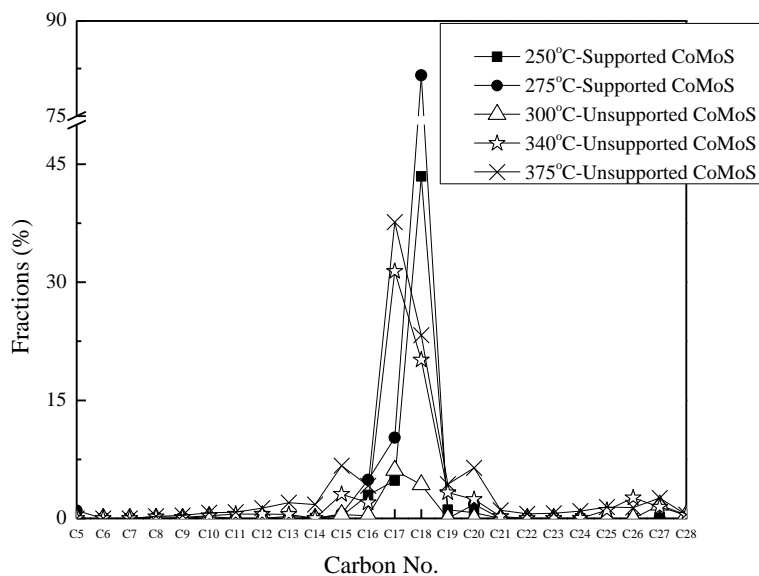


Figure 5-9 Carbon No. distributions of hydrocarbons in liquid product

The higher ratios of C18/C17 were attributed to increases in C18 (Figure 5-9). Catalyst support tended to promote the HDO process. HDO could have mainly occurred on the sulfur vacant active sites of the catalysts, because large amounts of unsaturated sulfur vacancies exist on supported CoMoS. This discussion also demonstrates that there was a high correlation between the production of C18 (over the supported CoMoS catalyst) and the existence of acidity on the support. Research by Ryymin E.M. et al. supports this result. They found that large number of Lewis acid sites on Al<sub>2</sub>O<sub>3</sub> supports benefits hydrogenation and dehydration reactions [22].

#### **5.3.3.3 Hydrogenation (C=C saturation) and dehydrogenation (C-H cracking)**

The content of compounds containing carbon-double bonds is important when considering fuel, because olefins content is related to fuel instability. The degree of hydrogenation was revealed by the selectivity of alkane and ratios of Hydrogen to Carbon found in the liquid products, as shown in Figure 5-10.

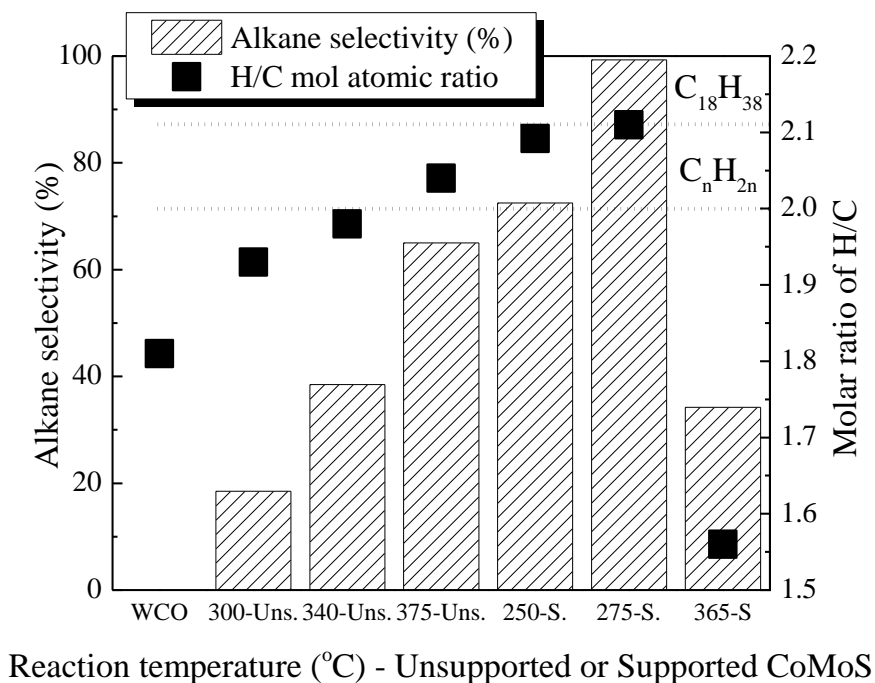


Figure 5-10 Alkane selectivity and ratio of hydrogen to carbon of liquid products

According to Figure 5-10, the alkane selectivity increased with an increasing reaction temperature, for all trials except the one that was run at 365 °C over the supported catalyst. This indicates that hydrogenation activity can also increase due to an increase in temperature. The majority of oxygenates could be removed from the product obtained by upgrading at 375 °C over the unsupported catalyst, but there was still a certain amount of unsaturated hydrocarbons that were left (shown in Figure 5-10). When using unsupported CoMoS at 375 °C, more than 30 % of the hydrocarbons still contained double bonds after

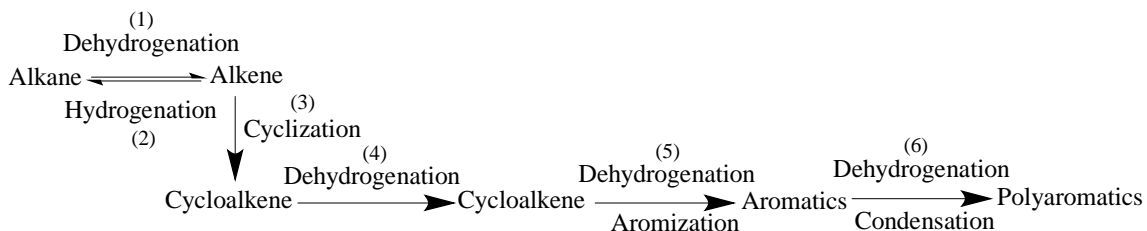
treatment. When using supported CoMoS at 275 °C, over 99 wt% hydrocarbons were successfully saturated. This suggests that supported CoMoS caused a higher hydrogenation activity compared to unsupported CoMoS. Also shown in Figure 5-10, much higher H/C molar ratios were observed in the supported CoMoS products than in the unsupported CoMoS products. This confirms the conclusion that catalyst support can strongly enhance hydrogenation activity. For supported catalyst products, The H/C ratio increased from 2.09 to 2.12 when the temperature was increased from 250 °C to 275 °C, and then decreased back to 1.56 when the temperature was further increased to 365 °C. This dramatic decrease in H/C ratio was caused by the significant dehydrogenation of paraffins (shown in Figure 5-11) that occurred at high temperatures, which produced aromatics (especially poly-aromatics). It is important to note that there were no aromatics detected in all products upgraded by unsupported CoMoS and low temperature supported CoMoS: these reactions ceased at cycloalkanes without further de-hydrogenation. TPR results led to the conclusion that hydrogenation tended to take place on the sulfur vacancies located at the edges of active metal sites. These findings agreed well with the literature [121, 122], where it was reported that hydrogenation took place on unsaturated metal sites. Likewise, it was also reported that the Lewis acid sites on Al<sub>2</sub>O<sub>3</sub> and TiO<sub>2</sub> supports increase the hydrogenation activity [70].

Alkenes were produced during the reactions 4 and 6 in Scheme 4-1. The presence of alkenes was due to C-H bonds cracking, which could be explained by the two routes shown in Scheme 4-1. The first route was the hydrodecarbonylation of a fatty acid, which

was supported by high temperatures [108] (Scheme 4-1-(b)-6). The second was the tautomerization of an aldehyde and subsequent HDO of the resulting enol into an olefin [109] (Scheme 4-1-(a)-4). This olefin remained in the products if conditions were not optimal for hydrogenation. Other researchers have reported the same observation [55, 60]; which was attributed to olefin subsistence due to a lack of hydrogen supply, shorter residence time, and poor catalyst activity. It was reported that SH groups promote hydrogenolysis [121, 122]. In this study, however, it was observed that supported CoMoS not only caused higher levels of hydrogenation and HDO at low temperatures, but also led to higher levels of dehydrogenation at high temperatures when compared to unsupported CoMoS.

Minor amounts of paraffin, a certain amount of olefins and cycloalkanes, and a large amount of oxygenates and aromatics, including benzene, azulene, naphthalene, acenaphthlene, fluorene, and anthracene, were detected by GC/MS in the product upgraded at 365 °C over the supported CoMoS catalyst. The lack of paraffinic compounds was not attributed to DO but to dehydrogenation, aromatization, and condensation. The formation of aromatic compounds was the outcome of sequential dehydrogenation reactions (shown in Scheme 5-2). Under certain conditions, olefins could have undergone cyclization (dehydrogenation of the olefin) to form cycloalkanes and/or cyclo-olefins. If cycloalkanes were produced, they might have also undergone additional dehydrogenation to form cyclo-olefins. Cyclo-olefins were then subjected to further dehydrogenation to produce aromatics [108]. Finally, aromatics underwent

condensation to form poly-aromatics. The occurrence of this process was supported by the presence of aromatics shown in Figure 5-11. Thus, dehydrogenation happened at excessively high temperatures over the supported CoMoS, because of the significantly enhanced rate of dehydrogenation that was observed at these elevated temperatures. This agreed well with the results of the catalytic cracking of animal fats, which produced aliphatic hydrocarbons at lower cracking temperatures (400 °C) and alkyl aromatic hydrocarbons at higher cracking temperatures (550 °C) [92].



Scheme 5-2 Hydrogenation and dehydrogenation pathways

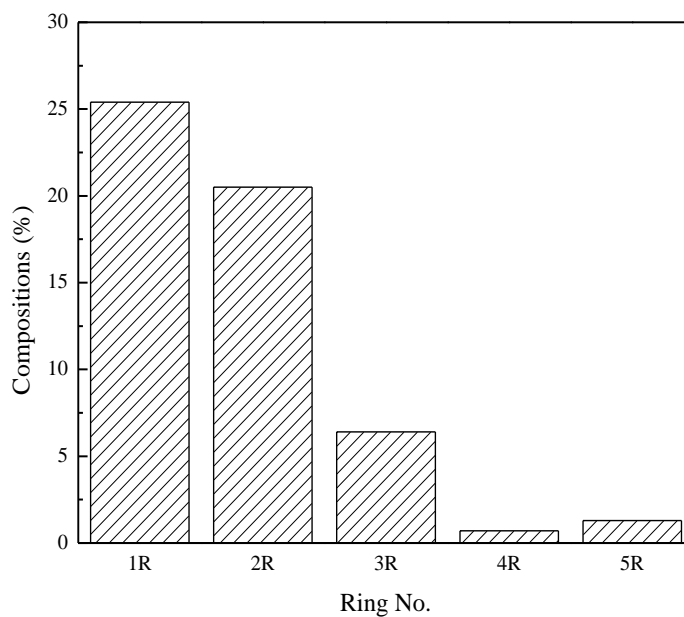


Figure 5-11 Aromatics ring No. distributions over supported catalyst at 365°C

#### 5.3.3.4 Other reactions

In the high temperature reaction processes (365 °C over supported catalyst, and 375 °C over unsupported catalyst) cyclization reactions occurred, as was indicated by the formation of cycloalkanes. The cyclization proceeded either from the isomerization of alkenes or the dehydrogenation of n-alkanes. The cyclization reaction was facilitated by the high accumulation of alkenes. Alexander et al. found [55] that cyclization reactions could also generate products from fatty acids with double bonds.

## 5.4 Conclusions

For deoxygenation process: the hydrocarbon fraction was close to 100 % in the products that were upgraded at 375 °C and 275 °C over unsupported CoMoS and supported CoMoS, respectively. Catalyst support changed the reaction-limiting step by accelerating the rate at which fatty acids were deoxygenated into alcohols by HDO. The increase of reaction temperature did not affect the main reaction pathways, but it slightly enhanced HDC capability.

For hydrocracking and polymerization process: unsupported catalyst was correlated with lower levels of hydrocracking and higher levels of polymerization when compared to supported catalyst. Lack of acidic support led to lower hydrocracking and higher polymerization capabilities.

For hydrogenation and dehydrogenation process: supported CoMoS not only exhibited higher hydrogenation and HDO abilities at low temperatures, but also exhibited higher dehydrogenation activity at high temperatures compared to unsupported CoMoS.

Acidic sites on catalyst support promote the dissociated of hydrogen, which can be effectively consumed during hydrotreating process, and further improve the hydrogenation and hydrodeoxygenation capabilities.

## **Chapter 6 Hydrotreating of triglycerides over CoMoS supported catalyst: Deactivation mechanisms of the catalyst**

### **6.1 Introduction**

Catalyst deactivation presents a challenge to process design and operation. A complete understanding of catalyst deactivation is of great importance for developing new catalysts or improving the lifetimes of existing catalysts [123, 124]. Compared to petroleum hydrotreating (which removes sulfur), the purpose of triglyceride hydrotreating is to remove oxygen. Therefore, it is vital to understand how oxygenates influence catalyst activity during triglyceride upgrading using sulfided hydrotreating catalysts. At the present moment, the deactivation mechanisms of sulfided catalysts during HDO have been comprehensively studied for model oils (representing biomass-derived oil) but rarely for real oils or triglyceride containing oils. In this work, the deactivation of the supported CoMoS catalyst during the HDO of real triglyceride oil was studied. Two areas of deactivation are proposed. The first consists of the effects occurring due to oxygenates, such as by-product water, the oxygenated compounds in the liquid products, and the oxide active components on the catalysts. The second consists of more traditional deactivation causes, such as the appearances of coke deposition and sintering. In-situ drying of the catalyst was carried out to investigate the magnitude of water formation effects on deactivation.

## 6.2 Experimental

The reaction conditions for the supported, sulfided CoMo catalysts were: a temperature of 275 °C, a pressure of 1100 psi, an LHSV at 3 h<sup>-1</sup>, and an H/O ratio at 50 ml/ml. The reaction time was 220 hours. Samples were taken at the 77<sup>th</sup>, 107<sup>th</sup>, 138<sup>th</sup>, 177<sup>th</sup>, and 213<sup>th</sup> hours. The five samples were given the tags “R<sub>i</sub>”, where i denote the numbers 1 to 5 (respective to chronological order).

## 6.3 Results

### 6.3.1 Variation of the properties, functional groups, and compositions of products with time-on-stream

#### 6.3.1.1 Variation of products’ properties

Table 6-1 indicates the results of the acidity tests. No water was detected in any sample.

Table 6-1 Density and TAN variation with time-on-stream

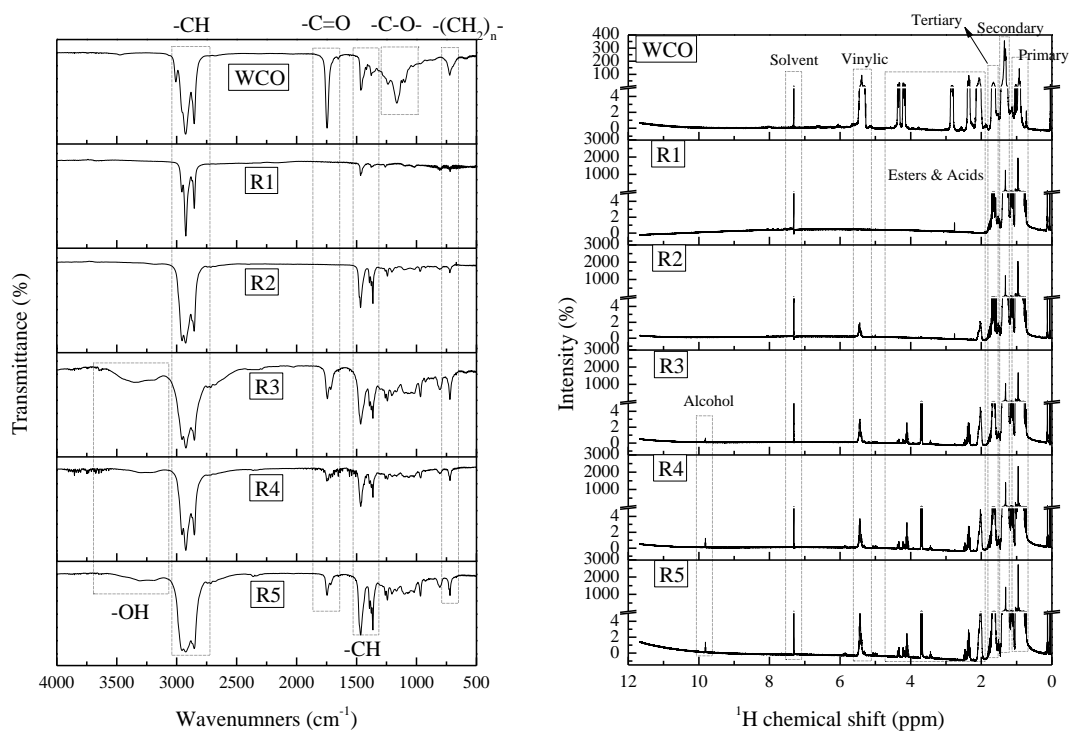
Sample	Feed	R1	R2	R3	R4	R5
TAN (mg KOH/g)	0.1	0.4	0.5	7.2	5.7	6.4

The TAN results show that some samples were significantly more acidic than the feed oil, even though the former had been hydrotreated. This increase of acidity was due to the appearance of some intermediates in those samples, which included acids, alcohols, and aldehydes. These intermediates were more acidic than the ester functional groups in the

feed triglycerides. Experiments R1 to R5 indicated that catalyst DO activity decreased because of the increased acidity, because they all exhibited incomplete oxygen conversion. A temperature of 365 °C was used to test the effects of high temperatures on catalyst activities, for the trials R1-R3. A large TAN variation ranging from 0.5 to 7.2 mg KOH/g was observed. When the temperature was lowered back to 275 °C, the DO activity of the catalyst dropped back down, but the TAN still remained as high as 5.7 mg KOH/g. This result revealed a decrease in DO activity due to temperature, so high temperature was found to be a cause of catalyst deactivation.

### **6.3.1.2 Variation of products' structure**

FTIR and H-NMR analysis (shown in Figure 6-1) were used to determine the structure characterization and distribution variations of the products over time-on-stream. Throughout all of the FTIR results, spectra consistently show a strong presence of alkane groups in the wavenumber ranges of 3000-2850  $\text{cm}^{-1}$  and 1500-1400  $\text{cm}^{-1}$ , as expected. However, as shown in Figure 6-1 (a), the samples from R3 to R5 exhibit peaks at around 3200  $\text{cm}^{-1}$  and in the range of 1750-1500  $\text{cm}^{-1}$ . These peaks are evidence of the existence of oxygenated compounds. The H-NMR results show evidence of higher concentrations of primary hydrogen (peaks ranged of 0-1.2 ppm), lower amounts of oxygen containing functional groups (peaks ranged of 2-4.4 ppm and around 10 ppm), and lower amounts of carbon-carbon double bonds (peaks ranged of 5.2-5.5 ppm) in the products than in the WCO (Figure 6-1 (b)). Carbon-carbon double bonds existed in the products R2 to R5, and a certain amount of oxygenates existed in the products R3 to R5 as well.



(a) FTIR results

(b) H-NMR results

Figure 6-1 Variation of functional groups with time-on-stream

### 6.3.2 Activity variation

After triglyceride hydrotreating, the products should ideally be 100 % paraffinic – all oxygen should be removed and all carbon-double bonds should be saturated. Three categories of reaction that help to achieve these goals are hydrogenation, DO, and cracking reactions.

### 6.3.2.1 Hydrogenation activity variation

Figure 6-2 shows the variations of oxygenate, alkane, and alkene selectivity observed in the reaction products against time-on-stream.

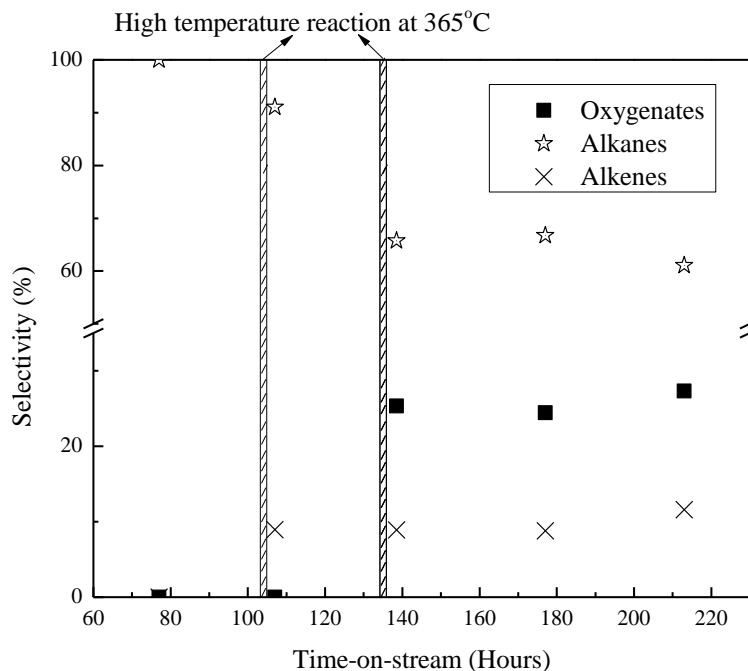


Figure 6-2 Selectivity of Alkanes, alkenes, and oxygenates with time-on-stream

When considering the usability of fuels, a high content of carbon-carbon double bonds is unfavorable because their presence makes the fuel unstable. It can be observed that the content of unsaturated hydrocarbons gradually increased with the increasing of time-on-stream, which indicates that hydrogenation activity decreased. During the first 100 hours of operation, all double bonds could be saturated. A temperature of 365 °C was introduced to test the effects of high temperature on the catalyst activities. This condition

started at about the 100<sup>th</sup> hour of time-on-stream and remained for 4 hours; the temperature was then lowered back to 275 °C. The olefin content in the hydrotreated oil rose from 0 % to 8.9 % before the temperature of 365 °C was employed. And then the high temperature was tested again to confirm its influence. It is worth mentioning that the second high temperature operation did not affect the hydrogenation activity too much and the final liquid product contained 10.6 % of olefins (Figure 6-2). The hydrogenation capability of the catalyst was significantly reduced because of the severely high temperature; therefore, it can be concluded that high temperature had a remarkable impact on catalyst hydrogenation activity. Moreover, the hydrogenation activity was stable during the time-on-stream range of 138.5 to 213 hours.

The olefins were present for two reasons: cracking reactions (resulting in olefins lighter than C15) and the insufficient hydrogenation capability of HDO during alcohol dehydration (resulting in olefins ranging from C15 to C18); these are shown in Figure 6-3. Regardless of whatever reason caused the decrease in catalyst hydrogenation activity, olefin content can be used to determine variations in catalyst hydrogenation capability. As shown in Figure 6-3, the main reason for the decrease in hydrogenation capability was the insufficient hydrogenation that occurred during the dehydration of alcohols.

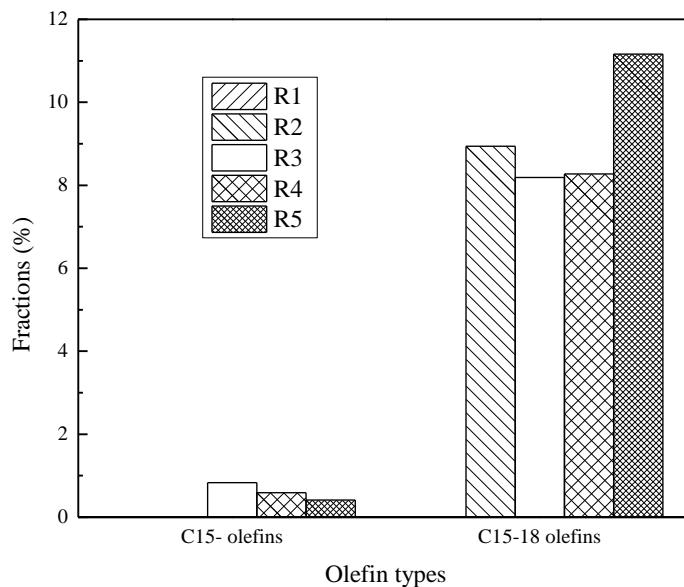


Figure 6-3 Distributions of different type olefins

### 6.3.2.2 Deoxygenation activity variation

As discussed in 4.2.3, the first reaction to occur during triglyceride hydrotreating was hydrogenation, in which unsaturated triglycerides were saturated. The second reaction was hydrogenolysis, in which triglycerides were broken down into diglyceride, monoglyceride, ester, and fatty acid intermediates. These intermediates could then undergo two further reaction pathways: HDO or HDC. In the HDO pathway, fatty acids reacted with hydrogen, forming aldehydes and water. These aldehydes could then react with hydrogen to produce alcohols, and the alcohols could undergo subsequent dehydration, producing hydrocarbons and water. The HDC pathway might have occurred through two distinct routes. The first route involved cracking and produced alkenes,

water, and carbon monoxide. The second route involved removing CO<sub>2</sub> to produce alkanes. Since one carbon molecule was lost from HDC and no carbon molecules were lost from HDO, the carbon numbers in the resulting hydrocarbons from HDC and HDO were one less than the carbon number of the fatty acid (HDC) and equivalent to the carbon number of the fatty acid (HDO). WCO was mainly composed of C18 fatty acids, so the occurrences of the two reaction pathways were easily deduced by comparing the C18 and C17 fractions of the final product. Figure 6-4 shows GC/MS results, which show the C18 and C17 fractions and C18 to C17 ratios. For all samples, even-numbered paraffins were dominant over odd-numbered paraffins, which suggest that HDO was generally more prevalent over HDC cracking reactions. As the time-on-stream increased, the fraction of C18 (and ratio of C18 to C17) decreased, especially after the temperature was increased to 365 °C for the second time. However, the fraction of C17 barely changed. Therefore, it can be concluded that the second 365 °C high temperature reaction only reduced HDO ability, but did not affect the HDC ability. It should be noted that the first 365 °C reaction did not significantly influence the DO capability. The significant decrease in the C18/C17 ratio from 107 to 138.5 hours was likely due to the formation of coke from alkenes, which were produced under temperatures as high as 365°C at the 133<sup>th</sup> hour. As coke precursors were built up within the catalyst bed, molecules were prevented from bonding with HDO active sites on the catalyst. The DO capabilities did not change within the range of 138.5 to 213 hours, which means that the DO activities were stable during this time.

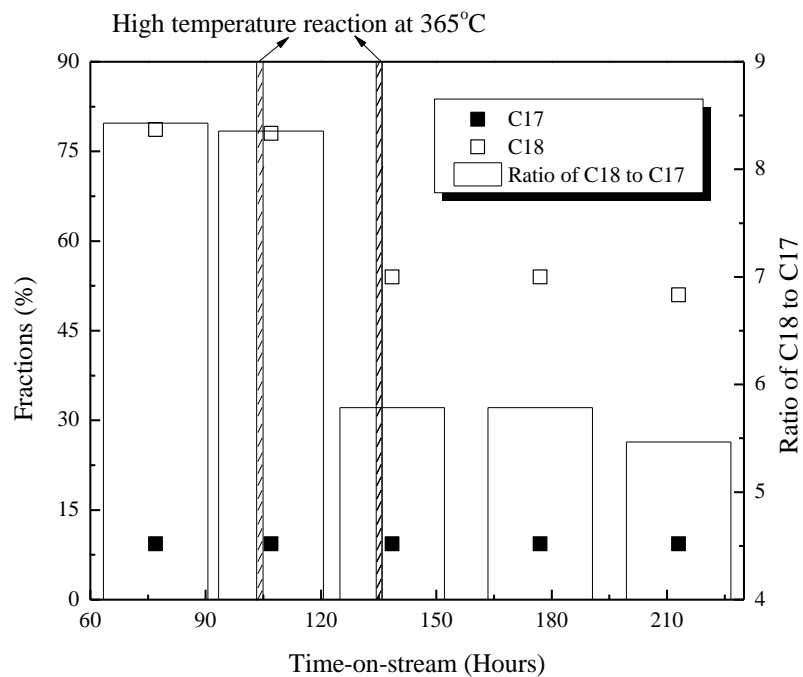


Figure 6-4 Variation of DO capabilities with time-on-stream

Figure 6-5 shows that most of the oxygenated compounds that were detected in the liquid products were alcohols; there were also some aldehydes, esters, and ethers. The ester compound, stearic acid propyl ester, was only found in the R5 samples. GC/MS results show that the only aldehyde present was octadecanal, which presented itself in the samples R3 to R5 in concentrations of 1.3-1.7 wt%. The alcohols existing in the products were hexadecanol and octadecanol, which were contained in concentrations of 0.8-0.9 % and 21.5-23.6 %, respectively. In particular, octadecanol was the primary oxygenate contained in the products, especially for the experiments R3-R5. The significant appearance of alcohols and hexadecanal helped to explain the TAN results. The presence

of even-carbon-numbered aldehydes and alcohols confirmed that the aldehyde to alcohol reaction that occurred during HDO was the rate-limiting step. It was also noted that both long-chain alcohols and long-chain hydrocarbons played an important role in the formation of wax-like solids at room temperature. As shown in Figure 6-2, all oxygen was eliminated from the products during the first 125 hours of operation. When WCO was hydrotreated at 365 °C for the second time in order to prove that high temperatures had an impact on catalyst activity, decreased DO was observed at the 125 th hour.

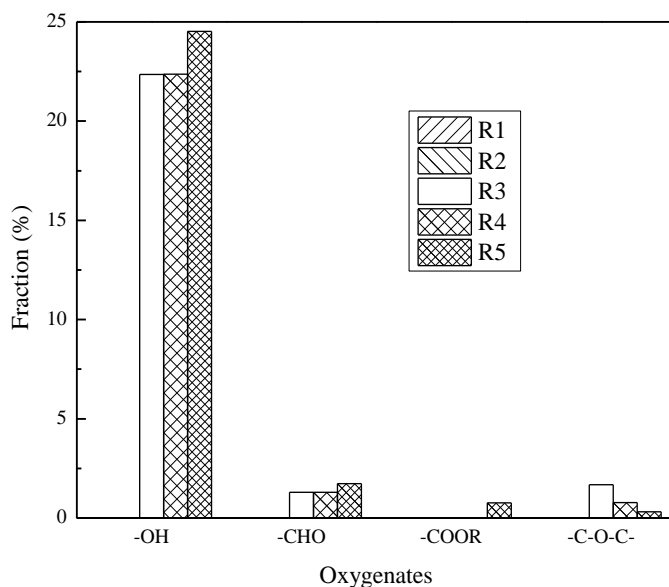


Figure 6-5 Variation of oxygenates in liquid products with time-on-stream

### 6.3.2.3 Cracking activity

Shown in Figure 6-6, C15 to C18 hydrocarbons had the highest concentrations among contained compounds in all products. Based on the composition of the feed oil, these results were expected. The cracking activity was determined by the content of C15<sup>-</sup> hydrocarbons in the products. The desired products of triglyceride hydrotreating were products in the diesel fraction, so cracking reactions were unwanted. During time-on-stream, no significant differences in cracking or polymerization capabilities were observed (Figure 6-6).

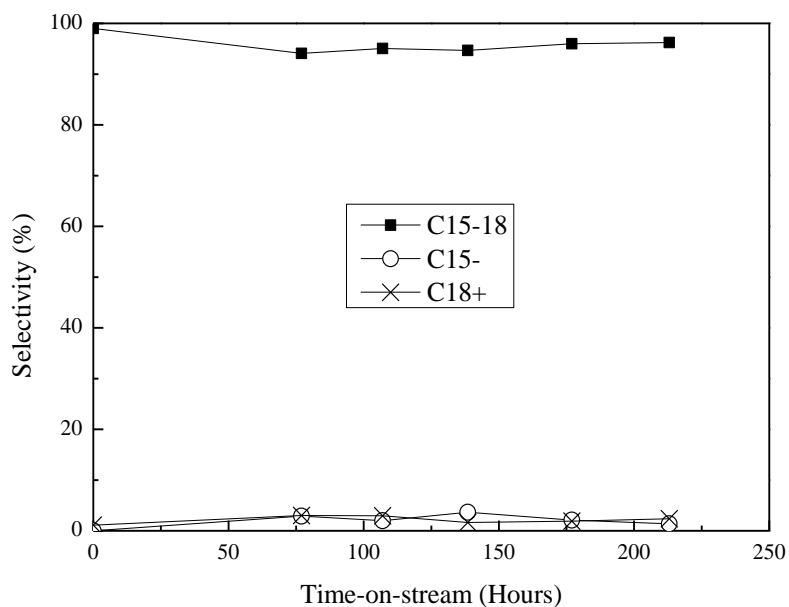


Figure 6-6 Variation of cracking and polymerization capabilities with time-on-stream

Based on the discussion above, two obvious effects of deactivation were observed: the rapid deactivation of hydrogenation activity due to coke deposition (after a time-on-stream of 100 hours) and the subsequent deactivation of HDO activity due to the catalyst pores plugging with produced coke (after a time-on-stream of around 130 hours). Coke depositions first showed selectivity towards hydrogenation active sites, and then went on to select HDO active sites.

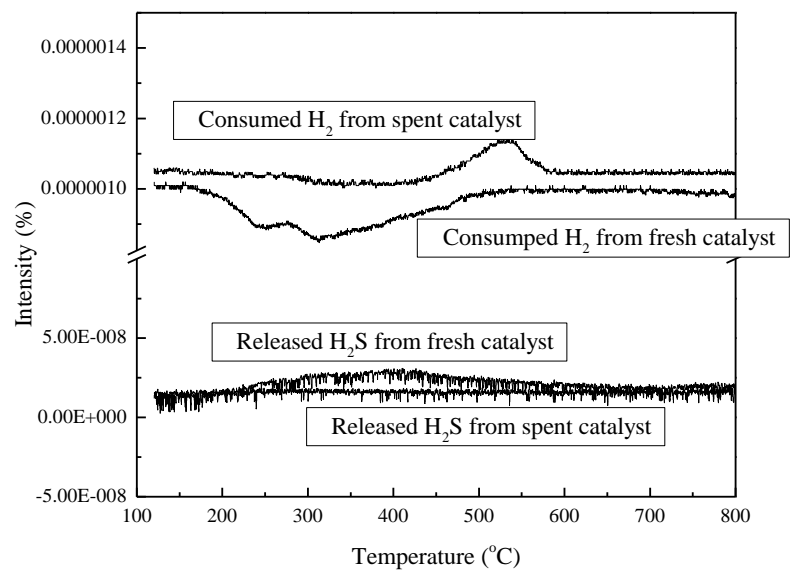
### 6.3.3 Characterization of fresh sulfided catalyst and spent catalyst

#### 6.3.3.1 Variation of the amount and strength of active sites

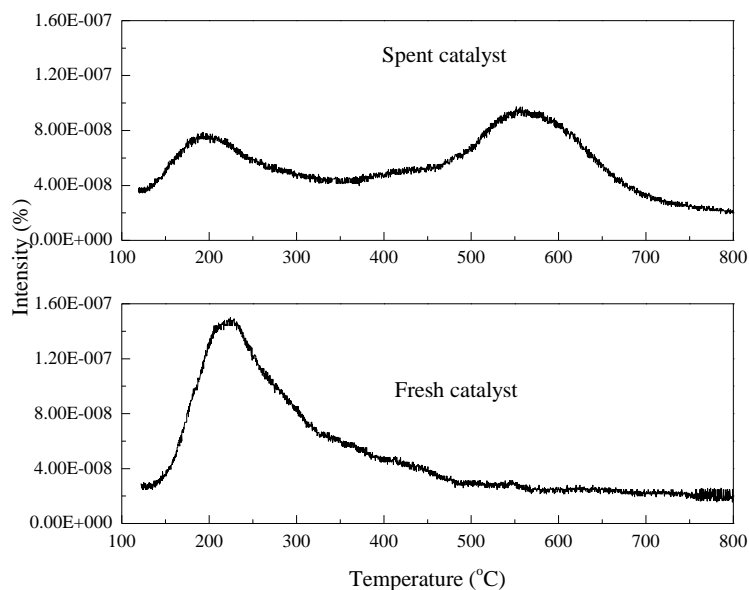
According to Figure 6-7 and Table 6-2, there was a significant difference in hydrogen consumption observed between the fresh sulfided and spent catalysts.

Table 6-2 The amount and strength of active sites on the fresh and spent catalysts

Amount (mmol/g)	H <sub>2</sub> consumption		H <sub>2</sub> S	Acidity			
	<460°C	>460°C		Weak	Medium	Strong	Total
Fresh catalyst	2.1	0.0	0.13	2.3	0.2	0.0	2.5
Spent catalyst	0.1	-0.1	0.00	0.6	0.3	1.5	2.3



(a) Strength and amount of hydrogenation and deoxygenation active sites



(b) Strength and amount of acidic sites

Figure 6-7 The strength and amount of active sites on the sulfided and spent catalysts

The amounts of H<sub>2</sub> consumed and H<sub>2</sub>S released are indicators of the amounts of hydrogenation and HDO active sites that existed on the catalysts. When the catalyst's testing temperature was lower than 460 °C, the total amount of hydrogenation active sites dramatically decreased from 2.08 mmol/g to 0.06 mmol/g. There was hydrogen released when the temperature was high than 460 °C. This occurred because the precursor to the coke produced was decomposed, and hydrogen was consequentially released. The effectiveness of hydrogenation active sites also decreased significantly during the reaction. Overall, the hydrogenation and HDO activities of the fresh catalyst were much higher than those of the spent catalyst. As shown in Figure 6-7, there was a small H<sub>2</sub>S peak in the TPR results of the fresh catalyst, but a significantly smaller H<sub>2</sub>S peak in the TPR results of the spent catalyst. This shows that the HDO capability of the catalyst obviously decreased during use.

The amount and strength of active sites on a catalyst can be representative of cracking capability. It was expected that acidity should have been decreased in the spent catalyst because of coke deposition, but this was not found to be the case. Figure 6-7 shows that the strength of acids on the spent catalyst was higher than that of the fresh sulfided catalyst. Table 6-2 shows a slight decrease in the total amount of acidity.

These results indicate that significant changes happening on the surfaces of the catalysts during reaction altered the amounts and strengths of the acidic sites. During the HDO

process, the active components of the sulfided catalyst ( $\text{MoS}_2$ ) could have been converted into metal oxides. Other researchers have made the same observations. Yuji Yoshimura et al. [125] detected the existence of  $\text{MoO}_3$  using X-ray photo electron spectroscopy (XPS), when coal derived oil (containing a large amount of oxygenates) was hydrotreated over a sulfided  $\text{CoMo}/\text{Al}_2\text{O}_3$  hydrodesulfurizing catalyst. It was reported that strong acidic sites could be generated when  $\text{MoO}_3$  was deposited on alumina, titania, and silica [126-128]. Even though the acids on  $\text{Al}_2\text{O}_3$  and  $\text{TiO}_2$  are typically Lewis acids only, Biying et al. found that Bronsted acids could be produced when  $\text{MoO}_3$  was loaded onto titania [127]. In addition, the formation of coke is facilitated on Lewis acids than on Bronsted acids [129, 130].

#### **6.3.3.2 The amount and type of coke formation on spent catalyst**

Figure 6-8 shows the existence of three peaks corresponding to  $\text{O}_2$ ,  $\text{CO}$ ,  $\text{CO}_2$ , and  $\text{H}_2\text{O}$ , which indicates that different kinds of coke were deposited on the spent catalysts [131]. Carlos et al. studied the characterization of residual coke during the burning of coked catalysts, and discovered that TPO was selective and that two burning zones were presented. These zones corresponded with the coke deposited in metallic active sites and the coke deposited in acidic active sites, which was more polymerized and poorer in hydrogen.

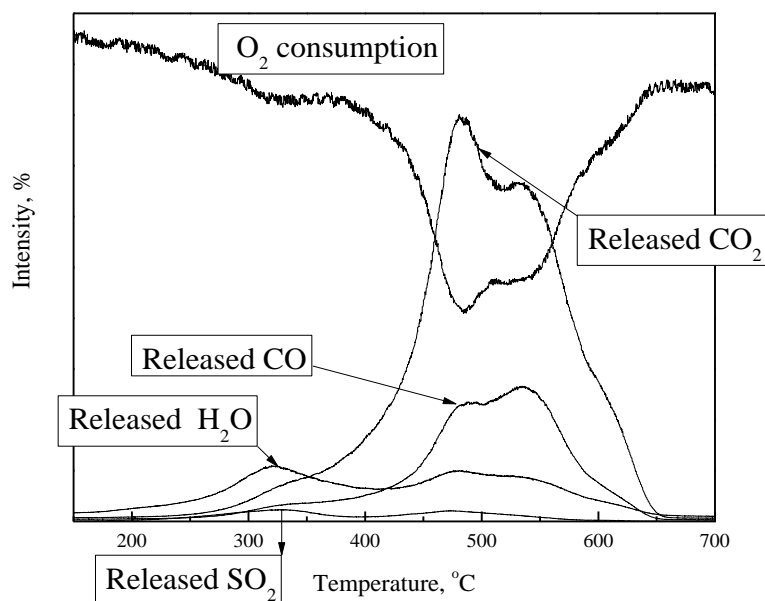


Figure 6-8 TPO result of the spent catalyst

In the research presented in this work, coke burning was conducted. Unwashed oil product and H<sub>2</sub>O were present in the first burning zone (120-400 °C). The precursors to coke were aromatics with less than three rings – this was known because the ratio of H/C of 3-ring aromatics was 0.7. These were detected in the second burning zone (400-500 °C). Poly-aromatics that had more than three rings were found in the third burning zone (at temperatures higher than 500 °C). As shown in Table 6-3, the SO<sub>2</sub> amount was an exception to the other values. The release of SO<sub>2</sub> was distributed in the first and second

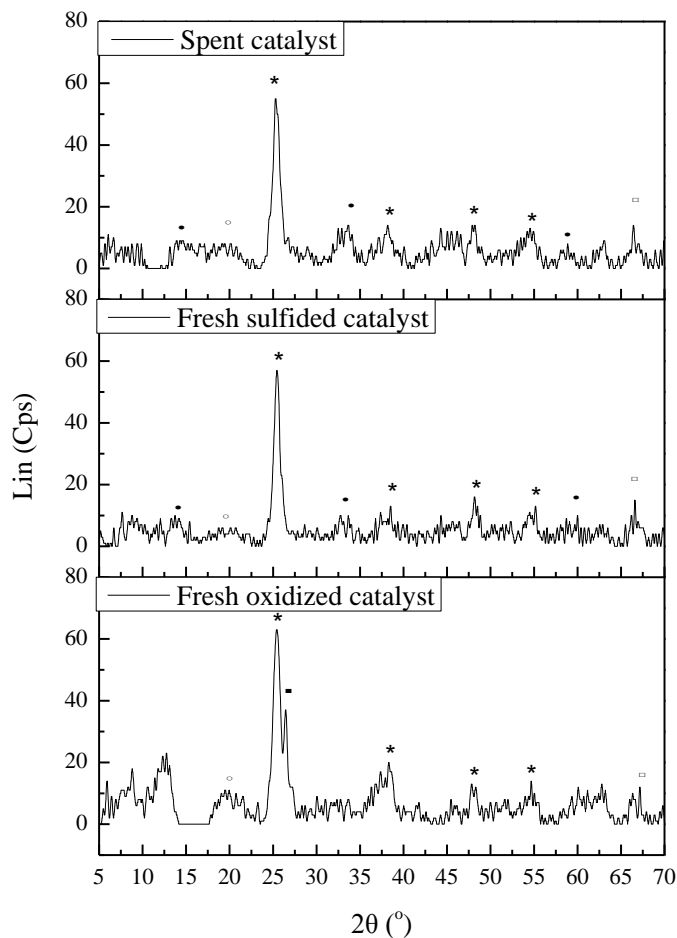
burning zones rather than in the second and third burning zones. Yoshimura et al. studied the weight losses of sulfided and oxidic CoMo/Al<sub>2</sub>O<sub>3</sub> catalysts by a TGA [132]. They found that the driving force converting MoS<sub>2</sub> and Co<sub>9</sub>S<sub>8</sub> into metal oxide and SO<sub>2</sub> was higher than the driving force converting carbon into CO<sub>2</sub> and CO. This fact is in accordance with the current study.

Table 6-3 Type and amount of the coke deposition on the spent catalyst

Amount (mmol/g)	SO <sub>2</sub>	CO <sub>2</sub>	CO	H <sub>2</sub> O	O <sub>2</sub>	H/C
(120-400°C)	0.7	0.0	0.5	6.4	-3.2	24.5
(400-500°C)	0.7	8.9	2.4	4.4	-13.2	0.8
(>500°C)	0.0	6.3	3.5	2.5	-6.8	0.5
Total	1.4	15.1	6.5	13.4	-23.2	-

### 6.3.3.3 Variation of crystal structure

The XRD results (in Figure 6-9) show that TiO<sub>2</sub> (PDF 21-1272) and  $\gamma$ -Al<sub>2</sub>O<sub>3</sub> (PDF 46-1131) were present in all of the three examples tested.



●:  $\text{MoS}_2$ ; ○:  $\text{SiO}_2$ ; \*:  $\text{TiO}_2$  (PDF# 21-1272); ■:  $\beta\text{-CoMoO}_4$  (PDF# 21-868); □:  $\gamma\text{-Al}_2\text{O}_3$  (PDF# 46-1131)

Figure 6-9 XRD spectra of the fresh and spent catalysts

$\text{TiO}_2$  (PDF 21-1272) had a better crystallinity over  $\gamma\text{-Al}_2\text{O}_3$  (PDF 46-1131) – this was shown by  $\text{TiO}_2$ 's higher intensity and sharper diffraction peak [64]. The broad peak at around  $2\theta = 20^\circ$  was from  $\text{SiO}_2$ . No obvious peaks for  $\text{MoO}_3$  or  $\text{CoO}$  were observed in the XRD patterns of the un-sulfided oxide catalyst, but a small peak attributing to  $\beta$ -

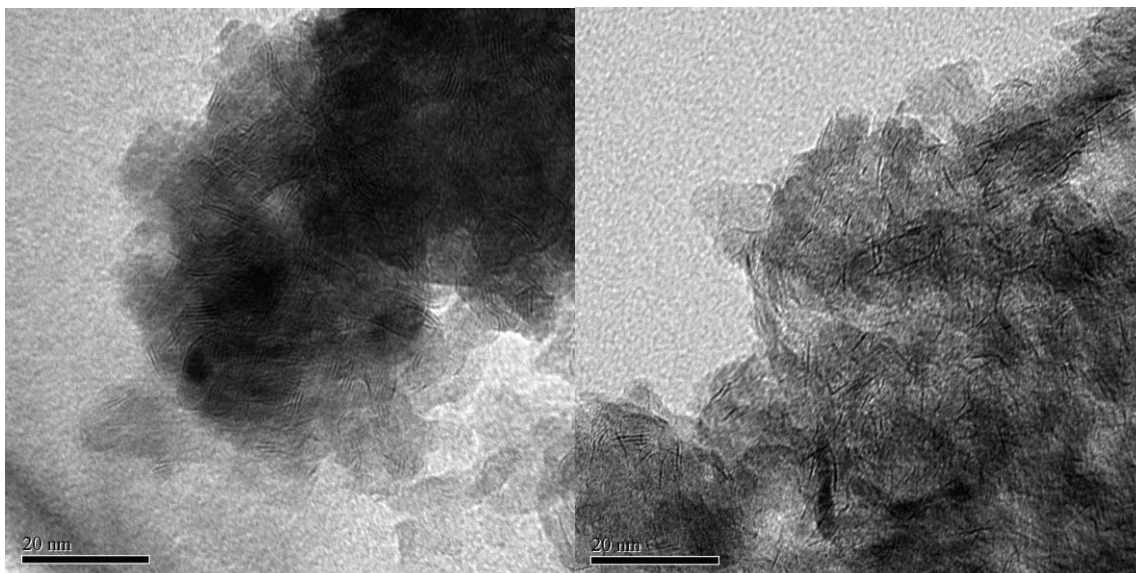
CoMoO<sub>4</sub> (PDF 21-868) was found at  $2\theta = 26.5^\circ$ . These peaks disappeared after the catalyst was sulfided. Characteristic peaks for MoS<sub>2</sub> appeared after the catalyst was sulfided. XRD could determine whether the sintering of active metals or catalyst support occurred during hydrotreating, but CoMo catalysts needed to be processed for a long time at more severe conditions to exhibit extensive MoS<sub>2</sub> sintering or segregated Co sulfided phase formation and support sintering [133]. The changes in Mo and Co dispersion that occurred between the fresh sulfided and spent catalysts were confined to a very limited range, which was reflected in the XRD patterns [134].

Laurent and Delmon found that the result of partial gamma-alumina support crystallisation formed into a hydrated boehmite phase, because of the existence of large amounts of water (the partial pressure of water was 2.5 MPa under a total pressure of 7 MPa) [10]. Boehmite specific peaks were not detected in the XRD results of the fresh sulfided catalysts or the spent catalysts (Figure 6-9). It can therefore be concluded that, based on XRD results, no obvious sintering phenomena were observed for the supported/sulfided CoMo catalyst during the triglyceride hydrotreating process.

#### **6.3.3.4 Variation of morphology**

TEM and EDX were used to determine and compare the morphologies of the fresh sulfided and spent catalysts. This helped to determine whether any active metals were lost or aggregated during the hydrotreating process. Representative TEM micrographs and the basic properties of the fresh and spent catalysts are shown in Figure 6-10 and Table 6-4, respectively. While hydrotreating with the catalyst, the layers of MoS<sub>2</sub> decreased

significantly and the length of crystalline decreased as well (from 5.84 to 5.10 nm). The stacks in the fresh sulfided catalyst consisted of an average of 2.34 layers, whereas most of stacks in the spent catalyst only had one layer left (average of 1.52 layers). For  $\text{TiO}_2$ , multi-layered  $\text{MoS}_2$  clusters possessed higher activities than single-layered  $\text{MoS}_2$  clusters – this can be explained by the theories of single-layered Co–Mo–S (I) and multi-layered Co–Mo–S (II) [135]. For sulfided catalysts, an increased stacking layer can weaken the polarization of aluminum ions on the alumina surface and can improve the ability of cobalt on molybdenum to form CoMoS active phases [64]. This multilayer theory can further explain the disappearances of  $\text{MoS}_2$  layers on the catalyst during triglyceride hydrotreating. The TPR results show that there was no  $\text{H}_2\text{S}$  released from the use of the spent catalysts, which supports the conclusion that the amount of active  $\text{MoS}_2$  decreased during reaction. This conclusion can also be supported by the fact that the fraction of edge metal atoms increased due to the loss of sulfur.



(a) Fresh sulfided catalyst      (b) Spent catalyst

Figure 6-10 TEM images of the fresh sulfided and spent catalysts

### 6.3.3.5 Variation of physical properties

Table 6-4 and Figure 6-11 show the variations in physical properties of the catalyst over the course of the reaction.

Table 6-4 Basic properties of the fresh sulfided and spent catalysts

Catalysts	Fresh sulfided catalyst	Spent catalyst
Average slab length (nm)	5.84	5.10
Average layer numbers	2.34	1.52
Fraction of edge metal atoms [113]	0.20	0.22
Surface area (m <sup>2</sup> /g)	150	48
Pore volume (cm <sup>3</sup> /g)	0.35	0.11
Average pore diameter (nm)	9.24	4.41

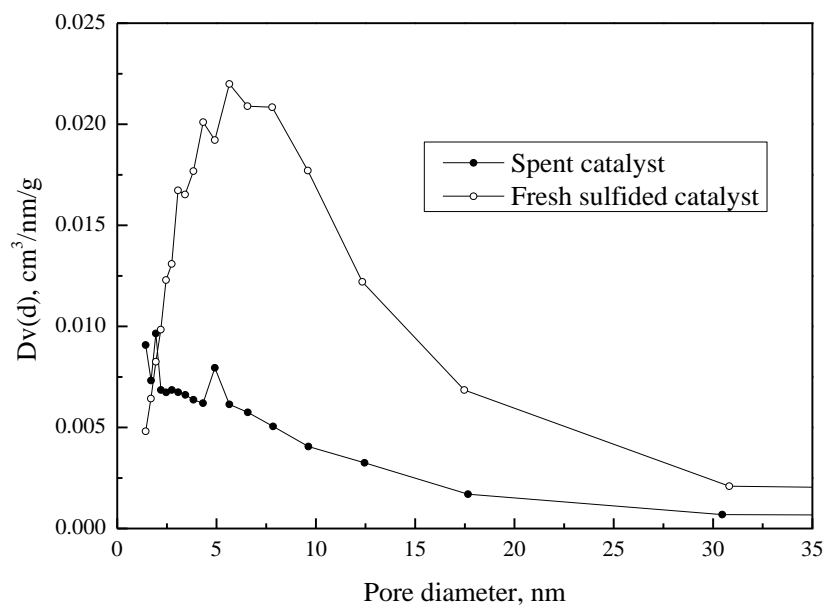


Figure 6-11 Variation of pore size distributions

The surface area, pore volume, and average pore size obviously decreased after the reaction. Coke formation on the surface of the catalyst may be responsible for this decrease.

### 6.3.3.6 Variation of elemental composition

As can be seen from Table 6-5, the differences between the elemental compositions of the fresh and spent catalysts (measured by the relative content of the element's atomic ratio to Al) were not more than 0.02, except for those of sulfur and carbon. This indicates that, besides sulfur and carbon, none of the compositional elements in the catalysts decreased during the hydrotreating process. Only the ratio of sulfur content decreased by

0.10, which reveals that sulfur was lost during the reaction. This conclusion was confirmed by NS-9000 results. During the hydroprocessing of coal-derived oil, the same phenomenon was attributed to the existence of oxygenates in the feed [136]. It is also noted that 21.53 % carbon was produced after 222 hours of reaction, indicating severe carbon deposition and coke formation.

Table 6-5 Elemental compositions of the fresh sulfided and spent catalysts

Element compositions	Al <sup>1</sup>	Si <sup>1</sup>	S <sup>1</sup>	Ti <sup>1</sup>	Co <sup>1</sup>	Mo <sup>1</sup>	S <sup>2</sup>	C <sup>3</sup>
Fresh sulfided catalyst <sup>4</sup>	1.00	0.06	0.39	0.33	0.11	0.57	0.46	0.00
Sulfided catalyst <sup>4</sup>	1.00	0.07	0.29	0.35	0.11	0.59	0.34	0.87

1, 2, and 3 tested by electron micro probe, NS-9000, and TPO, respectively;

4 is the relative content of atomic ratio to Al.

## 6.4 Discussion

Concerning the hydrotreating of triglycerides using supported CoMo catalysts, two categories of catalyst deactivation mechanism are proposed in this work. The first category encompasses the existence of both coking (coke covers the active sites on the catalyst's surface) and sintering (the crystal undergoes phase change). These are the same factors that cause catalyst deactivation in petroleum hydrotreating. The second category involves all sources of deactivation caused by oxygenates. These are not found in petroleum hydrotreating processes because of the low oxygen content in petroleum feed. Oxygenates include byproduct water, oxygenated compounds in the products, and

remaining metal oxide components on the catalysts that produced from metal sulfide being exchanged by oxygenates in the feed.

#### **6.4.1 Causes for deactivation of catalyst**

##### **6.4.1.1 Coke deposition**

The physical contact of coke with the catalyst surface resulted in the blocking of active sites and the plugging of pores [136]. The chemisorption might have increased the chance for condensation to form coke. Coke forms by sequential dehydrogenation reactions. The formation starts from olefins and includes (a) olefin cyclization to form substituted cycloalkane, (b) the dehydrogenation of cycloalkane into cycloalkene, (c) the dehydrogenation of cycloalkene into aromatics, and (d) aromatics forming into polyaromatics. These coking pathways advance via carbonium ions intermediates on B acids [137] – this was in accordance with  $\text{NH}_3$ -TPD results found in this study, which can further confirm the conclusion that B acids existed on the surfaces of catalysts during the triglyceride hydrotreating process.

##### **6.4.1.2 Sintering and poisoning**

Sintering usually refers to the activity loss caused by crystal growth and active metal migration/aggregation on a catalyst; in general, sintering is irreversible. Judging from XRD and TEM results, sintering was not observed in both the supports and active metal phases of the catalysts during hydrotreating.

Poisoning involves a chemical interaction of extraneous feedstock molecules (normally, basic nitrogen compounds and metal-containing feedstock, such as V, Ni, Ti, and Fe) with the catalyst active sites [136]. In this study, none of these poisoning substrates were present in the feed, so poisoning did not contribute significantly to deactivation.

## **6.4.2 Oxygenate deactivation**

### **6.4.2.1 Byproduct water**

Water was a by-product of the triglyceride hydrotreating process. To examine the effects of moisture during experimentation, catalysts were dried with nitrogen in-situ, at the 215<sup>th</sup> hour of time-on-stream.

As shown in Table 6-6, after the spent catalyst was dried, 12.3 % of hydrogenating activity and 18.3 % deoxygenation activity were recovered. The HDO activity was also recovered by 11.7 %, but there were no significant changes in HDC activity – these changes correlated well with the activity losses exhibited due to time-on-stream. On stream, the HDO capability decreased much more than the non-decreasing HDC capability (shown in Figure 6-4). This shows that moisture was a key factor in catalyst deactivation; by-product water greatly hindered hydrogenation and HDO. Yoshimura et al. [138] observed similar results when studying the effects of water content on hydrodenitrogenation activity. Lavopa et al. [71, 138] also arrived to the same conclusion.

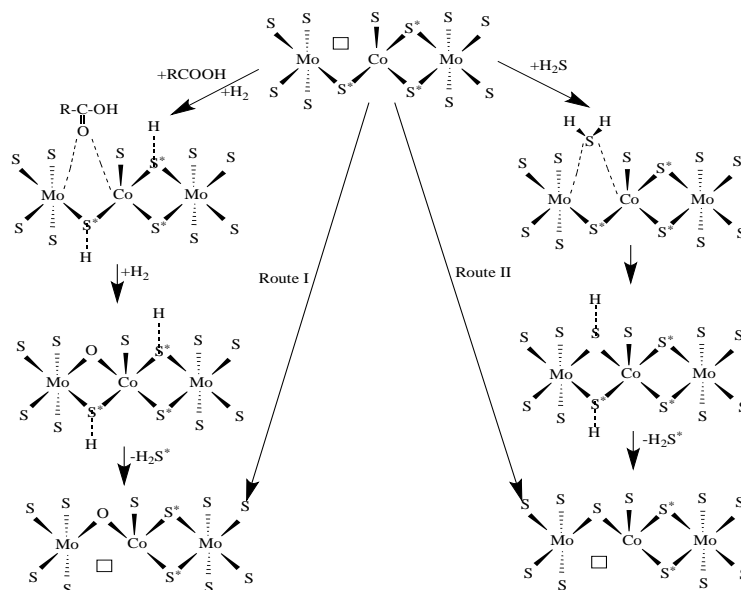
There were no changes in cracking and polymerization capabilities that occurred due to water. It is possibly attributed to the fact that the by-product, water, was occupied on the hydrogenation active sites and coordinatively unsaturated sites (for HDO).

Table 6-6 The effect of water condensation on catalyst activities

Fractions	Before drying (%)	After drying (%)	Activity recovery (%)
Alkane	56.0	63.4	13.2
alkene	10.6	9.3	12.3
oxygenates	33.4	27.3	18.3
C17	12.1	12.2	0.8
C18	47.8	53.4	11.7
C15-	1.4	1.4	0.0
C15-18	96.2	96.3	0.1
C18+	2.4	2.4	0.0

#### 6.4.2.2 Oxygenated compounds in liquid products

The aliphatic ester HDO reaction mechanism seemed to be dominant in the experiments conducted in this work. This reaction is the same as the classical mechanism involving sulfur vacancies in the HDS process [70, 139-142]. The reaction mechanism for HDO on sulfur vacancies is proposed in Scheme 6-1, according to the hydrodesulfurization theory proposed by Qian et al. [38].



Scheme 6-1 HDO reaction mechanism and transformation between labile sulfur and vacancies on the sulfided CoMo/Al<sub>2</sub>O<sub>3</sub>. S\*: 3S; (□) Anion vacancy.

Route I, HDO; route II, sulfur exchange.

Scheme 6-1 demonstrates the following process: oxygen in the reactants is transferred to the catalyst, sulfur on catalyst active site is released in the form of H<sub>2</sub>S, and the position of active site is transformed in the active phase. Sulfur is replaced by oxygen during the HDO process. Therefore, one of the reasons for catalyst deactivation during triglyceride hydrotreating was the exchange of oxygen (from oxygenates) with sulfur in the active phases of the catalysts [138].

### 6.4.2.3 Oxide active components on the catalysts

Table 6-7 lists thermodynamic data for possible reactions of sulfur/oxygenate exchange in MoS<sub>2</sub>. Reactions were deemed favorable when  $\Delta G_f < 50$  kJ/mol [143].

Table 6-7 Thermodynamic data for reactions of sulfur exchanged by oxygenates

Possible reactions	$\Delta G_f @ 275^\circ\text{C}$ (kJ/mol)
$3\text{C}_{17}\text{H}_{35}\text{COOH}(\text{l})^* + \text{MoS}_2(\text{s}) + 8\text{H}_2(\text{g}) \rightarrow \text{MoO}_3(\text{s}) + 2\text{H}_2\text{S}(\text{g}) + 3\text{C}_{18}\text{H}_{38}(\text{l})^* + 3\text{H}_2\text{O}(\text{l})$	48.3
$2\text{C}_{17}\text{H}_{35}\text{COOH}(\text{l})^* + \text{MoS}_2(\text{s}) + 3\text{H}_2(\text{g}) \rightarrow \text{MoO}_2(\text{s}) + 2\text{H}_2\text{S}(\text{g}) + 3\text{C}_{18}\text{H}_{38}(\text{l})^* + \text{H}_2\text{O}(\text{l})$	-80.7

\* According to the values from literature the reaction temperature was 260°C [144]

The thermodynamic data clearly indicated that there was a tendency for some MoS<sub>2</sub>-like structures to be converted into MoO<sub>3</sub>, even during the hydrotreating process. This might have occurred due to some of the Mo undergoing oxidation from Mo<sup>4+</sup> to Mo<sup>6+</sup> under high temperatures and in the presence of oxygen containing compounds. In the experiments, insufficient quantities of sulfur were used to maintain the catalyst in its sulfided form. Other authors discovered the same MoS<sub>2</sub> conversions when investigating coal-derived feed hydroprocessing [136, 138]. The main active phase of the catalyst before being sulfided was MoO<sub>3</sub>, so resulfiding the catalyst could recover the decrease in activity caused by loss of sulfur. Ferrari et al. [75] reported that increasing the amount of sulfur (resulfiding) could restore some activity to the catalyst.

## 6.5 Conclusions

There were three causes for deactivation of the supported CoMoS catalyst used in this study: coke deposition, by-product water, and loss of sulfur. A high reaction temperature (at 365 °C) promotes coke formation, which further led to catalyst deactivation. By-product water partially caused deactivation, but in-situ drying could be used to recover the hydrogenation activity and the HDO activity of the catalyst. Loss of sulfur also caused deactivation, but resulfiding was shown to be a potential option for reactivating the spent catalyst. Hydrogenation capability was first affected by high temperature operation, and then the HDO capability. Deactivation had no significant impact on the catalyst's cracking, polymerization, or HDC activities.

# Chapter 7 Catalytic cracking of oleic acid to fuels and chemicals: roles of catalyst acidity and basicity on product distribution and reaction pathways

## 7.1 Introduction

Literature has reported on the reaction process for the catalytic cracking of oxygenates to petroleum-like products with metal oxide catalysts – most of the reported work has been performed using acid catalysts. In contrast, the effects of basic sites on catalyst performance have not been sufficiently discussed. In this study, the specific roles that acidity, basicity, and type of acidic sites on the catalyst play on the product distributions of oleic-acid-derived products have been investigated.

## 7.2 Experimental

The operational parameters of this performance evaluation are listed in Table 7-1.

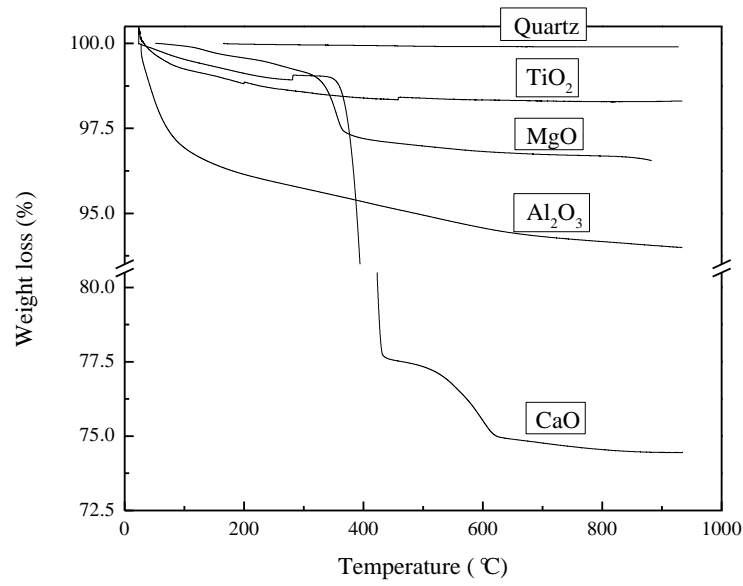
Table 7-1 Activity evaluation parameters of metal oxide catalysts

Operational parameters	Values
Reaction temperature (°C)	470±1 [145]
Mass ratio of catalyst to feed	2.5±0.2 (TiO <sub>2</sub> , 0.4)
Mass ratio of catalyst to quartz	1:2 (TiO <sub>2</sub> , 1:17)
Mass of feed (g)	1.2±0.1
Injection time (s)	180±30 (TiO <sub>2</sub> , 1140)
N <sub>2</sub> flow rate (ml/min)	30

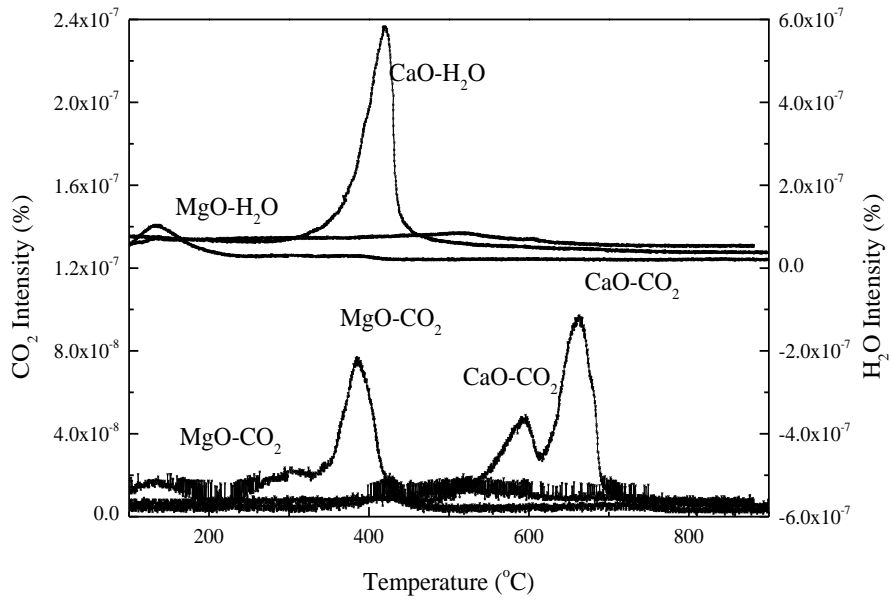
## **7.3 Results and discussion**

### **7.3.1 Catalyst thermal treatment**

Catalyst thermal treatment results are shown in Figure 7-1 (a) and (b).



(a) Weight loss and derived weight loss of catalysts



(b) Released substrates

Figure 7-1 Thermal treatment of metal oxide catalysts

The weight loss of titania and alumina were only due to absorbed water. No weight loss occurred during quartz thermal treatment. The obvious weight losses of CaO and MgO during thermal treatment corresponded to released water and CO<sub>2</sub>. Therefore, CaO and MgO underwent in-situ drying with nitrogen at a temperature of 800 °C for 2 hours before being subjected to performance evaluations.

### 7.3.2 Catalysts characterization

#### 7.3.2.1 Physical properties

Table 7-2 shows the physical properties of all the tested catalysts. Compared to other catalysts, the neutral quartz catalyst has barren pore structures, an extremely low surface area, and a rather small pore volume. Acidic catalysts generally have higher surface areas and pore volumes compared to alkaline catalysts. This was in accordance with the observed pore size distributions, shown in Figure 7-2.

Table 7-2 Surface areas and pore volume of metal oxide catalysts

Catalysts	Surface area (m <sup>2</sup> /g)	Pore volume (cm <sup>3</sup> /g)	Average pore size (nm)
Quartz	0.1	4.8E-4	19.4
MgO	11.6	0.2	69.8
CaO	13.7	0.1	29.0
TiO <sub>2</sub>	56.9	0.9	59.6
Al <sub>2</sub> O <sub>3</sub>	152.9	0.5	14.1

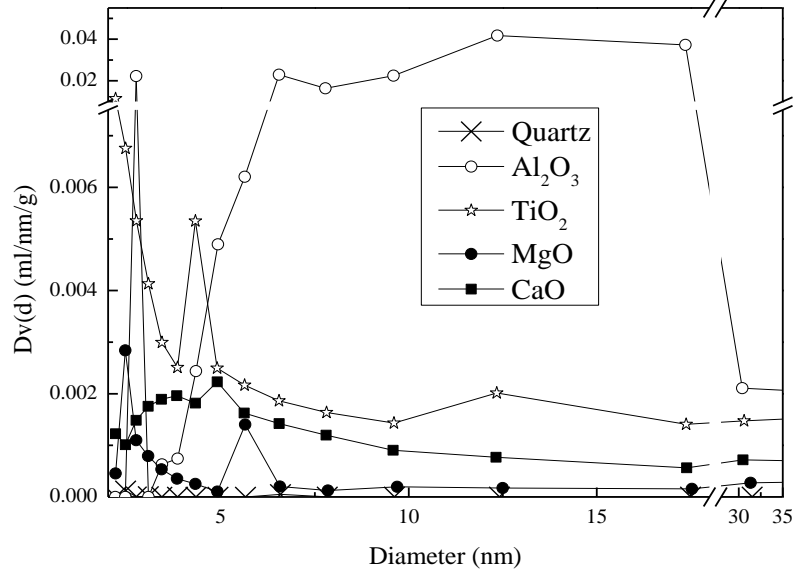


Figure 7-2 Pore size distributions of metal oxide catalysts

### 7.3.2.2 Amount and strength of active sites

Table 7-3 Amount of active sites on metal oxide catalysts

Properties	Amount of active sites ( $\times 10^{-2}$ mmol/g)			
	Weak	Medium	Strong	Total
Titania	39.8	10.8	8.0	58.6
Alumina	14.0	3.9	7.5	25.4
MgO	20.7	0.0	0.0	20.7
CaO	0.0	0.0	153.8	153.8

The amounts and strengths of active sites on the acidic and alkaline catalysts are listed in Table 7-3. Compared to  $\text{Al}_2\text{O}_3$ ,  $\text{TiO}_2$  had a high amount of acids with high strengths.

Both the amounts and the strengths of the CaO active sites were higher than those of MgO. There were no active sites on quartz.

### 7.3.2.3 Type and strength of acids on acidic catalysts

Figure 7-3 shows the Py-FTIR spectra of (a)  $\text{Al}_2\text{O}_3$  and (b)  $\text{TiO}_2$ . The peaks at around  $1450\text{ cm}^{-1}$ ,  $1540\text{ cm}^{-1}$ , and  $1490\text{ cm}^{-1}$  are indicative L acids, B acids, and both acids, respectively [101]. Only L acids appeared on these two catalysts.

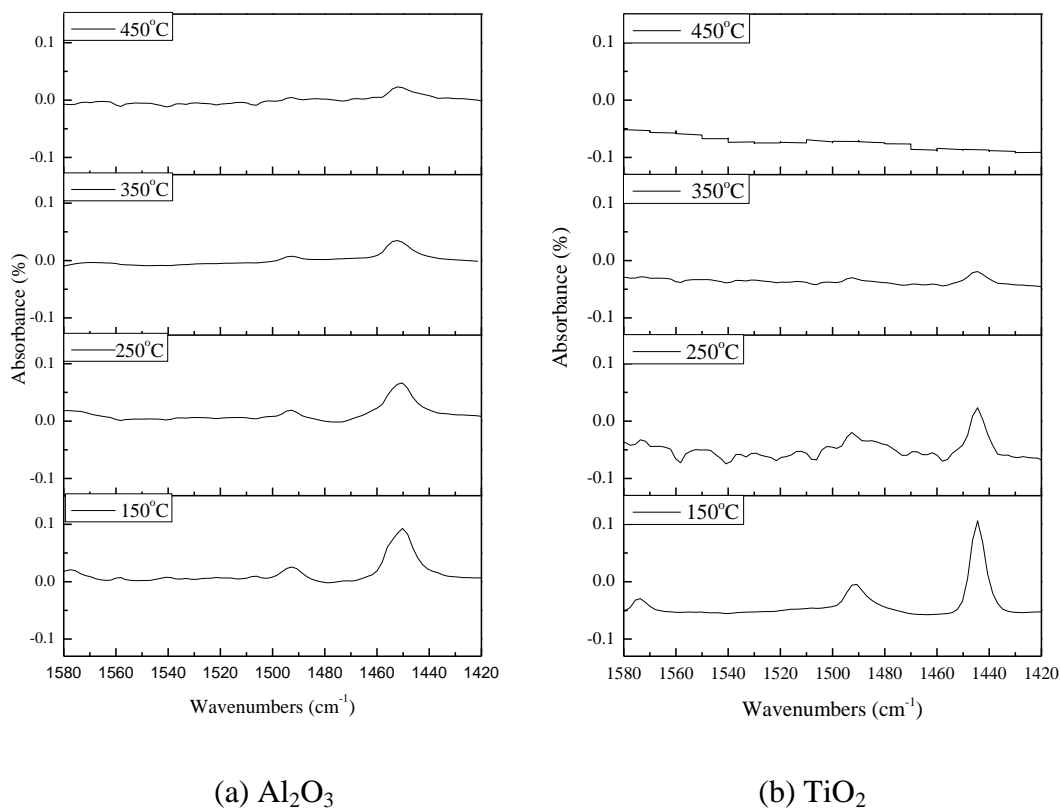


Figure 7-3 Py-FTIR spectra of acidic metal oxide catalysts

### 7.3.2.4 Product distribution

The product yield distributions for the different catalysts are shown in Table 7-4. The total product yields reached  $100\pm 5.0$  % during all experiments. As expected, the conversion of quartz-upgraded products was as low as 35 %: around 65 % of the oleic acid was left in the liquid products, and catalytic cracking resulted in lower liquid yields, higher gas yields, and higher coke yields.

Table 7-4 Product distributions

Yields (wt%)	Oil	Coke	Gas hydrocarbons	Water	CO/CO <sub>2</sub>	H <sub>2</sub>	Total
Quartz	93.4	0.1	0.9	0.5	2.6	0.1	97.5
Al <sub>2</sub> O <sub>3</sub>	82.5	5.1	3.0	1.6	10.6	0.4	103.2
TiO <sub>2</sub>	75.3	2.0	3.6	0.9	16.3	1.4	99.5
MgO	67.5	5.3	5.5	2.3	14.9	0.1	95.6
CaO	29.0	51.2	3.8	0.0	19.8	1.0	104.8

All liquids spontaneously separated into two fractions: oil product and water. The oil product yields of the catalysts decreased in the following order: quartz (93.4 wt%) > alumina (82.5 wt%) > titania (75.3 wt%) > MgO (67.5 wt%) > CaO (29.0 wt%). For all catalysts, the total amount of water, carbon oxides, and hydrogen were found to increase during the catalytic process. This indicates that the catalysts enhanced dehydration, DC reactions, and dehydrogenation. Other researchers have observed the same behaviour [85]. It has been reported that activated alumina is an effective catalyst for the decarboxylation of fatty acids (under atmospheric pressures and at 450 °C) – liquid product yields have

ranged between 65 % and 79 % with n-alkanes and n-alkenes [83]. Idem reported contradictory results: relatively higher gas and coke yields were obtained when working with alumina as opposed to working with base catalysts [84].

There were variations in DO that occurred when WCO was upgraded with the different types of catalysts. All these catalysts exhibited DO more by the removal of CO and CO<sub>2</sub> than by the removal of water. The liquid yield, the gas hydrocarbon yield, and the coke yield all appear to be closely associated with the types of active sites that exist on the catalysts. Higher liquid yield, lower gas hydrocarbon yield, and lower coke yield were achieved first by quartz, then by acidic catalysts, and lastly by alkaline catalysts. Increasing the strength of active sites on the catalysts caused lower liquid yields and higher gas hydrocarbon yields in the products. Increasing the amount of active sites on the catalysts lowered the coke yields. CaO was an exception, however, its use led to a higher gas hydrocarbon yield and a lower coke yield when compared to MgO.

Certain amounts of hydrogen were detected by GC-RGA. Serrano et al. studied the feasibility of producing hydrogen, and received 0.1 % hydrogen through the decomposition of vegetable and microalgal oils [146].

The oxygen removal rates and light oil yields of the oil products are shown in Table 7-5. The amount of active sites on a catalyst strongly affects the oxygen removal rate.

Although the oxygen removal rate of  $\text{Al}_2\text{O}_3$  was lower than that of  $\text{TiO}_2$  and the alkaline catalysts, the light oil yield of  $\text{Al}_2\text{O}_3$  was the highest among all catalysts. Idem reported the same trend: higher OLP yields were obtained when working with alumina, whereas lower OLP yields appeared when working with base catalysts [84].

Table 7-5 Oxygen removal rate and valuable product distributions

Yields (wt%)	Oxygen removal rate	Light oil yields, to feed	Valuable products yields
Quartz	18.5	20.8	21.5
$\text{Al}_2\text{O}_3$	73.0	40.8	43.1
CaO	97.7	16.6	19.3
MgO	99.4	22.0	26.2
$\text{TiO}_2$	100.0	29.1	31.8

### 7.3.2.5 Product compositions

Table 7-6 shows the contents of inorganic gases and coke in the products of each catalyst. In the DO of oleic acid under the tested conditions, DCO occurred more often than decarboxylation. Tani et al. [31] found similar results: when palm oil was upgraded by silica and MgO-silica catalysts, DO occurred more by DCO than by dehydration. During the same process, however, higher yields of  $\text{CO}_2$  were obtained in comparison to CO yields [31]. CaO is a good dehydrogenation catalyst because of its high hydrogen production ability. CaO is also an exception due to its low carbon monoxide high carbon dioxide contents and high coke content. As for the other catalysts, more active sites

resulted in higher concentrations of hydrocarbon gases and coke. When the reaction temperature was at 470 °C, CaO reacted with CO<sub>2</sub>, producing CaCO<sub>3</sub> (see Figure 7-1). The water gas shift reaction was then accelerated, resulting in carbon monoxide and water being consumed to release CO<sub>2</sub> and H<sub>2</sub>.

Table 7-6 Inorganic gas and coke contents

Concentration (wt%)	Quartz	Al <sub>2</sub> O <sub>3</sub>	TiO <sub>2</sub>	CaO	MgO
CO <sub>2</sub>	1.5	5.3	5.1	11.4	2.6
CO	2.6	8.8	8.8	0.5	4.8
H <sub>2</sub> *10	1.6	8.1	18.6	22.3	1.0
Coke	0.0	0.7	0.3	7.1	0.8

Table 7-7 shows the contents of gas hydrocarbons in the products. C1-C3 olefin and paraffin were the principal organic gas products. Generally, the olefin content was higher than the paraffin content for each carbon number. Only the CaO upgraded product showed different results – the content of methane was relatively higher than all other organic gases. This might have occurred due to the high concentrations of hydrogen reacting with CO to form methane. It is worth noting that the content of paraffin upgraded by CaO was higher than the content of olefin upgraded by CaO for each carbon number. The high concentrations of hydrogen may have led to olefin being saturated in the CaO upgrading process. Idem et al. observed a similar phenomenon when they compared the gas products upgraded by silica and silicalite [84]. Other authors have

mentioned that the hydrogenation of C=C bonds may occur, even under an inert gas [147-149].

Table 7-7 Organic gas product compositions

Concentration (wt%)	Quartz	Alumina	Titania	CaO	MgO
CH <sub>4</sub>	0.15	0.46	0.37	1.15	0.27
C <sub>2</sub> H <sub>4</sub>	0.27	0.48	0.36	0.49	0.38
C <sub>2</sub> H <sub>6</sub>	0.15	0.50	0.36	0.86	0.27
C <sub>3</sub> H <sub>6</sub>	0.20	0.61	0.33	0.45	0.31
C <sub>3</sub> H <sub>8</sub>	0.08	0.44	0.20	0.56	0.14
C <sub>4</sub> H <sub>8</sub>	0.10	0.21	0.16	0.24	0.17
C <sub>4</sub> H <sub>10</sub>	0.03	0.19	0.09	0.37	0.07
C <sub>5</sub> H <sub>10</sub>	0.07	0.25	0.12	0.20	0.12
C <sub>5</sub> H <sub>12</sub>	0.06	0.05	0.10	0.32	0.13
C <sub>6</sub> H <sub>12</sub>	0.06	0.06	0.18	0.11	0.18
C <sub>6</sub> H <sub>14</sub>	0.03	0.11	0.11	0.17	0.13

The group and elemental compositions of the oil products are shown in Figure 7-4 and Table 7-8.

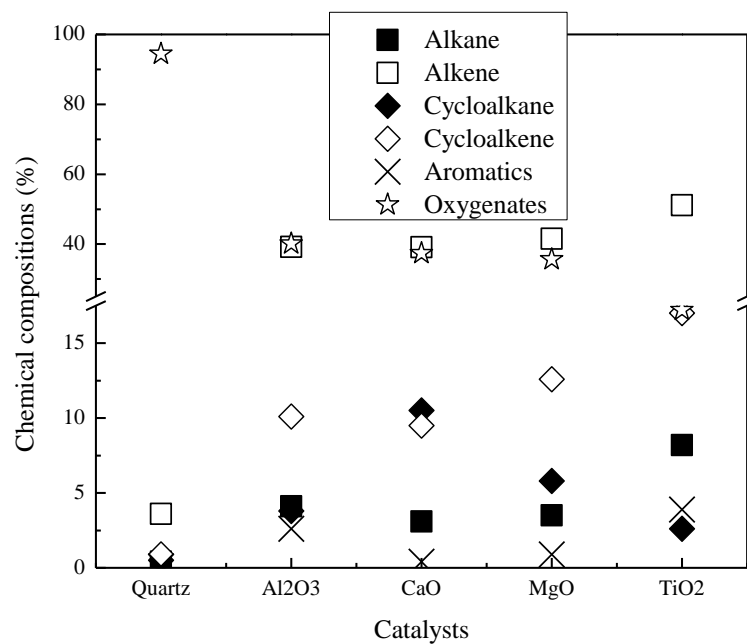


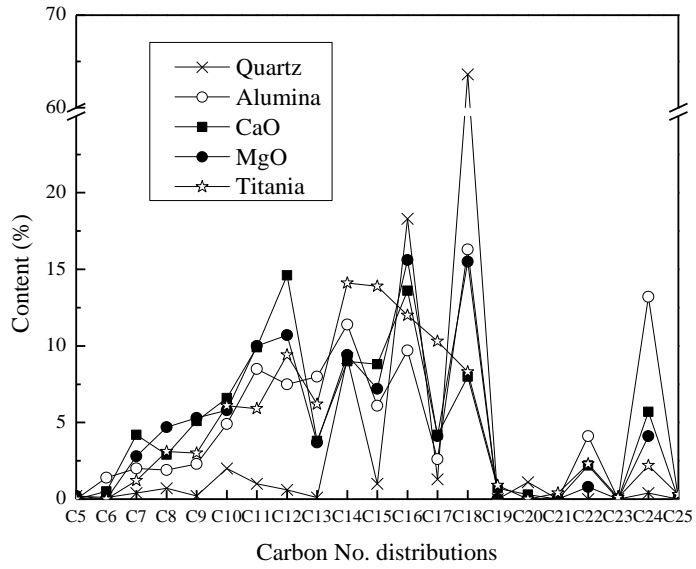
Figure 7-4 Chemical compositions of liquid products

Table 7-8 Liquid product elemental compositions

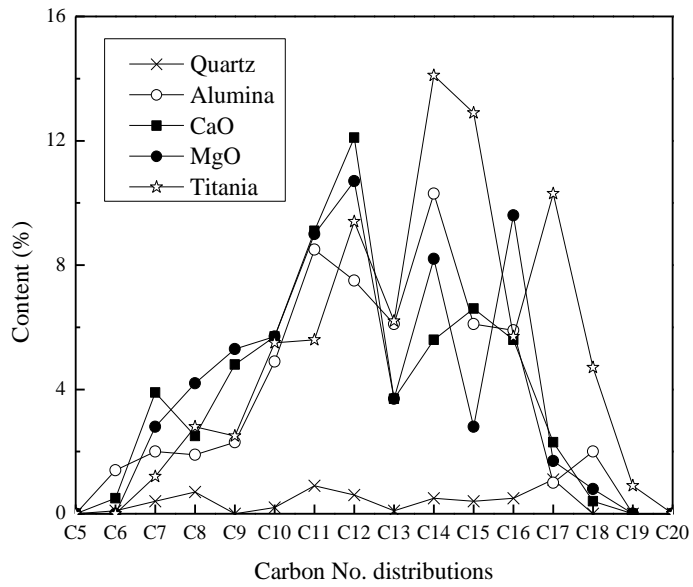
Content (%)	Quartz	Al <sub>2</sub> O <sub>3</sub>	CaO	MgO	TiO <sub>2</sub>
Oxygen element	9.9	3.7	0.9	0.1	0.0
Mol. Ratio of H/C	1.87	1.83	1.75	1.80	1.81

The carbon numbers distributions of OLPs, and the carbon number distribution of hydrocarbons in OLPs are shown in Figure 7-5. In general, the occurrence of chemical compounds in the products did not differ greatly between acidic and alkaline catalysts. The OLPs contained hydrocarbons between the ranges of C6 to C18, and C22 to C24. These hydrocarbons included alkanes, alkenes, cycloalkanes, cycloalkenes, aromatics,

and oxygenates. Most oxygenates could be removed by using acidic and alkaline catalysts. The oils with the lowest oxygenate contents (in order of increasing oxygen content) were those produced by using titania, followed by MgO and CaO, and then by alumina. It was easy to determine the low aromatic contents and small differences in hydrogen/carbon molar ratios in the products upgraded by acidic and alkaline catalysts. Oxygen content corresponded well with oxygenate content for all oil products. Demirbas et al. [150] reported the same trend, as well as low concentrations of aromatics.



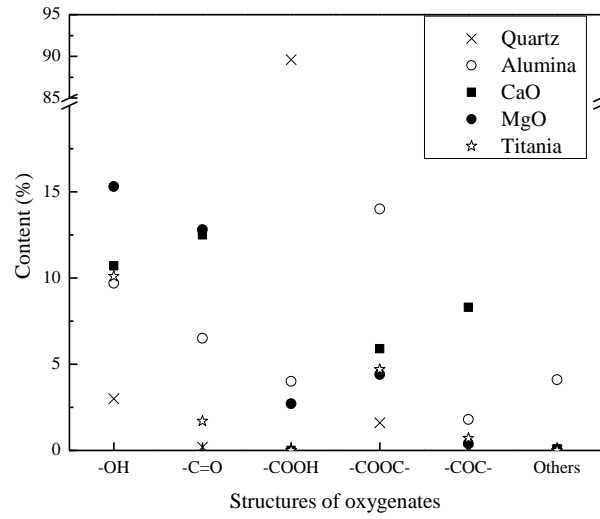
(a) Total liquid products



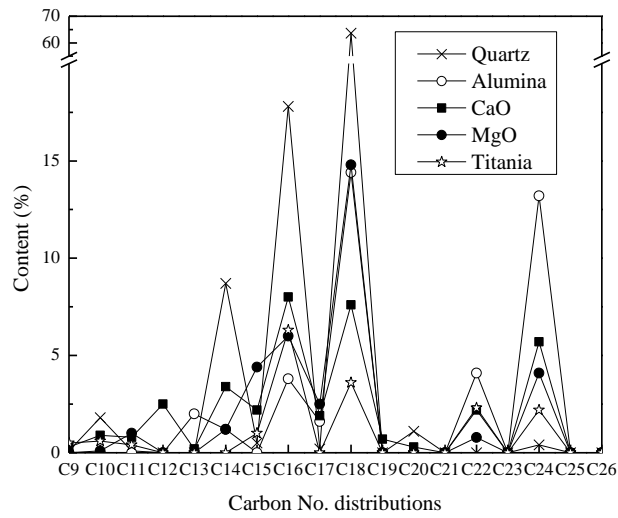
(b) Hydrocarbons in liquid products

Figure 7-5 Carbon No. distributions

The oxygenate compositions of the oil products are shown in Figure 7-6 and Table 7-9.



(a) Structures of oxygenates



(b) Carbon No. distributions of oxygenates

Figure 7-6 Structures and carbon No. distributions of oxygenates in liquid products

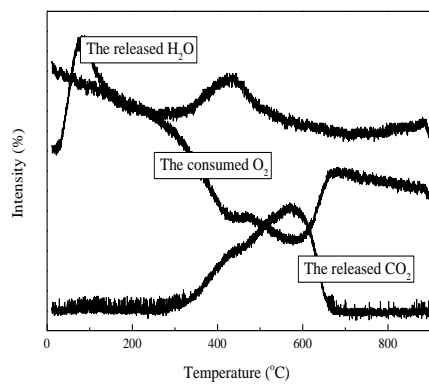
Table 7-9 Oxygenate compositions

Content (wt%)	Quartz	CaO	MgO	Al <sub>2</sub> O <sub>3</sub>	TiO <sub>2</sub>
Acid	89.6	0.0	2.7	4.0	0.0
Alcohol	3.0	10.7	14.2	9.7	9.7
Ketone	0.2	11.1	6.1	0.8	1.7
Di-ester	0.5	5.8	4.4	14.0	2.2
Di-epoxide	0.0	3.7	0.4	1.8	0.7
Aldehyde	0.0	1.4	6.7	5.7	0.0
Epoxide	0.0	4.1	0.0	0.0	0.0
Ester	1.1	0.1	0.0	0.0	2.5
Furan	0.0	0.5	0.0	0.0	0.0
Di-alcohol	0.0	0.0	0.8	0.0	0.4
Phenol	0.0	0.0	0.3	0.0	0.0
others(4-ketone+2-phenol)	0.0	0.1	0.0	4.1	0.0
sum	94.4	37.4	35.6	40.1	17.2

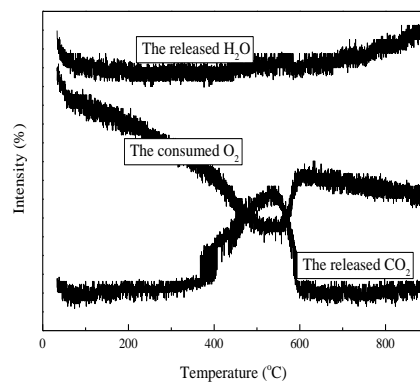
Aldehydes, esters, ketones, and alcohols were found in the OLPs. Certain amounts of di-epoxides, epoxides, acids, and esters were present in some samples. Low conversions and high concentrations of fatty acids were achieved when working with quartz. It was noted that there was 4.1 % 1',4-dihydroxy-2,3'-dimethyl, [1,2'-Binaphthalene]-5,5',8,8'-tetrone in the products upgraded by alumina. Ketones and aldehydes were found in the catalytic reactions, but were not detected during thermal cracking. Esters were found to be present during both catalytic and non-catalytic reactions.

Figure 7-7 shows the TPO analysis results of all investigated catalysts except for the quartz. The reason why quartz was omitted was that no oxygen was consumed and no water or CO<sub>2</sub> was released during its use (the same applies to oxygen TGA results in Figure 7-8).

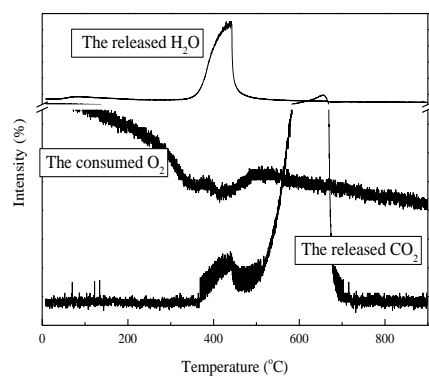
As shown in Figure 7-7, the different catalysts exhibited significantly different TPO results. For the alumina results, the water that was released below 250 °C should have been the water that was later absorbed by the alumina. The weight loss observed between 250 °C and 700 °C was due to the production of coke – because oxygen was consumed within this range. For titania, the TPO results were very simple and clear: only coke was burnt out in the range of 300-600 °C. For CaO, the water and CO<sub>2</sub> that was released when the temperature was lower than 500 °C were from coke; when the temperature was higher than 500 °C, the CO<sub>2</sub> released should have come from the decomposition of CaCO<sub>3</sub> because no oxygen was consumed during this time. The MgO results were similar to the CaO results in which only the temperature and the amount of CO<sub>2</sub> released from the metal carbonate differed. For MgO, coke was burnt out when the temperature was higher than 400 °C, and CO<sub>2</sub> was released from MgCO<sub>3</sub> in the temperature range 150-400 °C. All relevant calculations, such as those used to determine the amounts of produced water, CO<sub>2</sub>, and coke content, were based on these TPO results.



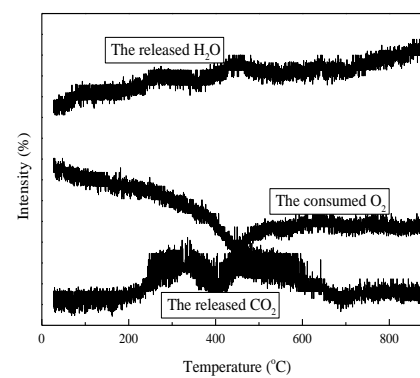
(a) TPO of spent  $\text{Al}_2\text{O}_3$



(b) TPO of spent  $\text{TiO}_2$



(c) TPO of spent  $\text{CaO}$



(d) TPO of spent  $\text{MgO}$

Figure 7-7 TPO results of spent catalysts

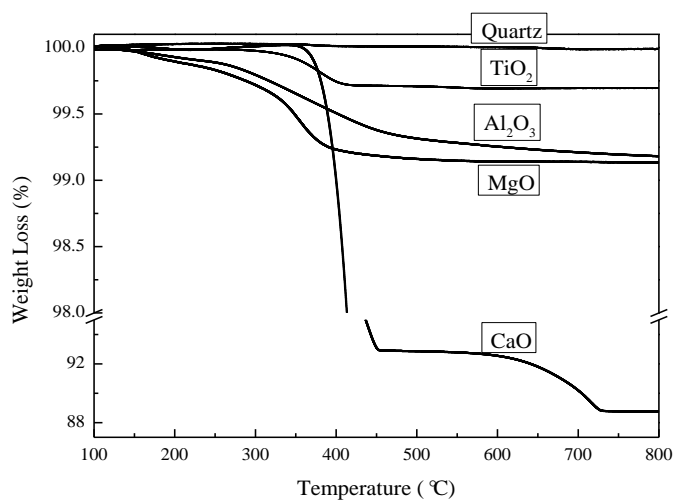


Figure 7-8 Weight loss of spent catalysts

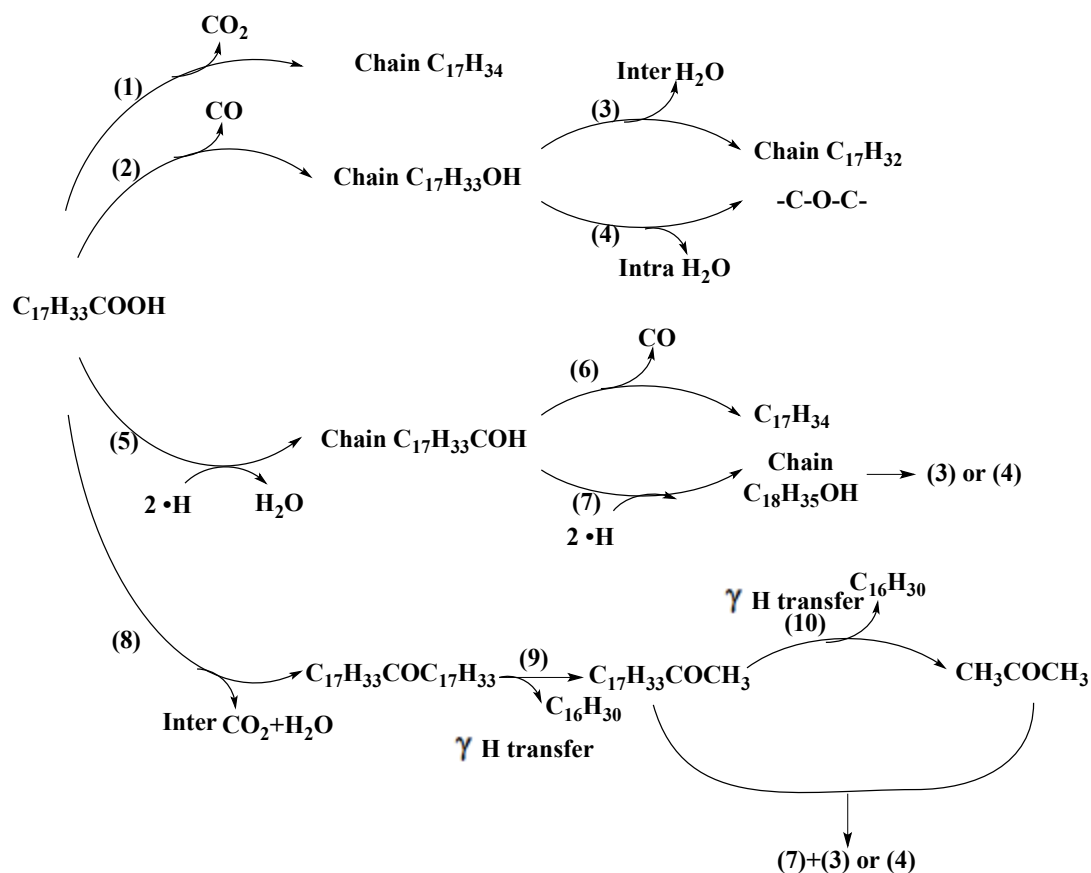
### 7.3.3 Reaction pathways

The molarity compositions of the DO products are shown in Table 7-10. As seen in the table, the DO of oleic acid under nitrogen at 470 °C mainly proceeded via DCO, which was indicated at by the high carbon monoxide yield. DCO<sub>2</sub> also occurred, as demonstrated by the presence of carbon dioxide (also shown in Table 7-6). As discussed previously, CaO was an exception among all the other catalysts, favoring DCO<sub>2</sub> over DCO.

Table 7-10 Molarity compositions of DO products

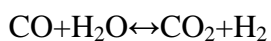
Molarity (mol/mol oleic acid)	CO	CO <sub>2</sub>	H <sub>2</sub> O
Quartz	0.13	0.05	0.06
CaO	0.02	0.89	0.00
Al <sub>2</sub> O <sub>3</sub>	0.52	0.21	0.19
MgO	0.82	0.27	0.30
TiO <sub>2</sub>	1.11	0.39	0.14

The deoxygenation pathways that occur during the treatment of oleic acid using metal oxide catalysts are summarized in Scheme 7-1: (1) oleic acid undergoes decarboxylation to form C17 mono-alkene and CO<sub>2</sub>; (2) decarbonylation occurs forming alcohol – this is followed either by inter-molecular dehydration to form C17 di-alkene, CO, and H<sub>2</sub>O, or intra-molecular dehydration to form –C-O-C- and water; (3) dehydration occurs and is either followed by decarbonylation to form C17 mono-alkene, CO, and H<sub>2</sub>O, or further dehydration to form alcohol; (4) intra-molecular decarboxylation and dehydration occur to form symmetrical ketones – this is followed by a  $\gamma$ -hydrogen transfer to release methyl ketones and C16 di-alkene, followed by another  $\gamma$ -hydrogen transfer by rearrangement or reduction to form alcohol.



Scheme 7-1 Oleic acid deoxygenation pathways over metal oxide catalysts

As discussed in Section 7.2.2.4,  $H_2$  can be formed by the dehydrogenation of oleic acid or its intermediates, and can be present on the catalyst surfaces. Hydrogen may then undergo a water-gas-shift reaction (Reaction 7-1) with  $CO_2$  the product of decarboxylation. Gosselink reported the same findings [147].



Reaction 7-1

### 7.3.3.1 Acidic catalysts

Alumina and titania catalysts were used to evaluate the effects of acidity on product distribution. Compared to other catalysts, yields of various products and compositions of gas products obtained with these two acidic catalysts were very close. This is because both had relatively high surface areas, large pore volumes, rich pore structures, and proper amounts and strengths of acidic sites; both also shared the same acid type (L acids only).

However, the titania and alumina catalysts differed in a few ways. The compositions of hydrogen and OLP obtained from titania (which had a higher acidity and strength) were significantly larger than those obtained from alumina. This is shown in Table 7-6 (which compares the hydrogen compositions of different catalyst products). This result is in accordance with the chemical composition of OLPs shown in Table 7-8 and Figure 7-4 – these show that the unsaturated hydrocarbon (alkene, cycloalkane, and aromatic) contents of the OLP upgraded by titania were much higher than the respective contents of the OLP upgraded by alumina. Moreover, the amount of oxygenates found in titania upgraded OLP was much lower than that of alumina upgraded OLP. These results show that more dehydrogenation and DO reactions occurred when using titania as opposed to using alumina; this may have been due to the fact that titania contained a higher amount of acidic sites. Table 7-4 shows that the gas hydrocarbon yield obtained for titania was also higher than that obtained for alumina. This can be attributed to over-cracking due to the high amount and strengths of acidic sites on the titania catalyst. The high degree of

aromatization reactions that occurred within the pores on the titania catalyst happened due to the larger average pore diameters (shown in Table 7-2).

As shown in Table 7-9, Figure 7-6, Scheme 7-1, and Table 7-10, the main mechanism in the DO of oleic acid into aliphatic hydrocarbons using acidic catalysts (L acids only) was DCO (step 2 in Scheme 7-1); the reaction limiting step was the dehydration of alcohols (step 3 in Scheme 7-1) because of the high concentrations of alcohols existing in acidic catalyst OLPs. This result agreed with the hydrocarbon no. distributions of the titania and alumina products. The product of DCO, C17 hydrocarbon, underwent cracking following the free radical mechanism to produce C14. C14 was the most prevalent hydrocarbon found in the acidic catalyst oil products (shown in Figure 7-5(b)).

### **7.3.3.2 Neutral catalyst**

Analysis of the gas products obtained by upgrading with quartz showed the existence of CO and CO<sub>2</sub>. This indicates that DO reactions proceeded through both DCO and DCO<sub>2</sub> mechanisms [151]. Analysis of the liquid products revealed that alkenes and fatty acids were the primary products. Fatty acids were especially prevalent – their content was as high as 94.4 %, with compound sizes of C18 (65 %), C16 (18 %), and C14 (8 %). Analysis of the oxygenates in the OLP showed a mixture of alcohols, esters, and acids. Results indicated that, at 470 °C and using a quartz catalyst, the rate of oleic acid conversion to the corresponding symmetrical ketone was low. This was indicated by the lack of ketones in the OLPs; Billaud obtained similar results [152]. Nearly no aromatic compounds and only a small number of alkane and cycloalkane species were detected in

the products, which implies that little secondary thermal cracking occurred. All of these results agree with previous research [153]. Considering the yields and compositions obtained by all investigated catalysts, the presence of catalyst reduced the amount of liquid product obtained and caused further removal of the acid group [81].

### **7.3.3.3 Alkaline catalysts**

Calcium oxide and magnesium oxide catalysts were used to assess the effects of basicity on product distribution. The yields of various products and the compositions of gas and OLPs are shown in Figure 7-4 to Figure 7-8 and Table 7-4 to Table 7-9. Compared to other catalysts, the OLP yields, the coke yields, the gas hydrocarbons yields, the oxygen removal rates, the compositions and carbon number distributions of the OLPs, and the oxygenate contents in the OLPs were very similar between the CaO and MgO products. This may be due to the similar surface areas, pore volumes, and active sites that the two basic catalysts share. There was a difference, however, between the water, carbon oxide, and hydrogen yields of calcium oxide and magnesium oxide. As discussed in section 7.2.2.5, CaO could have reacted with CO<sub>2</sub> at temperatures of around 470°C producing CaCO<sub>3</sub> (see Figure 7-1), and the water-gas-shift reaction could have subsequently been accelerated. This would have resulted in carbon monoxide and water reacting to release CO<sub>2</sub> and H<sub>2</sub>, explaining the higher yields and concentrations of carbon oxide and hydrogen found in CaO than in MgO products. CaO exhibited a relatively high dehydrogenation capability, which could be confirmed by the higher aromatic, cycloalkane, and alkene concentrations in its products. The MgO product contained more water than the CaO product – this could have been due to the production of free radicals

on the MgO surface that reacted with oxygenates to release water. Additionally, the CO<sub>2</sub> produced during the MgO catalytic process may have reacted with H<sub>2</sub> to form CO and H<sub>2</sub>O. This conclusion was supported by the high concentrations of CO and H<sub>2</sub>O, as well as the low concentrations of CO<sub>2</sub> and H<sub>2</sub> found in the MgO products. Differing from literature [84], the alkaline catalysts used in this study did not inhibit secondary cracking, which could have been indicated by low oil and high gas yields.

The amounts of fatty acids left in the liquid products upgraded by alkaline catalyst were drastically lower than in all the other catalyst products except for that of titania. This was probably due to the saponification of the fatty acid by the base [81]. However, the removal of the acid functions in the products did not necessarily lead to the complete elimination of oxygen groups. The liquid products still consisted of ketones and aldehydes with –C=O, alcohols with –OH, esters (especially di-esters) with –COOC-, and epoxides (especially di-epoxides) with –C-O-C-. This is shown in Figure 7-6 and Table 7-9.

MgO and CaO promoted the decarboxylation reaction to produce more CO<sub>2</sub> and hydrocarbons. The explanation is as follows: MgO/CaO can form into MgCO<sub>3</sub>/CaCO<sub>3</sub> through a reaction with carboxylic acid (step 1 and 8 in Scheme 7-1). CaCO<sub>3</sub> is stable enough; therefore, high temperatures (>700 °C) are needed to decompose it back to CaO (the reaction temperature was 470 °C) [154]. However, MgCO<sub>3</sub> was able to be easily decomposed into CO<sub>2</sub> and MgO under the reaction conditions. In practice, the TGA-MS

analysis results (Figure 7-1) showed that both  $\text{MgCO}_3$  and  $\text{Mg(OH)}_2$  could be decomposed into  $\text{MgO}$  at  $450\text{ }^\circ\text{C}$ .

As shown in Table 7-9, Figure 7-6, Scheme 7-1, and Table 7-10, the main mechanism for the DO of alkaline catalysts to produce chain hydrocarbons was decarboxylation (step 1 and 8 in Scheme 7-1). The least occurring reactions were the reduction of ketones into alcohols and the dehydration of alcohols – this was deduced from the high contents of ketones and alcohols found in the alkaline catalyst upgraded OLPs.

#### **7.3.3.4 Aromatization**

As shown in Figure 7-4 and Table 7-8, the aromatic contents of all the catalyst products (neutral, base, L acids only) were lower than 3.9 wt%. Thus, the similarities between the product distributions of the acidic catalysts (titania and alumina) and all the other catalysts show clearly that L acids were not a dominating factor in the aromatization of oleic acid.

Cerny et al. observed that there was over 40 % and around 85 % aromatics in the  $<150\text{ }^\circ\text{C}$  and  $>150\text{ }^\circ\text{C}$  fractions when they upgraded USY with equal amounts of B and L acid catalyst [145]. Omar et al. found that when upgrading fatty acids, adding ZSM-5 catalyst (with both B and L acids) produced an appreciable quantity of aromatic compounds. They proposed that aromatics were produced either from cycloalkenes or alkenes that were promoted by catalyst addition [153]. Therefore, it is likely that the existence of B acids on the catalyst increased the formation of aromatics [155]. Frety et al. came to the

same conclusion. Sometimes L and B acids can change into one another during the reaction process in the presence of water – this could explain the higher yields of aromatic hydrocarbons obtained when the titania and alumina catalysts (L acids only) were used, compared to both the quartz (non-acid catalyst) and alkaline catalysts.

Li et al. [156] found that, at high temperatures, higher amounts of aromatics were obtained from the catalytic pyrolysis of cottonseed rather than from the thermal pyrolysis of the same substance at the expense of the olefins in the gasoline fraction. Padamaja et al. observed the same phenomena [157]. Idem et al. suggested that the larger aromatic yields were due to mild secondary cracking reactions within the catalyst pores with high shape selectivity [84]. In addition, Omar et al. found that high power treatment (by microwave [153]) may be another reason for why aromatics might form on catalyst surfaces that do not contain B acids.

#### **7.4 Conclusions**

Under an inert N<sub>2</sub> atmosphere, the liquid product yields of different catalysts were found to be between 29.0 wt% and 93.4 wt% of the feed, but could have been lower depending on which active sites were used. The catalysts with the highest oxygen removal capabilities (97.7-100.0 wt%) were CaO, MgO, and titania, whereas the catalyst with the lowest oxygen removal capability (18.5 wt%) was quartz. Even though the oxygen removal rate of the alumina reaction only reached 73.0 wt%, the light oil yield and the valuable product yield were the highest among all investigated catalysts. Liquid products were composed mainly of hydrocarbons ranging from 6 to 18 in the terms of carbon

number. Oxygenates were also present with carbon numbers of 10 to 18, 20, 22, and 24. The majority of hydrocarbons in the OLPs were found to be alkenes and cycloalkenes, and there were also cycloalkanes and alkanes present in smaller amounts; aromatic contents were all lower than 3.9 wt%. DC was the dominating DO reaction that occurred under the tested conditions. Acidic catalysts deoxygenated the feed compounds into aliphatic hydrocarbons by DCO; the reaction-limiting step was the dehydration of alcohols. Increasing the acidity of the catalysts was beneficial to DO, but it also benefitted secondary cracking. Alkaline catalysts deoxygenated the feed compounds into chain hydrocarbons by DCO<sub>2</sub>; the lowest occurring reactions were the reduction of ketones to alcohols and alcohol dehydration. The saponification of oleic acid by the alkaline catalysts also occurred. CaO had a higher dehydrogenation capability than MgO, but the hydrogen free radicals on the MgO surfaces were more effective at reacting with oxygenates to release water. The existence of B acids was found to be important in the formation of aromatics.

## **Chapter 8 High deoxygenation and low aromatization performance of kaolin-based cracking catalysts for WCO upgrading**

### **8.1 Introduction**

Kaolin is an abundant material with some mild acidic sites. Researchers have found that using treated kaolin [93] as a catalyst can improve coke selectivity and yield distribution, significantly reduce sulfur content in the petroleum catalytic cracking gasoline products [94], and enhance metal tolerance performance during the petroleum cracking process [95, 96]. Furthermore, if kaolin-based catalysts can work well with the WCO upgrading process, then irreversible catalyst deactivation should no longer be a problem because these catalysts have been proven to work well even under severe petroleum catalytic cracking conditions [15-20]. This research investigates the effect of the treatment of kaolin (thermal treatment and chemical treatment) on WCO catalytic cracking upgrading. The aim is to produce high yield, low oxygen content, and low aromatic content diesel fraction OLP.

### **8.2 Experimental**

As discussed in section 3.3.4.1, ATK was prepared from natural kaolin (calcined at 800 °C) and then treated by an HCl solution. BTK was prepared from natural kaolin (calcined at 1000 °C) and an NaOH solution. PTK was dried overnight in an oven at 105 °C and was not chemically but thermally treated (during the matrix preparation process in section 3.3.4.2), whereas ATK and BTK were undergone both thermally and chemically treated.

The performance evaluation of the novel catalysts was carried out under these conditions: a water inlet flow rate of 3 ml/min, a temperature of  $470 \pm 3$  °C, a mass ratio of catalyst to feed of  $3.3 \pm 0.3$ , and a weight hourly space velocity of  $10.5 \pm 1.2$  h<sup>-1</sup>.

## 8.3 Results

### 8.3.1 Kaolin treatments

Figure 8-1 shows the weight loss, derived weight, and amount of released water observed during kaolin treatment over a large temperature range. Weight loss mainly occurred between 400-700 °C – this matched very well with the location of the released water curve. During this process, alumina and silica could be released [94, 158]. Therefore, acid and alkaline solutions were used to extract the released alumina and silica, respectively.

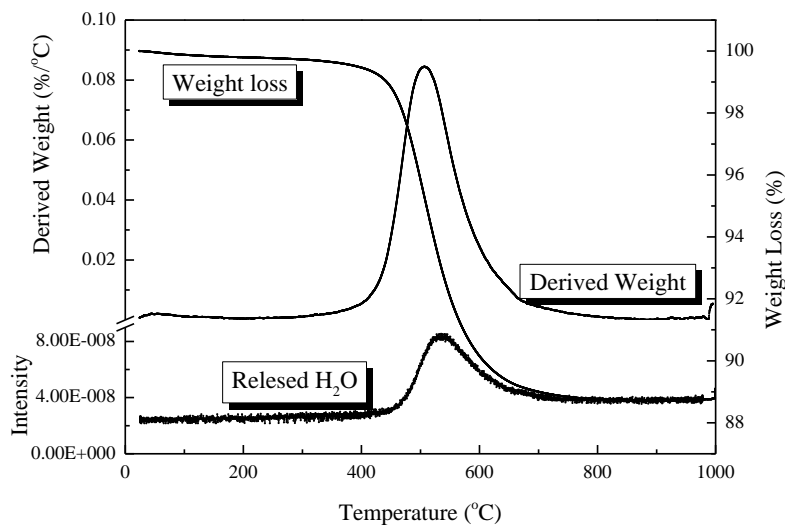


Figure 8-1 Thermal treatment of kaolin

The X-ray diffraction patterns of the kaolin-based catalysts are shown in Figure 8-2. The natural kaolin was primarily composed of kaolinite and quartz. The peaks at 12° and 24° were assigned to the hydroxyl stretching vibrations peaks of kaolinite [96, 159]. These peaks disappeared after treatment, even in PTK (which was only thermally treated at 550 °C). The crystalline nature was destroyed during thermal treatment and therefore treated kaolin changed into amorphous. CC was also found to be amorphous from its respective XRD spectrum. In Figure 8-2, the vibration of alumina was obviously observed in BTK and CC. This means alumina could have been exposed after both thermal treatment and alkaline extraction had already occurred.

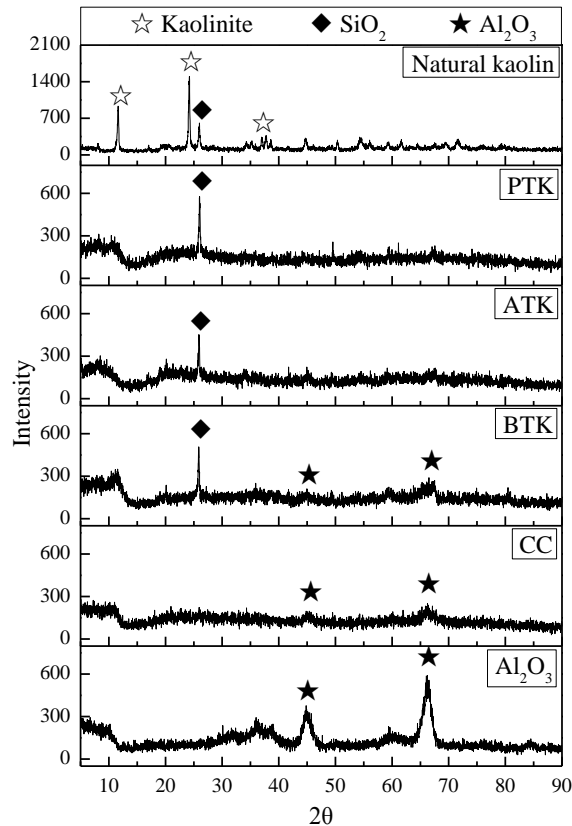


Figure 8-2 XRD patterns

## 8.3.2 Catalyst characterization

### 8.3.2.1 Acid type, amount, and density

Table 8-1 shows the acid type, amount, strength, and density of acids of the different catalysts. Concerning the states of the treated kaolin catalysts during reaction, the acidity of ATK and BTK both decreased. This happened in BTK especially – its total amount of acidity was halved over the course of the alkaline treatment. Although natural kaolin and PTK initially contained only weak acids, the strengths of these acids were increased after treatment. Therefore, both acid and base treatment generated medium and strong acidity in the catalysts. For ATK, the acidity decreased when alumina was removed from the acid treating process. For BTK, the acidity could have decreased due to the neutralization of acidic sites during the base treating process. The exposed alumina on BTK (shown in Figure 8-2) caused an increase in acid strength on BTK. CC has the highest acid density, followed by ATK and then PTK, and BTK has the lowest acid density among all of these catalysts.

Table 8-1 Acid properties of kaolin-based catalysts and CC

Properties	Acidity (*10 <sup>-2</sup> mmol/g)					
	Weak	Medium	Strong	Total	L	B
Natural kaolin	2.3	0.0	0.0	2.3	-	-
BTK	1.8	0.6	0.5	2.9	2.7	0.2
ATK	2.2	1.4	2.0	5.6	4.1	1.5
PTK	5.9	0.0	0.0	5.9	4.0	1.9
CC	29.8	14.0	4.1	47.9	24.4	23.5

\* calculated by the peak area at 150°C, other catalysts by the peak area at 100°C because of the small absorption peaks

All of the kaolin-based catalysts had relatively higher amounts of Lewis acid sites than those of B acidic sites. This was true for BTK, whose ratio of B acids to L acids was lower than 0.09. CC had around the same amounts of B and L acids. Other researchers have found the same results – acids found on kaolin-based catalysts are usually mainly Lewis acids [94, 96]. The trend of the catalyst acid densities from highest to lowest was CC > ATK > PTK > BTK. Both the kaolin-based catalysts and the CC catalyst had the same trend for total Lewis acid density, as well as for total B acidic density.

Although CC had the same total amount of B acids to Lewis acids, the ratios of B acids to L acids for CC were: 0.004 at 150 °C, 0.022 at 250 °C, 2.229 at 350 °C, and 2.542 at 450 °C. This indicated that weak acids were primary L acids whereas strong acids were mainly B acids. The pyridine absorption peaks of the kaolin-based catalysts near 1450  $\text{cm}^{-1}$  and 1540  $\text{cm}^{-1}$  disappeared at 250 °C. This was because the kaolin-based catalysts had relatively low amounts of acidic sites and pyridine was less alkaline than ammonia, meaning some weak acid sites could not be detected by pyridine (but were detectable by  $\text{NH}_3$ ). Another possible reason for the disappearances of the peaks is that the pyridine molecules were much larger than the ammonia molecules, and therefore pyridine could not fit through some small pores but ammonia could. This is in accordance with the micropore surface area results in Table 8-2: kaolin-based catalysts had much higher micropore surface areas compared to CC catalyst.

### 8.3.2.2 Physical properties

Table 8-2 summarizes the physical properties of the catalysts. All treatments improved both the surface area and the pore volume of the natural kaolin. CC had a relative higher surface area and a lower pore volume than the treated kaolin catalysts.

Table 8-2 Physical properties of kaolin-based catalysts and CC

Properties	Surface area (m <sup>2</sup> /g)	Pore volume (ml/g)	Micropore surface area (m <sup>2</sup> /g)
Natural kaolin	9.7	0.1	-
BTK	61.0	0.4	5.4
PTK	58.8	0.5	8.8
ATK	37.4	0.4	13.5
CC	179.3	0.2	8.1

### 8.3.3 Product distribution and oxygen removal rate

The product distributions and oxygen removal rates are shown in Table 8-3. The organic liquid yields and the gas hydrocarbon yields seem to be closely associated with the total acidity and acid densities of the catalysts. Higher liquid yields and lower gas hydrocarbon yields were achieved at lower total acidities and lower acid densities. Coke formation was affected more by the densities of the weak acids – higher density of weak acid caused higher coke yields to be produced. Among all the kaolin-based catalysts, acid treated kaolin was the most effective for DO: the oxygen removal rate increased from 81.8 % to 93.8 % when pretreated kaolin was replaced by ATK. BTK removed less oxygen than

ATK – its lower total acidity and lower acid density (in comparison to the other catalysts) may have been responsible for it.

Table 8-3 Product distribution and oxygen removal rate

Yield (wt%)	Organic liquid	Gas	Solid <sup>1</sup>	H <sub>2</sub> O	C <sup>2</sup> in H <sub>2</sub> O	Oxygen removal rate
BTK	82.6	4.9	2.3	5.2	1.3	59.5
PTK	74.4	4.0	6.5	9.3	1.7	81.8
ATK	74.4	4.8	4.8	10.2	1.5	93.8
CC	67.5	12.8	6.0	8.3	0.9	90.8

1: Calculated by weight loss between 200-650°C, drying under 160°C; 2: C-carbon

Close examination of the catalyst properties suggests that surface area and pore volume were not the key factors contributing to DO, whereas acid type, acid amount, acid density, and acid strength all strongly affected the oxygen removal rate. However, overly high acid properties also led to a decrease in the oxygen removal rate – this was shown by the lower oxygen removal rate of CC compared to that of ATK.

### 8.3.4 Product analysis

#### 8.3.4.1 Organic gases

The majority of gas hydrocarbon products were C1-C4 hydrocarbons (shown in Table 8-4). One of the reasons for the high concentration of C2 and C3 was the existence of glycerin (C3) structures in the WCO (shown in Table 3-1). Corma et al. [160] published

similar results that the contents of ethylene and propene were as high as 16 % and 56 % when an aqueous glycerol solution was upgraded by FCC equilibrium catalysts.

Table 8-4 Organic gas concentrations

Concentration (wt%)	ATK	BTK	PTK	CC
C1-C2	17.7	12.0	14.3	6.1
C3	7.7	3.7	13.6	26.0
C4	2.4	1.7	5.9	11.1
C5+	1.4	2.1	3.0	3.4
Sum	29.1	19.4	36.7	46.6

If C3 is not under consideration, C1 and C2 hydrocarbons were the most produced organic gases during the upgrading of WCO by kaolin-based catalysts. C4 was the primary organic gas product observed during the CC upgrading process. This indicates that different reaction pathways occurred when WCO interacted with different catalysts; this may have been correlated with the acidities and the type of acids on the catalysts. It is noted that PTK upgraded products contained relatively larger amounts of C3 and C4 (compared to the amounts of C1-C2) than ATK or BTK upgraded products.

#### 8.3.4.2 OLPs

Water content in the oil phase was tested by titration, and there was no water found in all OLPs. The elemental compositions of the OLPs are shown in Figure 8-3.

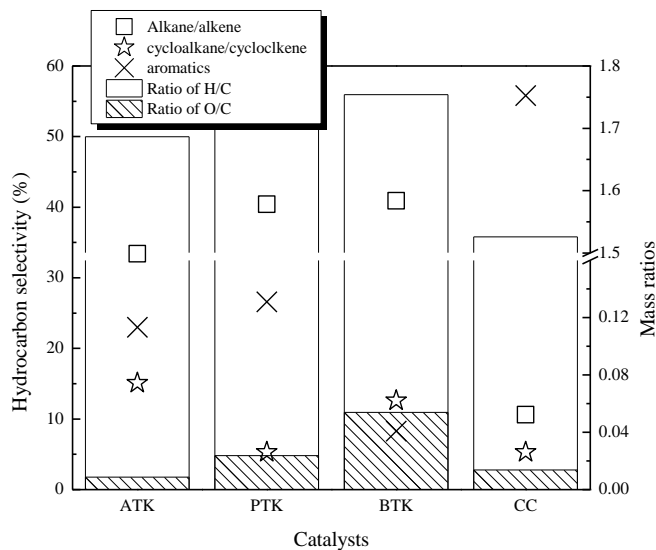


Figure 8-3 Hydrocarbon selectivity and mass ratios of elements

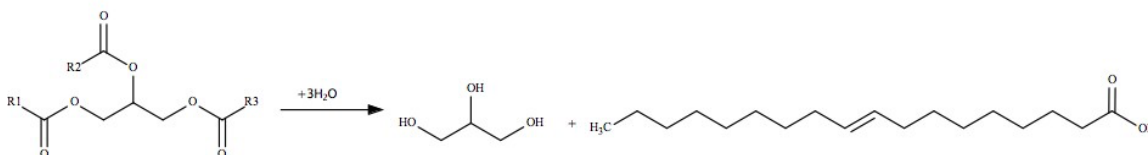
Low oxygen content was observed in all OLPs, except for the one that was upgraded by BTK. Compared to kaolin-based catalysts, the commercial catalyst had an impressive ability to eliminate oxygen. This was confirmed by the molar ratio of oxygen to carbon results.

In the CC upgraded OLP, the composition of aromatics was non-ideal because aromatic content was high (55.8 %) and the primary hydrocarbons found in the product (Figure 8-3). In contrast, chain hydrocarbons were the main components (accounting for 33.4-40.9 %) of the kaolin-based catalyst upgraded OLPs. These results further confirmed that

different reaction pathways occurred due to the switch between kaolin-based catalysts and CC.

## 8.4 Discussion

Using steam as a carrier gas, triglycerides were hydrolyzed into glycerol and fatty acids during the cracking process. Scheme 8-1 shows this process. Afterwards, the produced glycerol underwent dehydration, cracking, and hydrogen transfer reactions to form short oxygenates and gaseous hydrocarbons.



Scheme 8-1 Triglyceride hydrolysis process (oleic acid was used as an example)

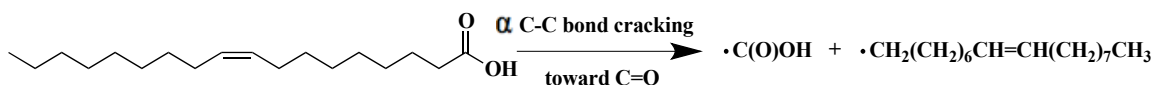
The produced fatty acids could undergo either oxygen-dependent reactions (DO) or oxygen-independent reactions (such as cracking and hydrogen transfers including cyclization, aromatization, and condensation).

### 8.4.1 Non-DO reactions

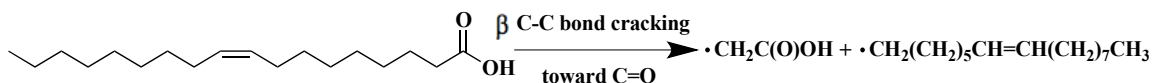
#### 8.4.1.1 Cracking

The bond dissociation energies of C-C bonds were the lowest in -COOH structures, higher in paraffins, and the highest in olefins [161]. The longer the chain, the lower the heat of formation – this meant that long chain compounds were much more reactive than

short chain compounds. Fatty acids were produced after the hydrolysis reaction; in Scheme 8-1, oleic acid was used as an example to illustrate the further reactions that the fatty acids underwent. C18, C17, and C16 could have been produced when DO followed dehydration, and the  $\alpha$  or  $\beta$  C-C bond toward C=O cracked.

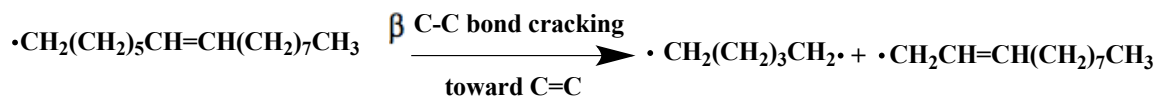


Scheme 8-2

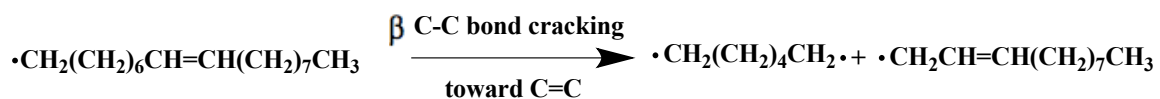


Scheme 8-3

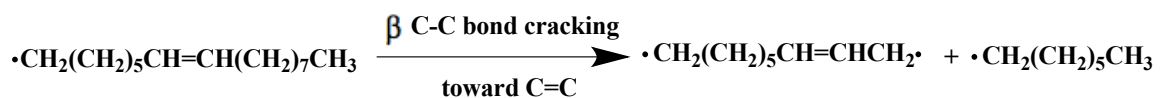
If the cracking reaction followed the free radical reaction mechanism, the  $\alpha$  or  $\beta$  C-C bond toward C=O (shown in Scheme 8-1) would have cracked, producing C(O)OH and C17 (Scheme 8-2) or CH<sub>2</sub>C(O)OH and C16 (Scheme 8-3); this occurred due to the low energies of formation. Subsequently, the remaining parts of the oleic acid would have undergone another  $\beta$  C-C bond (from C=C bond) cracking. This could have either occurred in the no. 7-8 C-C bond ( $\beta$  C-C bond from the other side of the C=C bond) to form C11 and C5 (Scheme 8-4) or C6 (Scheme 8-5), or in the no. 11-12 C-C bond to form C7 and C9 (Scheme 8-6) or C10 (Scheme 8-7).



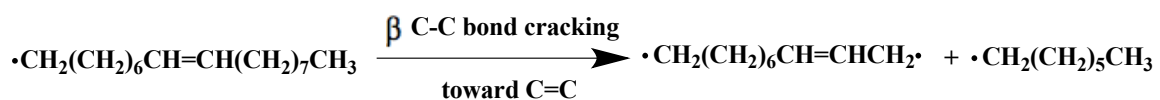
Scheme 8-4



Scheme 8-5



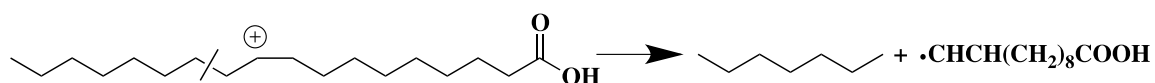
Scheme 8-6



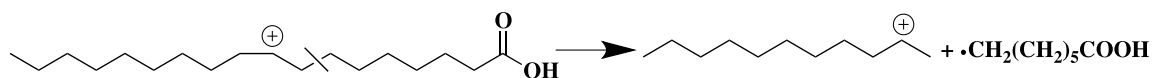
Scheme 8-7

If the cracking reaction followed the carbonium ion reaction mechanism, the first step would have been the formation of a carbonium ion (from carbon no. 9 and 10 in the original oleic acid, or carbon no. 3 or 4 when DO occurred due to the cracking of an  $\alpha$  or

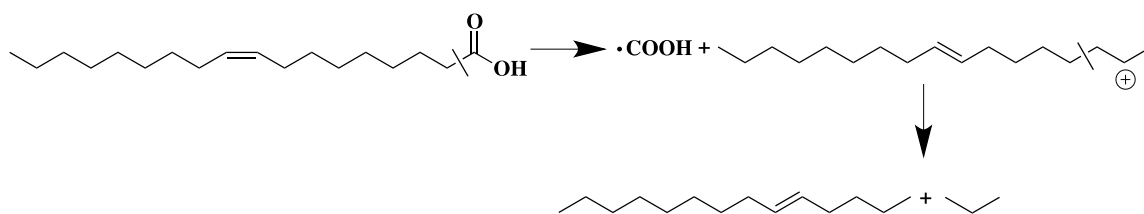
$\beta$  C-C bond toward C=O) from the protonation of the fatty acid's unsaturated bond on the acidic sites of the catalysts. This would have been followed by the cracking of the  $\beta$  C-C bond of C=C, which would have produced C7 and C11 (Scheme 8-8), C3 and C14 (Scheme 8-9) (or C4 and C13, (Scheme 8-10)), or C3 and C13 (Scheme 8-11) (or C4 and C12 (Scheme 8-12)). Schemes 8-9 to 8-12 show that the products could have existed in two different forms (8-9 or 8-10 and 8-11 or 8-12) because of the low stability of the primary carbonium ion, which could be later converted into a secondary or tertiary carbonium ion [162].



or



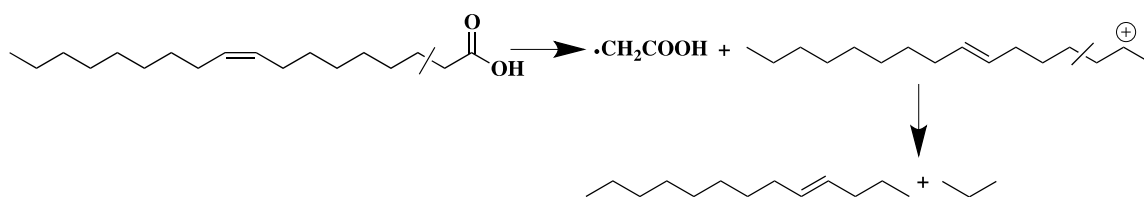
Scheme 8-8



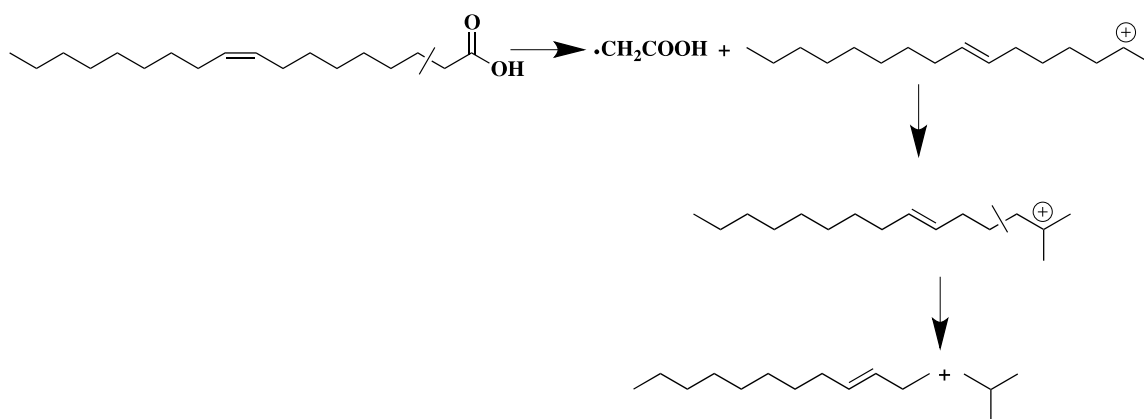
Scheme 8-9



Scheme 8-10



Scheme 8-11



Scheme 8-12

Figure 8-4 shows the carbon number distribution of OLPs and the carbon number distribution of oxygenates present in the OLPs. It is noticeable that the product distributions indicating cracking are highly associated with the catalyst used.

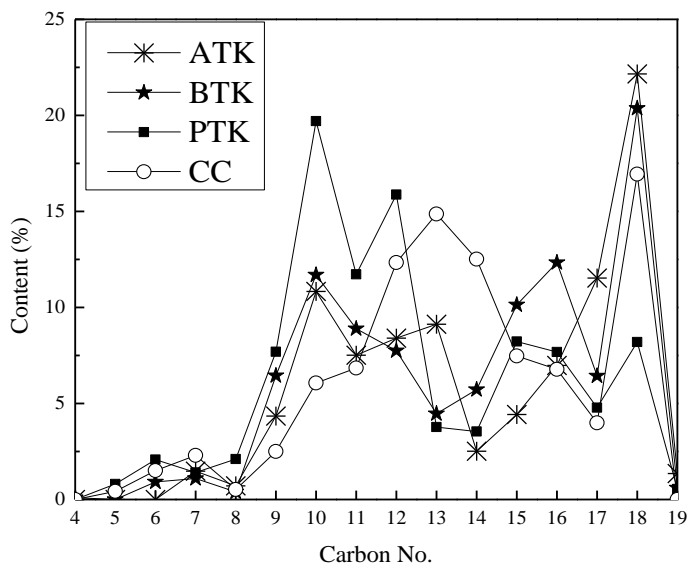


Figure 8-4 Carbon No. distributions of OLPs

HC: hydrocarbons

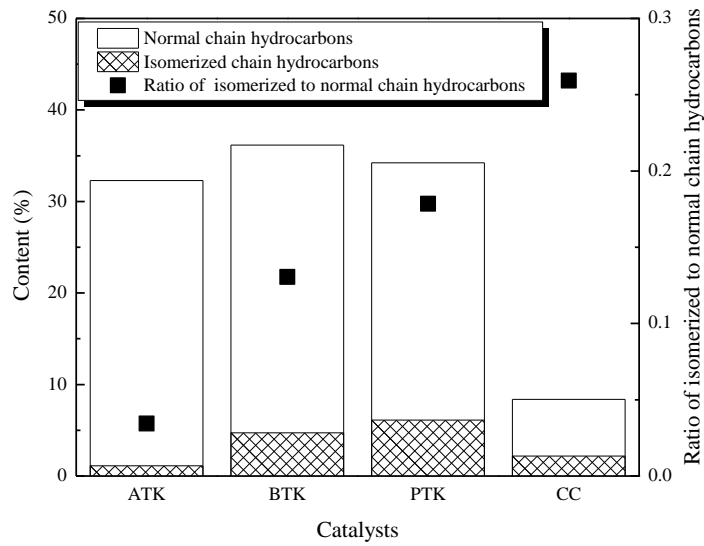
According to Figure 8-4, the carbon number distributions of all OLPs fell significantly into the diesel fraction (carbon numbers of 8 to 21) [163]. There were obviously some cracking reactions that occurred, and the products from cracking were concentrated in the carbon number ranges of 9-12 for kaolin-based catalysts, and 11-15 for CC.

CC caused a relatively lower liquid product content than the kaolin-based catalysts. This is in accordance with the OLP yield results in Table 8-3, which show that high acid density, high acidity, and a large amount of strong acids should have been responsible for this difference.

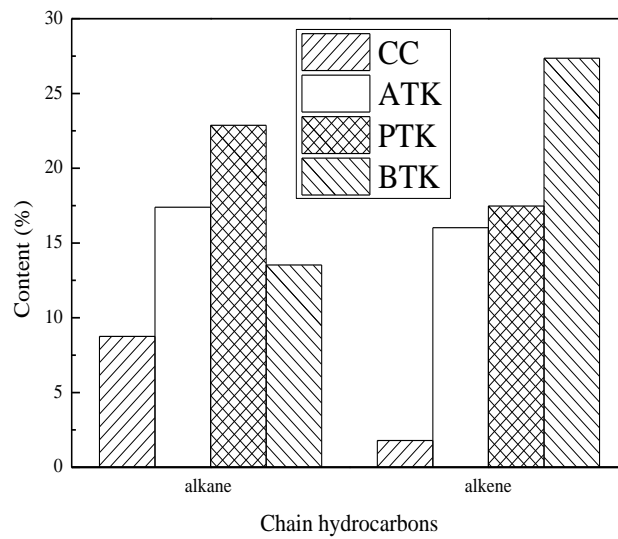
According to the carbon number distributions in Figure 8-4, all kaolin-based catalysts had a peak at carbon no. 10. This revealed that kaolin-based catalysts favored the free radical reaction mechanism. The CC upgraded OLP had its highest peak at carbon no. 13, which indicates that CC favored the carbonium ion reaction mechanism. It is worth mentioning that the PTK upgraded OLP had a peak at carbon no. 12, which was also one of the products of the carbonium ion reaction (see Scheme 12). The conclusion that PTK favored the carbonium ion mechanism to a certain degree was corroborated by the high concentrations of C<sub>4</sub> found in the PTK gas products (see Table 8-4). Antoine et al. [164] conducted research on C-C bond scissions in fatty acid methyl esters using density functional theory. They also observed  $\beta$  C-C bond breakages similar to the ones observed in the conducted experiments.

#### **8.4.1.2 Hydrogen transfer reaction**

In compliance with the carbonium ion mechanism, primary carbonium ions could also be converted into secondary or tertiary carbonium ions, to produce isomerized chain hydrocarbons by isomerization (Figure 8-5 (a)), alkenes by cracking (Figure 8-5 (b)), and cycloalkanes, cycloalkenes, and aromatics by cyclization and aromatization (Figure 8-6).



(a) Normal and isomerized chain HC



(b) Saturated and unsaturated chain HC

Figure 8-5 Compositions of chain hydrocarbons in liquid products

PTK and especially CC exhibited high hydrogen transfer activities compared to BTK and ATK, due to their relatively high contents of aromatic hydrocarbons including 1-3 rings aromatics (shown in Figure 8-6). Differences in hydrogen transfer activities may have been correlated with the different acid densities and acid strengths of the catalysts.

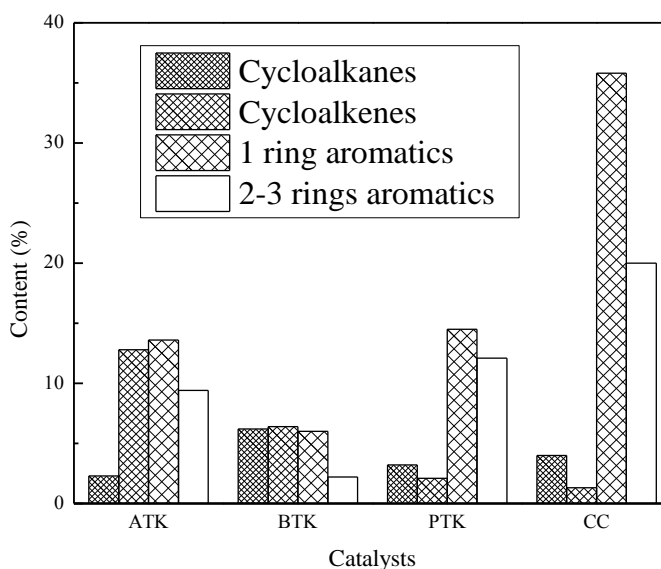


Figure 8-6 Distribution of ring hydrocarbons

Aromatization activity was lower in treated kaolin products than in pretreated kaolin and CC upgrading products. And, the former two produced higher amounts of cycloalkanes and cycloalkenes. This indicates that the treatments done to kaolin could have resulted in products with better reaction selectivity. Produced 1-ring aromatics could have been released or been further reacted to form 2-ring and 3-ring aromatics by condensation.

Only the CC upgraded OLP contained 3-ring aromatics, which indicates that CC had the highest hydrogen transfer capability. In the petroleum cracking process, strong B acids are favorable in the cracking of resids [165]. In the triglyceride cracking process, however, strong B acids promoted aromatization and condensation.

It is likely that CC upgrading primarily followed the carbonium ion reaction mechanism, because of the high concentrations of aromatics and iso-hydrocarbons found in the CC upgraded OLPs and the large amounts of C3 and C4 found in the gas products. Kaolin-based catalysts more readily followed the free radical reaction mechanism, because of the high concentrations of alkanes and alkenes (especially alkenes) as well as the high concentrations of C1 and C2 found in the products (shown in Table 8-4, Figure 8-3, and Figure 8-5 (b), respectively). This may have also depended on the acid types, densities, and strengths of the catalysts. CC was primarily composed of strong B acids, whereas the acids on kaolin-based catalysts were mainly L acids.

#### **8.4.2 DO reactions**

Table 8-5 shows the molarity ratios of CO, CO<sub>2</sub>, and H<sub>2</sub>O (based on per mol of WCO). The molecular weight of WCO was assumed to be 884 g/mol because it contained 91 wt% of C18 fatty acids, and 71 wt% of it was comprised of oleic acid (see Table 3-1 and Figure 3-5).

Table 8-5 Molarity compositions of DO products<sup>1</sup>

Molarity (mol/mol WCO)	ATK	PTK	BTK	CC
CO <sub>2</sub>	0.3	0.3	0.6	0.3
CO	0.9	0.9	1.0	0.9
H <sub>2</sub> O	5.0	4.6	2.6	4.1
H <sub>2</sub> O-CO	4.2	3.7	1.6	3.2
Dehydration/DCO <sub>x</sub> <sup>2</sup>	3.6	3.0	1.0	2.6

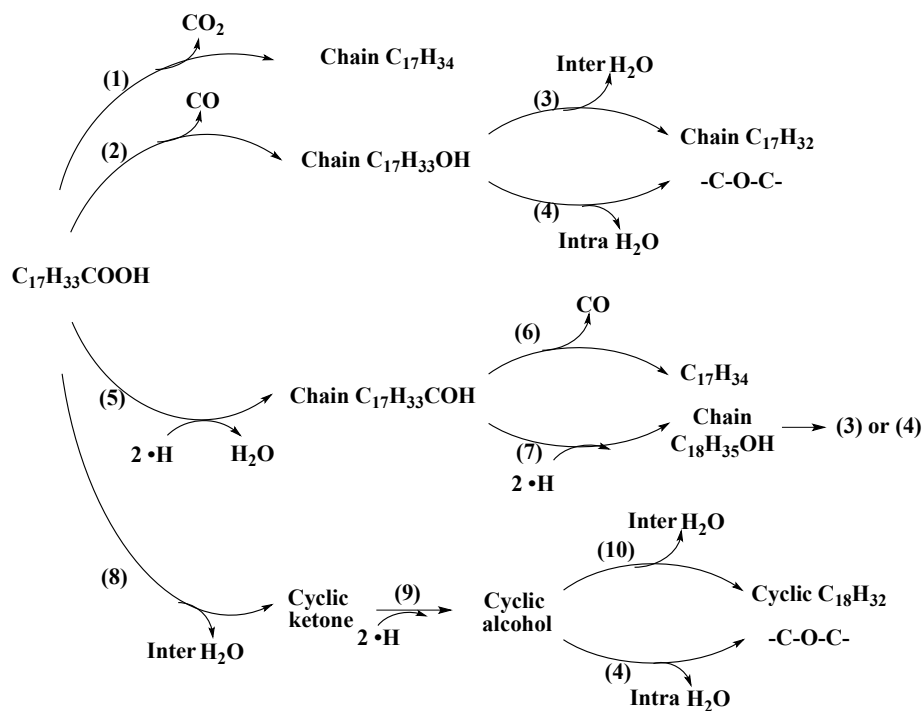
1: Further reaction of glycerol from hydrolysis step could produce CO<sub>x</sub> and H<sub>2</sub>O as well

2: DCO<sub>x</sub> means DO as form of CO or CO<sub>2</sub>

Shown in Table 8-5, both the kaolin-based and commercial catalysts eliminated more oxygen by the removal of water than by the removal of CO<sub>2</sub> and CO (they all produced the same amounts of H<sub>2</sub>O at the same time, so Table 8-5 also shows the amount of H<sub>2</sub>O minus CO – the net content of H<sub>2</sub>O produced from dehydration). Comparing the produced amounts of CO to CO<sub>2</sub>, it can be concluded that the DO of WCO favored decarbonylation over decarboxylation in all catalyst upgrading processes. An unexpected result was that most of the oxygen was removed in the form of water, even though hydrogen is required to release water and no hydrogen was introduced during cracking process. The reason for this was that fatty acids could react with the hydrogen produced from dehydrogenation, and this hydrogen could be effectively consumed since it was produced in-situ [147, 166]. This result could be confirmed by the hydrogen balance results. Other researchers have also reported that dehydration was the primary DO

reaction during industrial petroleum FCC equilibrium catalysts upgrading process [32, 44]. Tian et al. found that the ratio of dehydration to DCOx ranged from 2.6 to 5.5 when upgrading triglycerides over FCC equilibrium catalysts [44]. The dehydration to DCOx ratio is much lower for BTK than it is for other catalysts. The higher H/C ratios of BTK upgraded OLPs could be responsible, because low dehydrogenation capability leads to low free hydrogen radical concentration (and therefore less water produced). Another possible reason may be the low acid density and low acidity of BTK.

Scheme 8-13 shows the deoxygenation reactions that during the cracking process, using oleic acid as an example compound.



Scheme 8-13 Reactions of DO during cracking process

Chain alkenes could be produced either by decarboxylation (reaction 1) or by DCO (reaction 2 and reaction 3). Chain alcohols, intermediates of DCO (reaction 2), could also form –C-O-C- through intra-molecular dehydration (reaction 4). Oleic acid could react with the hydrogen radicals produced from dehydrogenation to form aldehydes and water (reaction 5), or could undergo inter-molecular dehydration to produce cyclic ketones (reaction 8). Both the chain aldehydes and cyclic ketones could react with the in-situ hydrogen radicals to produce chain alcohols (reaction 7) and cyclic alcohols (reaction 9), and the alcohols could either go through inter-molecular dehydration or intra-molecular dehydration to release chain alkenes (reaction 3) or cyclic alkenes (reaction 10) and –C-O-C- (reaction 4). Oleic acid could undergo esterification with the produced alcohols to produce esters. Benson et al. also reported that fatty acids could undergo inter-molecular and intra-molecular dehydration to produce ketones and esters [167].

As shown in Figure 8-7, BTK upgraded OLP contained over 14 % oxygenates (carbon no. of 18), indicating that DO occurred before cracking.

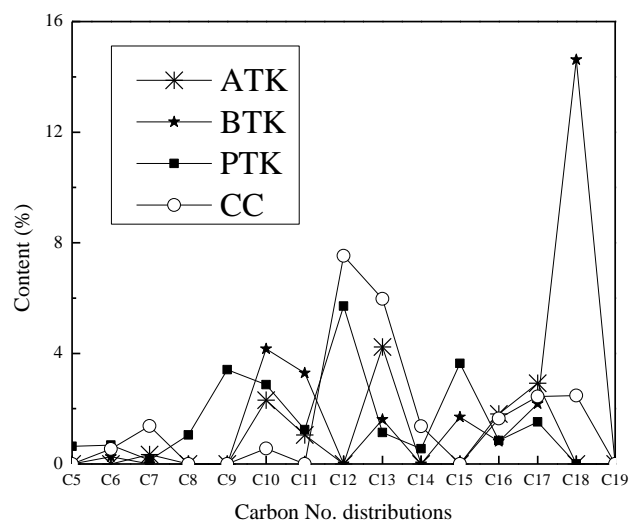


Figure 8-7 Carbon No. distributions of oxygenates

Note: oxygenates in Figure 8-7 without acids.

As shown in Figure 8-8, the ATK and BTK upgraded OLPs had high contents of ketones and fatty acids, whereas the PTK and CC upgraded OLPs had high contents of alcohols, and contained some esters and ethers. More than 60 % of the  $-C=O$  containing compounds in the ATK and BTK upgraded OLPs were cyclic ketones. Therefore, reaction 9 was the rate-limiting step when WCO was upgraded by treated kaolin catalysts. More than 80 % of the  $-OH$  containing compounds in the PTK and CC upgraded OLPs were chain alcohols. Therefore, reaction 3 and reaction 4 were the rate-limiting steps when WCO was upgraded by these two catalysts. The BTK upgraded product contained a large amount of oxygenates (as shown in Figure 8-8) because of BTK's low acidity. CC and PTK had much higher dehydrogenation capabilities compared to the kaolin-based

catalysts, which meant that they could produce higher amounts of hydrogen free radicals for converting ketones into alcohols. These alcohols were intermediates for producing esters, ethers, and epoxides. On the other hand, low concentrations of hydrogen radicals were produced when using treated kaolin. These were not enough to react with appreciably with ketones, so there were high ketone, low alcohol, low ester, low ether, and low epoxide contents present in the treated kaolin upgraded OLPs. Small molecular acids can be released when oleic acid undergoes C-C bond cracking.

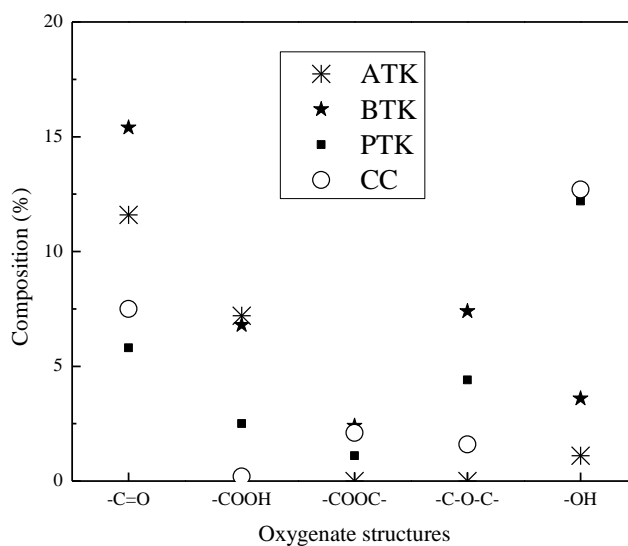


Figure 8-8 Types of oxygenates

3.2 wt% and 4.5 wt% of hexenyl cyclopentanone were found in the ATK and BTK upgraded OLPs, and 2.1 wt% of dimethyl decanol and 2.4 wt% of phenyl heptenol were

found in the PTK and CC upgraded OLPs. The existence of these compounds could confirm the proposed oxygenate producing reactions.

## 8.5 Conclusions

After treatment, the surface area and pore volume of natural kaolin were enlarged. Medium and strong acidic sites were also generated. ATK was found to be much more reactive for DO than PTK – the oxygen removal rate increased from 81.8 % to 93.8 % when untreated kaolin was replaced by ATK.

Acidity and acid density are factors critical to cracking activity rendering higher liquid yields and lower gas hydrocarbon yields at lower total acidities and lower acid densities of the catalyst. The physical properties of catalysts are not the key factors in WCO DO, but the acid properties strongly affect DO. Overly high acid densities and strengths reduced the oxygen removal rate. The compositions of the OLPs were significantly influenced by the type, strength, and density of the acidic sites on the catalysts. The cracking process by the reference catalyst, CC, primarily followed the carbonium ion reaction mechanism, whereas the cracking processes by the kaolin-based catalysts complied more with the free radical reaction mechanism. CC could eliminate the most oxygen but produced too many unexpected aromatic hydrocarbons. On the other hand, acid treated kaolin catalysts exhibited high yield and high quality liquid products with low oxygen content, low aromatic content, and high ratio of hydrogen to carbon. Both kaolin-based and CC catalysts eliminated more oxygen by the removal of water than by

the removal of CO<sub>2</sub> and CO. The DO of WCO favored DCO over DCO<sub>2</sub> in all catalyst upgrading process.

## **Chapter 9 Integration of catalytic cracking and hydrotreating for triglyceride deoxygenation**

### **9.1 Introduction**

The newly developed cracking catalyst, ATK (see Chapter 8), was evaluated in the FCC reactor. Its performance was compared to that of the petroleum commercial catalyst (CC) as well as the alumina catalyst. The resulting catalytic cracking liquid products were then hydrotreated in a batch reactor at 275-325 °C and under 250-500 psi, using a commercial supported CoMoS catalyst (see Chapter 3). The products of this new integrated technology were compared with the products of direct hydrotreating, by analyzing the compositions and calculating the hydrogen consumptions.

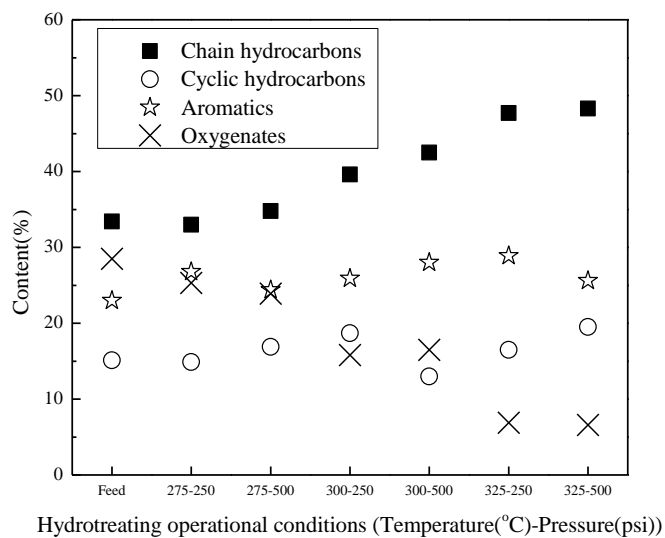
### **9.2 Experimental**

ATK was evaluated in the FCC reactor at 470 °C and under atmospheric pressure, and steam was used as the carrier gas. After undergoing catalytic cracking with ATK, the product was hydrotreated in a batch reactor (at 275-325 °C and 250-500 psi). This integrated process was named ATK-HDO. The products from ATK-HDO were compared with those obtained from: catalytic cracking with alumina followed by hydrotreating (Alumina-HDO, at 325 °C and 500 psi), catalytic cracking with CC followed by hydrotreating (CC-HDO, at 325 °C and 500 psi), and using hydrotreating only (at 325 °C and 500/1000 psi).

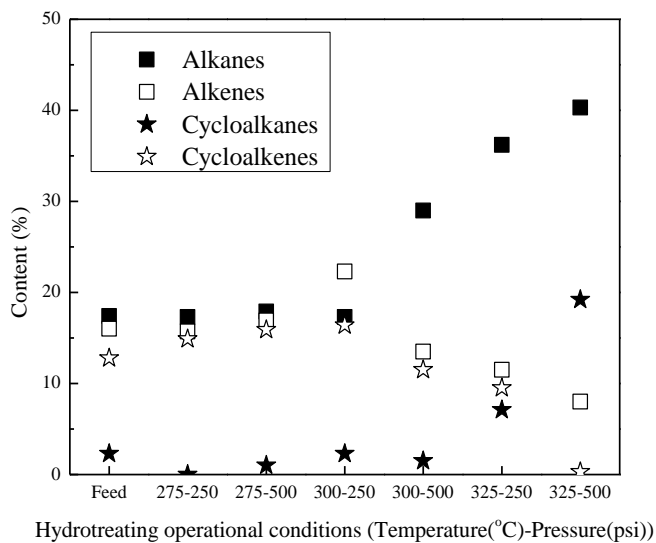
The total mass received from both the catalytic cracking process and the hydrotreating process could reach  $100 \pm 5$  %. The ultimate goal is to increase the liquid yield, lower the hydrogen consumption, and enhance the product quality using this process.

### **9.3 Results and discussion**

Hydrotreating of the ATK cracked liquid products was conducted under several different conditions. The liquid product compositions and the hydrocarbon compositions are shown in Figure 9-1 (a) and (b), respectively.



(a) Chemical composition distributions



(b) Hydrocarbon distributions

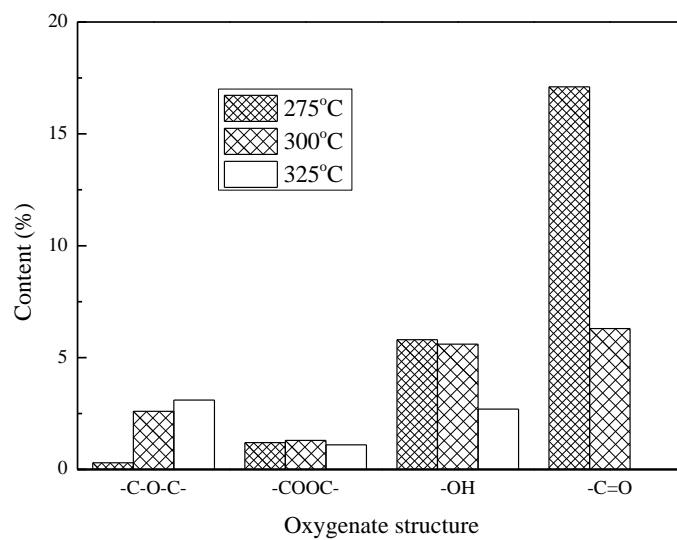
Figure 9-1 The compositions of ATK-HDO upgrading products

For the OLPs' compositions shown in Figure 9-1 (a), when the temperature was increased the chain hydrocarbon content increased and the oxygenate content decreased, but there were no significant changes in cyclic hydrocarbon and aromatic contents. It is clear that the oxygenate content did not significantly change between different pressures when the temperature was kept constant. This indicates that it was the reaction temperature rather than the hydrogen pressure that was the key factor for deoxygenation during the integrated process.

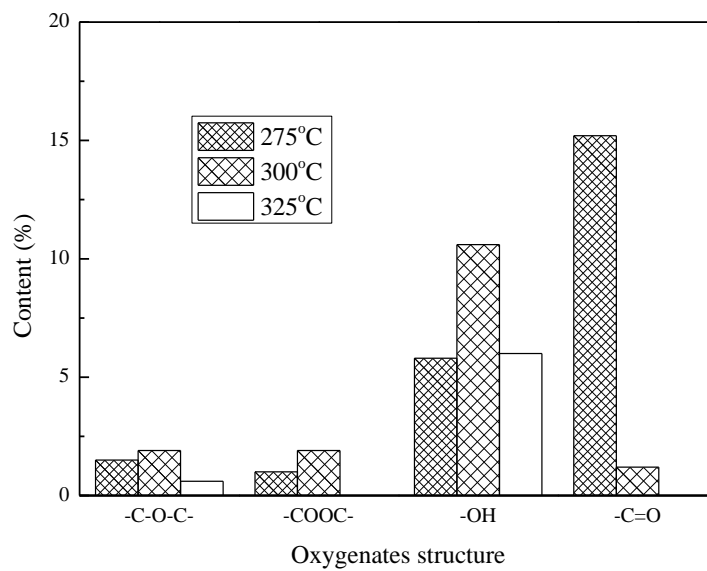
As shown in Figure 9-1 (b), at 300 °C and under 250 psi there was an obvious increase in alkene content but no big changes in other hydrocarbon contents. This increase occurred because alkenes are the products of oxygenate hydrotreating. When the hydrogen pressure increased to 500 psi, the contents of alkenes and cycloalkenes decreased, whereas the content of alkanes significantly increased. The reason for this is that the hydrogenation of alkenes and cycloalkenes into alkanes started when the temperature was at 300 °C and the hydrogen pressure was at 500 psi. When the temperature increased to 325 °C, the contents of the alkenes and cycloalkenes continued to decrease and the contents of alkanes and also cycloalkanes increased. This reveals that the hydrogenation of cycloalkanes into alkanes was the reaction-limiting step at 325 °C. For both the DO and hydrogenation of WCO during the integrated process, the optimal reaction temperature was 325 °C and the optimal hydrogen pressure was 500 psi. Under the optimal reaction conditions of the integrated process using ATK (ATK-HDO), the OLP

contents of oxygenate, cycloalkene, and alkene were lowered to 6.6 wt%, 0.3 wt%, and 8.0 wt%, respectively.

The oxygenates contained in the OLPs under pressures of 250 psi and 500 psi are shown in Figure 9-2 (a) and (b), respectively. Even though there were no obvious variations in the total oxygenate contents of the OLPs (at the same temperature and different pressures, see Figure 9-1 (a)), the specific oxygen structures differed.



(a) at 250psi



(b) at 500psi

Figure 9-2 The oxygenate structures of ATK-HDO upgrading products

As shown in Figure 9-2 (a), the contents of  $-C=O$  and  $-OH$  decreased and the content of  $-C-O-C-$  increased when the temperature was increased. This demonstrates that the DO of  $-C-O-C-$  into a hydrocarbon was the lowest occurring reaction among all DO processes for a pressure of 250 psi. At 325 °C, all  $-C=O$  was converted into  $-OH$ . When the hydrogen pressure increased to 500 psi, the conversion of  $-COOC-$  reached 100 % and the content of  $-C-O-C-$  also decreased; the content of  $-OH$  increased, however. This reveals that the DO of  $-OH$  became the reaction-limiting step when the hydrogen pressure increased from 250 psi to 500 psi at a temperature of 325 °C.

The OLPs upgraded by several different catalysts were all hydrotreated under optimal hydrotreating conditions, and the WCO was also directly hydrotreated (HDO) under the same conditions to be used as a reference. The chemical compositions of OLPs from the integrated process are shown in Figure 9-3. The oxygenate content in the direct HDO OLP was as high as 89.6 %, much higher than in the other OLPs that were first upgraded by cracking catalysts (17.9 % in the CC-HDO OLP and around 6.3 % in the alumina/ATK-HDO OLP). Concerning the hydrocarbon contents of the OLPs, the alumina-HDO OLP was primarily composed of chain hydrocarbons (including 24.3 % unsaturated), whose content was as high as 85.8 %. The CC-HDO OLP was mainly comprised of aromatics (50.4 %). The composition of the ATK-HDO OLP was somewhere in the middle, comprised of 40.3 % chain hydrocarbons, 27.6 % aromatics, and 25.5 % cyclic hydrocarbons. Overly high concentrations of long-chain hydrocarbons

in the liquid products led to a high cloud point and a high freezing point. Overly high aromatic contents made it so the oil products were not fully combustible, so aromatics contents were attempted to be limited in the oil products. Based on these all conclusions, ATK-HDO was selected as the best option for creating of drop-in biofuels.

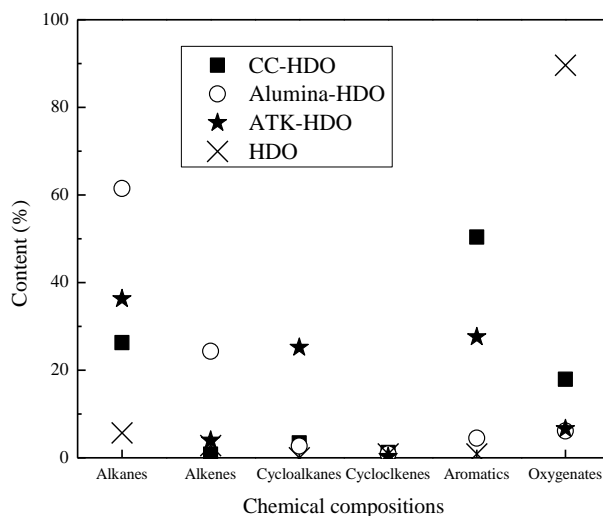


Figure 9-3 Chemical compositions of liquid products under optimal conditions

Because of the high concentration of oxygenates found in the direct HDO OLP at 325 °C and under 500 psi, the hydrogen pressure was increased to 1000 psi for this trial. The results are shown in Figure 9-4. At 325 °C, the conversion rates under the pressures 500 psi and 1000 psi were 22.3 % and 56.1 %, respectively. Even though the alkane content increased from 5.7 % to 40.9 %, the oxygenate content remained as high as 48.8 %.

Therefore, there was a gap in the DO ability between the direct hydrotreating and the integrated catalytic-cracking/hydrotreating technologies.

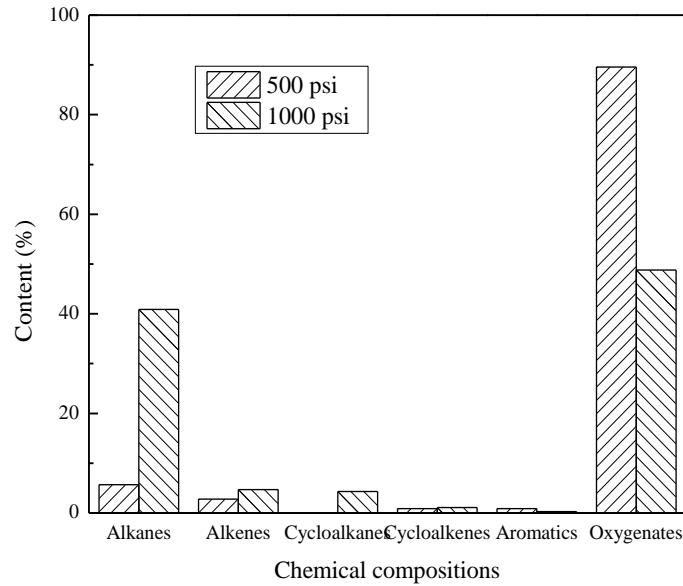


Figure 9-4 Chemical compositions of directly hydrotreating WCO

The organic liquid product yield, gas product yield, and oxygen removal rate of catalytic cracking processes are shown in Table 9-1. All of the three catalysts could achieve more than a 90 % oxygen removal rate, but ATK and alumina had especially high DO capabilities (as high as 93.8 %). The liquid product yields of CC and alumina were lower than that of ATK. This was due to over-cracking that occurred when WCO was upgraded by CC, which resulted in a high gas hydrocarbon yield (see Table 9-1). The DCO<sub>2</sub> and DCO reactions were more prevalent in alumina than they were in ATK and CC – this can

be explained by the high yield of CO/CO<sub>2</sub>. Lower liquid yields were received during DO by DC than by dehydration.

Table 9-1 Product distribution and oxygen removal rate of catalytic cracking process

Yield (wt%)	OLP	CO/CO <sub>2</sub>	Hydrocarbon gases	Oxygen removal rate
CC	67.5	5.6	7.2	90.8
ATK	74.4	3.4	1.4	93.8
Al <sub>2</sub> O <sub>3</sub>	65.9	9.2	3.8	93.9

The liquid and gas product yields of the hydrotreating processes are shown in Table 9-2. The liquid product yields could have reached 94.7-99.7 %, whereas the gas product yields were 0.2-2.1 %. This reveals that there were low amounts of cracking reactions in the hydrotreating process under the investigated conditions. It should be noted that the integrated technology and the direct hydrotreating favored DCO and DCO<sub>2</sub>, respectively.

Table 9-2 Product distribution of hydrotreating process

Yields (wt%)	CC	ATK	Alumina	WCO	WCO-1000psi
Hydrocarbon gases	0.40	1.95	0.40	0.02	2.30
CO	0.08	0.12	0.13	0.01	0.02
CO <sub>2</sub>	0.05	0.02	0.01	0.19	0.46
OLP	99.7	98.0	94.7	98.8	98.8

The hydrogen consumptions during the hydrotreating process are shown in Figure 9-5. It can be seen that hydrogen consumption for CC-HDO, ATK-HDO, alumina-HDO, and directly HDO are 4.0, 2.4, 3.9, and 8.8 mol hydrogen per mol WCO. Using oleic acid as an example, the calculation hydrogen consumption to remove all oxygen and saturate all carbon double bonds is 15 mol hydrogen for per mol WCO. This means that the integrated technology could have reduced the amount of hydrogen consumption needed, especially for ATK-HDO. Even though the conversion of the direct hydrotreating process was as low as 22.3 %, its hydrogen consumption was still three times that of ATK-HDO's under the same conditions.

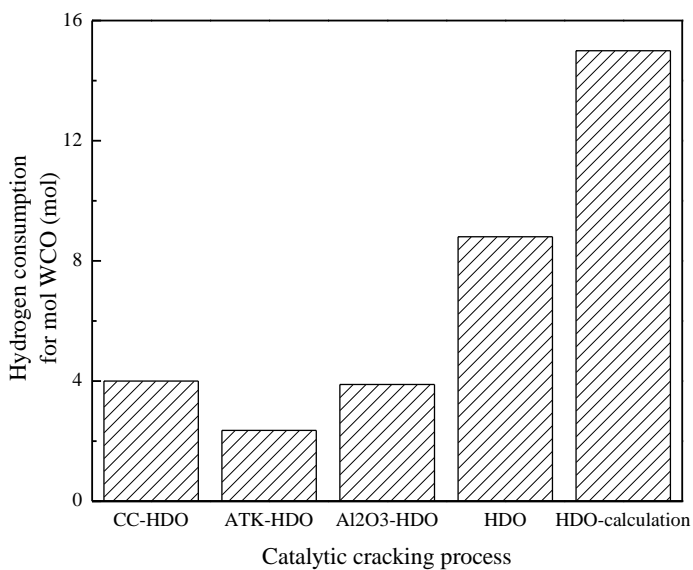


Figure 9-5 Hydrogen consumptions during hydrotreating process

## 9.4 Conclusions

In summary, the integrated catalytic cracking and hydrotreating technology was successfully applied for the triglyceride DO process, producing a higher liquid yield and a higher oxygen removal rate, all at low levels of hydrogen consumption. Most unsaturated compounds and oxygenates could be removed. Some long-chain hydrocarbons could undergo cracking, cyclization, or aromatization, forming short-chain or iso-paraffins, cyclic hydrocarbons, or aromatics. The lowest amount of hydrogen was consumed during the WCO ATK-HDO process.

## **Chapter 10 Conclusions and recommendations**

### **10.1 Conclusions**

This study consisted of three parts: an investigation on the feasibility of employing hydrotreating for the upgrading of triglyceride-based oils, the development of a novel catalytic cracking catalyst, and the evaluation of the newly produced catalytic-cracking/hydrotreating dual technology. This technology was compared with existing hydrotreating technology in order to further confirm the effectiveness of the designed cracking catalyst, acid treated kaolin. The conclusions of this work are summarized below.

#### **10.1.1 Hydrotreating of triglycerides**

Hydrogenation and DO were the dominant reactions at 275-325 °C; HDO reactions were the most prevalent DO reactions that occurred at 365 °C. The DO capability increased when the reaction temperature increased from 250 to 275 °C. The hydrogenation capability increased when the temperature increased from 250 to 275 °C then decreased when the temperature increased from 275 to 300 °C. An increase in the volumetric ratio of H<sub>2</sub> to oil increased the DO and hydrogenation capabilities, but could not produce significant effects when the ratio was higher than 100 ml/ml. When the concentrations of WCO and CLO in the feed increased, DO and hydrogenation capabilities decreased. When the LHSV increased, DO and hydrogenation capabilities decreased as well. The reaction temperature increasing from 275 to 300 °C was the only factor that obviously increased the cracking capability. Higher reaction temperatures and higher concentrations

of WCO in the feed caused DCO<sub>2</sub> to be favored over DCO. HDO was the most dominant reaction pathway for removing oxygen from WCO (and CLO). The selectivity of HDC (DCO<sub>2</sub>/DCO) over HDO was increased by decreasing the hydrogen supply or by increasing the WCO concentration in the feed.

The roles of catalyst support (for the CoMoS hydrotreating catalyst) and reaction temperature were investigated for the triglyceride hydrotreating process. Increasing the temperature did not affect the main reaction pathways, but it slightly enhanced HDC capability. Catalyst support was shown to enhance the HDO pathway and to change the rate-limiting steps of the reactions – this was achieved by accelerating the rate at which fatty acids were deoxygenated into alcohols by HDO. Lack of acidic support led to lower hydrocracking and high polymerization capabilities. The existence of catalyst support and the increase of reaction temperature were shown to have strongly enhanced hydrogenation activity. When compared to unsupported CoMoS, supported CoMoS not only had higher hydrogenation and HDO abilities at low temperatures, but it also had a higher dehydrogenation activity at high temperatures.

The three causes for the deactivation of the CoMoS supported catalysts are: the appearance of coke deposition, the production of by-product water, and the loss of sulfur from the catalyst. Working under high temperatures (at 365 °C) led to the easy formation of coke, further contributing to catalyst deactivation. By-product water partially caused catalyst deactivation, but in-situ drying could notably recover some of the hydrogenation

and HDO activity that was lost. Loss of sulfur caused deactivation in the catalyst, but resulfiding could be an option for reactivating the spent catalyst. Deactivation occurred by first decreasing hydrogenation capability and then by decreasing HDO capability. Deactivation caused no significant impacts on the cracking, polymerization, and HDC activities.

### **10.1.2 Development of novel cracking catalyst**

Acidic, neutral, and alkaline metal oxides were used for catalytic cracking. Although higher oxygen removal rates (97.7-100.0 wt%) were obtained by working with CaO, MgO, and titania, the light oil and valuable product yields of alumina were rather high (alumina also had a decent oxygen removal rate of 73.0 wt%). DC was the dominating DO reaction that occurred under the tested conditions. DCO was the main mechanism for transforming oleic acid into aliphatic hydrocarbons (using acidic catalysts), and the reaction-limiting step was the dehydration of alcohols. Acidity of the catalyst was beneficial to DO but was also beneficial to secondary cracking. DCO<sub>2</sub> was the main mechanism for transforming oleic acid into chain hydrocarbons (using alkaline catalysts), and the lowest occurring reactions in this process were the reduction of ketones to yield alcohols and alcohol dehydration. CaO exhibited the highest dehydrogenation capability, but the free hydrogen radicals on the surface of MgO were more effective when reacting with oxygenates to release water. The existence of B acids on the catalyst was found to be important to the formation of aromatics.

Novel kaolin-based catalysts were developed for the catalytic cracking of triglycerides. Acidity and acid density were critical to cracking activity: higher liquid yields and lower gas hydrocarbon yields were achieved using catalysts with lower total acidities and lower acid densities. The physical properties of the catalysts were not the key factors of WCO DO, whereas the acid properties of the catalysts strongly affected the DO. Overly high acid densities and strengths reduced the oxygen removal rate, however. The compositions of the OLPs were significantly influenced by the type, strength, and density of acidic sites on the catalysts. The cracking process by the reference catalyst, CC, primarily followed the carbonium ion reaction mechanism, whereas the cracking process by the kaolin-based catalysts complied more with the free radical reaction mechanism. CC eliminated more oxygen but produced excessive amounts of unexpected aromatic hydrocarbons. On the other hand, acid treated kaolin catalysts could produce high yield and high quality liquid product with low oxygen content, low aromatic content, and high ratio of hydrogen to carbon. Both kaolin-based and CC catalysts eliminated more oxygen through the removal of water than through the removal of CO<sub>2</sub> and CO. The DO of WCO favored DCO over DCO<sub>2</sub> in all catalyst upgrading processes.

### **10.1.3 Development of integration technology**

The catalytic-cracking/hydrotreating dual technology was successfully applied for the DO of triglycerides: it could produce high liquid yields and high oxygen removal rates, all at low levels of hydrogen consumption. Most unsaturated compounds and oxygenates could be removed. Some long-chain hydrocarbons could undergo cracking, cyclization, or aromatization, turning into short-chain or iso-paraffins, cyclic hydrocarbons, or

aromatics. The lowest amount of hydrogen was consumed during WCO ATK-HDO process.

## **10.2 Recommendations**

ATK is an effective catalytic cracking catalyst for triglyceride upgrading and is also hydrothermally stable. The regeneration of ATK is a key factor when considering its use for commercial purposes. Further study concerning the deactivation and regeneration of ATK could therefore be very useful.

A high liquid yield and high oxygen removal rate (at low levels of hydrogen consumption) were obtained by using the integrated catalytic-cracking/hydrotreating technology. A batch reactor was used for the hydrotreating process in the technology comparison in Chapter 9. It would have been better to use a continuous fixed-bed reactor for this part of the experiment.

In Chapter 7, only the acidic catalysts containing solely Lewis acids were used. All the data for the effects of Bronsted acids were obtained from literature. Further experiments could be done to further determine the impacts of Bronsted acids on the compositions of the liquid products.

In Chapter 4 and Chapter 6, for the effects of operational parameters on the triglyceride hydrotreating and the deactivation of supported CoMoS sections, the kinetic model and

reaction rate law could be further done, which is extremely important for industrial reactor design. The data presented herein is appropriate for a kinetic study with regards to the suggested optimal reaction parameters. According to our results, the reaction pathways totally changed when the reaction temperature was increased up to 365°C. Therefore, the kinetics study under high reaction temperature is very useful. However, further experiments under different reaction temperatures are required to be done if the high temperature reaction kinetic needs to be simulated.

## Bibliography

- [1] C. News, Ontario sets new greenhouse gas pollution reduction target. <http://www.cbc.ca/news/canada/toronto/ontario-sets-new-greenhouse-gas-pollution-reduction-target-1.3074911>, in, CBC News, 2015.
- [2] [http://www.bioenergywiki.net/Renewable\\_fuel\\_targets](http://www.bioenergywiki.net/Renewable_fuel_targets), in.
- [3] G. Canada, <http://www.ec.gc.ca/lcpe-cepa/eng/regulations/DetailReg.cfm?intReg=202>, (2015).
- [4] I. <http://www.iea.org>, World Energy Outlook 2008, Chapter 11, International Energy Agency, IEA/OECD, in, Paris, 2008.
- [5] G.W. Huber, A. Corma, Synergies between bio- and oil refineries for the production of fuels from biomass, *Angewandte Chemie-International Edition*, 46 (2007) 7184-7201.
- [6] P.M. Mortensen, J.D. Grunwaldt, P.A. Jensen, K.G. Knudsen, A.D. Jensen, A review of catalytic upgrading of bio-oil to engine fuels, *Applied Catalysis a-General*, 407 (2011) 1-19.
- [7] D. Kubicka, J. Horacek, Deactivation of HDS catalysts in deoxygenation of vegetable oils, *Applied Catalysis a-General*, 394 (2011) 9-17.
- [8] M. Badawi, J.F. Paul, S. Cristol, E. Payen, Y. Romero, F. Richard, S. Brunet, D. Lambert, X. Portier, A. Popov, E. Kondratieva, J.M. Goupil, J. El Fallah, J.P. Gilson, L. Mariey, A. Travert, F. Mauge, Effect of water on the stability of Mo and CoMo hydrodeoxygenation catalysts: A combined experimental and DFT study, *Journal of Catalysis*, 282 (2011) 155-164.

- [9] O.I. Senol, T.R. Viljava, A.O.I. Krause, Hydrodeoxygenation of aliphatic esters on sulphided NiMo/ $\gamma$ -Al<sub>2</sub>O<sub>3</sub> and CoMo/ $\gamma$ -Al<sub>2</sub>O<sub>3</sub> catalyst: The effect of water, *Catalysis Today*, 106 (2005) 186-189.
- [10] E. Laurent, B. Delmon, Influence of water in the deactivation of a sulfided NiMo  $\gamma$  Al<sub>2</sub>O<sub>3</sub> catalyst during hydrodeoxygenation, *Journal of Catalysis*, 146 (1994) 281-291.
- [11] I. Graca, J.M. Lopes, M.F. Ribeiro, F.R. Ribeiro, H.S. Cerqueira, M.B.B. de Almeida, Catalytic cracking in the presence of guaiacol, *Applied Catalysis B-Environmental*, 101 (2011) 613-621.
- [12] Z.Y. Ng SH., Shi Y, Ding LH, Chen S., Gieleciak S., Hager D., Catalytic conversion of plant oil to clean transportation fuels, in, *Pacificchem*, 2010.
- [13] A. Corma, G.W. Huber, L. Sauvanaud, P. O'Connor, Processing biomass-derived oxygenates in the oil refinery: Catalytic cracking (FCC) reaction pathways and role of catalyst, *Journal of Catalysis*, 247 (2007) 307-327.
- [14] I. Graca, J.M. Lopes, H.S. Cerqueira, M.F. Ribeiro, Bio-oils upgrading for second generation biofuels, *Industrial & Engineering Chemistry Research*, 52 (2013) 275-287.
- [15] A. Corma, J. Mengual, P.J. Miguel, Steam catalytic cracking of naphtha over ZSM-5 zeolite for production of propene and ethene: Micro and macroscopic implications of the presence of steam, *Applied Catalysis a-General*, 417 (2012) 220-235.
- [16] A. Corma, J. Mengual, P.J. Miguel, Stabilization of ZSM-5 zeolite catalysts for steam catalytic cracking of naphtha for production of propene and ethene, *Applied Catalysis a-General*, 421 (2012) 121-134.
- [17] A.G. Gayubo, A. Alonso, B. Valle, A.T. Aguayo, M. Olazar, J. Bilbao, Hydrothermal stability of HZSM-5 catalysts modified with Ni for the transformation of bioethanol into hydrocarbons, *Fuel*, 89 (2010) 3365-3372.

- [18] A.G. Gayubo, A.T. Aguayo, A. Atutxa, R. Prieto, J. Bilbao, Role of reaction-medium water on the acidity deterioration of a HZSM-5 zeolite, *Industrial & Engineering Chemistry Research*, 43 (2004) 5042-5048.
- [19] A.G. Gayubo, A.T. Aguayo, A. Atutxa, R. Prieto, J. Bilbao, Deactivation of a HZSM-5 zeolite catalyst in the transformation of the aqueous fraction of biomass pyrolysis oil into hydrocarbons, *Energy & Fuels*, 18 (2004) 1640-1647.
- [20] A.G. Gayubo, A.T. Aguayo, M. Olazar, R. Vivanco, J. Bilbao, Kinetics of the irreversible deactivation of the HZSM-5 catalyst in the MTO process, *Chemical Engineering Science*, 58 (2003) 5239-5249.
- [21] N. Taufiqurrahmi, S. Bhatia, Catalytic cracking of edible and non-edible oils for the production of biofuels, *Energy & Environmental Science*, 4 (2011) 1087-1112.
- [22] K. Liu, F.T.T. Ng, Effect of the nitrogen heterocyclic compounds on hydrodesulfurization using in situ hydrogen and a dispersed Mo catalyst, *Catalysis Today*, 149 (2010) 28-34.
- [23] N.A. Owen, O.R. Inderwildi, D.A. King, The status of conventional world oil reserves-Hype or cause for concern?, *Energy Policy*, 38 (2010) 4743-4749.
- [24] E.I. Administration, <http://www.eia.gov/beta/aeo/ - /?id=1-AEO2015&region=0-0&cases=ref2015&start=2012&end=2040&f=A&linechart=1-AEO2015.3.~1-AEO2015.30.~~~1-AEO2015.36.~1-AEO2015.35.~~~~~1-AEO2015.9.~1-AEO2015.10.~~&map=&ctype=linechart>, in: *Annual Energy Outlook 2015*, 2015.
- [25] C. Marcilly, Present status and future trends in catalysis for refining and petrochemicals, *Journal of Catalysis*, 216 (2003) 47-62.
- [26] J. Row, A. Doukas, Fuel quality in Canada: Impact on tailpipe emissions prepared for the Association of International Automobile Manufacturers of Canada, in, *The Pembina Institute*, 2008.

- [27] [http://en.wikipedia.org/wiki/Second\\_generation\\_biofuels](http://en.wikipedia.org/wiki/Second_generation_biofuels), in.
- [28] M. Al-Sabawi, H. de Lasa, Kinetic modeling of catalytic conversion of methylcyclohexane over USY zeolites: Adsorption and reaction phenomena, *Aiche Journal*, 55 (2009) 1538-1558.
- [29] Y.K. Ong, S. Bhatia, The current status and perspectives of biofuel production via catalytic cracking of edible and non-edible oils, *Energy*, 35 (2010) 111-119.
- [30] M. Al-Sabawi, J.W. Chen, S. Ng, Fluid catalytic cracking of biomass-derived oils and their blends with petroleum feedstocks: A review, *Energy & Fuels*, 26 (2012) 5355-5372.
- [31] H. Tani, T. Hasegawa, M. Shimouchi, K. Asami, K. Fujimoto, Selective catalytic decarboxy-cracking of triglyceride to middle-distillate hydrocarbon, *Catalysis Today*, 164 (2011) 410-414.
- [32] X. Dupain, D.J. Costa, C.J. Schaverien, M. Makkee, J.A. Moulijn, Cracking of a rapeseed vegetable oil under realistic FCC conditions, *Applied Catalysis B-Environmental*, 72 (2007) 44-61.
- [33] T.Y. Leng, A.R. Mohamed, S. Bhatla, Catalytic conversion of palm oil to fuels and chemicals, *Canadian Journal of Chemical Engineering*, 77 (1999) 156-162.
- [34] Y.S. Ooi, R. Zakaria, A.R. Mohamed, S. Bhatia, Catalytic cracking of used palm oil and palm oil fatty acids mixture for the production of liquid fuel: Kinetic modeling, *Energy & Fuels*, 18 (2004) 1555-1561.
- [35] S. Bhatia, C.T. Leng, P. Tarnunaidu, Modeling and simulation of transport riser reactor for catalytic cracking of palm oil for the production of biofuels, *Energy & Fuels*, 21 (2007) 3076-3083.

- [36] B. Watkins, C. Olsen, K. Sutovich, J. Deady, N. Petti, S. Wellach, New opportunities: for coprocessing renewable feeds in the refinery process, *Hydrocarbon Eng.*, 14 (2009) 49-58.
- [37] P. Dejaifve, J.C. Vedrine, V. Bolis, E.G. Derouane, Reaction pathways for the conversion of methanol and olefins on H-ZSM-5 zeolite *Journal of Catalysis*, 63 (1980) 331-345.
- [38] N. Taufiqurrahmi, A.R. Mohamed, S. Bhatia, Deactivation and coke combustion studies of nanocrystalline zeolite beta in catalytic cracking of used palm oil, *Chemical Engineering Journal*, 163 (2010) 413-421.
- [39] Y. He, S.E. Barnes, D.W. Crunkleton, G.L. Price, Comparison of ginger oil conversion over MFI, BEA, and FAU, *Fuel*, 96 (2012) 469-475.
- [40] P. Tamunaidu, S. Bhatia, Catalytic cracking of palm oil for the production of biofuels: Optimization studies, *Bioresource Technology*, 98 (2007) 3593-3601.
- [41] Y.S. Ooi, S. Bhatia, Aluminum-containing SBA-15 as cracking catalyst for the production of biofuel from waste used palm oil, *Microporous and Mesoporous Materials*, 102 (2007) 310-317.
- [42] H. Li, B. Shen, J.C. Kabalu, M. Nchare, Enhancing the production of biofuels from cottonseed oil by fixed-fluidized bed catalytic cracking, *Renewable Energy*, 34 (2009) 1033-1039.
- [43] P. Bielansky, A. Weinert, C. Schonberger, A. Reichhold, Catalytic conversion of vegetable oils in a continuous FCC pilot plant, *Fuel Processing Technology*, 92 (2011) 2305-2311.
- [44] H. Tian, C.Y. Li, C.H. Yang, H.H. Shan, Alternative processing technology for converting vegetable oils and animal fats to clean fuels and light olefins, *Chinese Journal of Chemical Engineering*, 16 (2008) 394-400.

- [45] J.A. Melero, J. Iglesias, A. Garcia, Biomass as renewable feedstock in standard refinery units. Feasibility, opportunities and challenges, *Energy & Environmental Science*, 5 (2012) 7393-7420.
- [46] R.K. Sharma, N.N. Bakhshi, Catalytic conversion of fast pyrolysis oil to hydrocarbon fuels over HASM-5 in a dual reactor system *Biomass & Bioenergy*, 5 (1993) 445-455.
- [47] T. Hua, Studies on catalytic cracking of fatty acid esters, in, China University of Petroleum (East China), 2008.
- [48] A.A. Lappas, S. Bezergianni, I.A. Vasalos, Production of biofuels via co-processing in conventional refining processes, *Catalysis Today*, 145 (2009) 55-62.
- [49] G. Fogassy, N. Thegarid, G. Toussaint, A.C. van Veen, Y. Schuurman, C. Mirodatos, Biomass derived feedstock co-processing with vacuum gas oil for second-generation fuel production in FCC units, *Applied Catalysis B-Environmental*, 96 (2010) 476-485.
- [50] F.D. Mercader, M.J. Groeneveld, S.R.A. Kersten, N.W.J. Way, C.J. Schaverien, J.A. Hogendoorn, Production of advanced biofuels: Co-processing of upgraded pyrolysis oil in standard refinery units, *Applied Catalysis B-Environmental*, 96 (2010) 57-66.
- [51] S. Bezergianni, A. Dimitriadis, A. Kalogianni, K.G. Knudsen, Toward hydrotreating of waste cooking oil for biodiesel production. Effect of pressure, H<sub>2</sub>/oil ratio, and liquid hourly space velocity, *Industrial & Engineering Chemistry Research*, 50 (2011) 3874-3879.
- [52] K. Murata, Y.Y. Liu, M. Inaba, I. Takahara, Production of synthetic diesel by hydrotreatment of *Jatropha* oils using Pt-Re/H-ZSM-5 catalyst, *Energy & Fuels*, 24 (2010) 2404-2409.
- [53] B. Veriansyah, J.Y. Han, S.K. Kim, S.A. Hong, Y.J. Kim, J.S. Lim, Y.W. Shu, S.G. Oh, J. Kim, Production of renewable diesel by hydroprocessing of soybean oil: Effect of catalysts, *Fuel*, 94 (2012) 578-585.

- [54] T.M. Sankaranarayanan, M. Banu, A. Pandurangan, S. Sivasanker, Hydroprocessing of sunflower oil-gas oil blends over sulfided Ni-Mo-Al-zeolite beta composites, *Bioresource Technology*, 102 (2011) 10717-10723.
- [55] A. Guzman, J.E. Torres, L.P. Prada, M.L. Nunez, Hydroprocessing of crude palm oil at pilot plant scale, *Catalysis Today*, 156 (2010) 38-43.
- [56] D. Kubicka, P. Simacek, N. Zilkova, Transformation of vegetable oils into hydrocarbons over mesoporous-alumina-supported CoMo catalysts, *Topics in Catalysis*, 52 (2009) 161-168.
- [57] S. Bezergianni, A. Dimitriadis, A. Kalogianni, P.A. Pilavachi, Hydrotreating of waste cooking oil for biodiesel production. Part I: Effect of temperature on product yields and heteroatom removal, *Bioresource Technology*, 101 (2010) 6651-6656.
- [58] S. Bezergianni, A. Dimitriadis, T. Sfetsas, A. Kalogianni, Hydrotreating of waste cooking oil for biodiesel production. Part II: Effect of temperature on hydrocarbon composition, *Bioresource Technology*, 101 (2010) 7658-7660.
- [59] S. Bezergianni, A. Dimitriadis, Temperature effect on co-hydroprocessing of heavy gas oil-waste cooking oil mixtures for hybrid diesel production, *Fuel*, 103 (2013) 579-584.
- [60] M. Toba, Y. Abe, H. Kuramochi, M. Osako, T. Mochizuki, Y. Yoshimura, Hydrodeoxygenation of waste vegetable oil over sulfide catalysts, *Catalysis Today*, 164 (2011) 533-537.
- [61] V.N. Bui, D. Laurenti, P. Afanasiev, C. Geantet, Hydrodeoxygenation of guaiacol with CoMo catalysts. Part I: Promoting effect of cobalt on HDO selectivity and activity, *Applied Catalysis B-Environmental*, 101 (2011) 239-245.
- [62] H.P. Zhang, H.F. Lin, Y. Zheng, The role of cobalt and nickel in deoxygenation of vegetable oils, *Applied Catalysis B-Environmental*, 160 (2014) 415-422.

- [63] H. Shimada, Morphology and orientation of MoS<sub>2</sub> clusters on Al<sub>2</sub>O<sub>3</sub> and TiO<sub>2</sub> supports and their effect on catalytic performance, *Catalysis Today*, 86 (2003) 17-29.
- [64] Qiherima, H.F. Li, H. Yuan, Y.H. Zhang, G.T. Xu, Effect of alumina supports on the formation of active phase of selective hydrodesulfurization catalysts Co-Mo/Al<sub>2</sub>O<sub>3</sub>, *Chinese journal of catalysis*, 32 (2011) 240-249.
- [65] Y. Sakashita, Y. Araki, H. Shimada, Effects of surface orientation of alumina supports on the catalytic functionality of molybdenum sulfide catalysts, *Applied Catalysis a-General*, 215 (2001) 101-110.
- [66] M.S. Rana, J. Ancheyta, S.K. Maity, P. Rayo, Maya crude hydrodemetallization and hydrodesulfurization catalysts: An effect of TiO<sub>2</sub> incorporation in Al<sub>2</sub>O<sub>3</sub>, *Catalysis Today*, 109 (2005) 61-68.
- [67] G. de la Puente, A. Gil, J.J. Pis, P. Grange, Effects of support surface chemistry in hydrodeoxygenation reactions over CoMo/activated carbon sulfided catalysts, *Langmuir*, 15 (1999) 5800-5806.
- [68] V.N. Bui, D. Laurenti, P. Delichere, C. Geantet, Hydrodeoxygenation of guaiacol Part II: Support effect for CoMoS catalysts on HDO activity and selectivity, *Applied Catalysis B-Environmental*, 101 (2011) 246-255.
- [69] A. Centeno, E. Laurent, B. Delmon, Influence of the support of CoMo sulfide catalysts and of the addition of potassium and platinum on the catalytic performances for the hydrodeoxygenation of carbonyl, carboxyl, and guaiacol-type molecules, *Journal of Catalysis*, 154 (1995) 288-298.
- [70] E.M. Ryymin, M.L. Honkela, T.R. Viljava, A.O.I. Krause, Competitive reactions and mechanisms in the simultaneous HDO of phenol and methyl heptanoate over sulphided NiMo/gamma-Al<sub>2</sub>O<sub>3</sub>, *Applied Catalysis A: General*, 389 (2010) 114-121.
- [71] V. Lavopa, C.N. Satterfield, Catalytic hydrodeoxygenation of dibenzofuran, *Energy & Fuels*, 1 (1987) 323-331.

- [72] M.W. Vogelzang, C.L. Li, G.C.A. Schuit, B.C. Gates, L. Petrakis, Hydrodeoxygenation of 1-naphthol: activities and stabilities of molybdena and related catalysts, *Journal of Catalysis*, 84 (1983) 170-177.
- [73] E. Laurent, B. Delmon, Study of the hydrodeoxygenation of carbonyl, carboxylic and guaiacyl groups over sulfided CoMo/ $\gamma$  Al<sub>2</sub>O<sub>3</sub> and NiMo/ $\gamma$  Al<sub>2</sub>O<sub>3</sub> catalysts. Influence of water, ammonia and hydrogen sulfide, *Applied Catalysis a-General*, 109 (1994) 97-115.
- [74] E. Laurent, B. Delmon, Influence of oxygen-containing, nitrogen-containing, and sulfur-containing-compounds on the hydrodeoxygenation of phenols over sulfided CoMo/ $\gamma$  Al<sub>2</sub>O<sub>3</sub> and NiMo/ $\gamma$  Al<sub>2</sub>O<sub>3</sub> catalysts, *Industrial & Engineering Chemistry Research*, 32 (1993) 2516-2524.
- [75] M. Ferrari, R. Maggi, B. Delmon, P. Grange, Influences of the hydrogen sulfide partial pressure and of a nitrogen compound on the hydrodeoxygenation activity of a CoMo/carbon catalyst, *Journal of Catalysis*, 198 (2001) 47-55.
- [76] T.R. Viljava, R.S. Komulainen, A.O.I. Krause, Effect of H<sub>2</sub>S on the stability of CoMo/Al<sub>2</sub>O<sub>3</sub> catalysts during hydrodeoxygenation, *Catalysis Today*, 60 (2000) 83-92.
- [77] O.I. Senol, E.M. Ryymin, T.R. Viljava, A.O.I. Krause, Effect of hydrogen sulphide on the hydrodeoxygenation of aromatic and aliphatic oxygenates on sulphided catalysts, *Journal of Molecular Catalysis a-Chemical*, 277 (2007) 107-112.
- [78] B. Valle, A.G. Gayubo, A. Alonso, A.T. Aguayo, J. Bilbao, Hydrothermally stable HZSM-5 zeolite catalysts for the transformation of crude bio-oil into hydrocarbons, *Applied Catalysis B-Environmental*, 100 (2010) 318-327.
- [79] Z.D. Yigezu, K. Muthukumar, Catalytic cracking of vegetable oil with metal oxides for biofuel production, *Energy Conversion and Management*, 84 (2014) 326-333.
- [80] C. Zhao, T. Bruck, J.A. Lercher, Catalytic deoxygenation of microalgae oil to green hydrocarbons, *Green Chemistry*, 15 (2013) 1720-1739.

- [81] J.R.S. Dosanjós, W.D. Gonzalez, Y.L. Lam, R. Frety, Catalytic decomposition of vegetable oil, *Applied Catalysis*, 5 (1983) 299-308.
- [82] P. Kirszensztejn, R. Przekop, A. Tolinska, E. Mackowska, Pyrolytic and catalytic conversion of rape oil into aromatic and aliphatic fractions in a fixed bed reactor on Al<sub>2</sub>O<sub>3</sub> and Al<sub>2</sub>O<sub>3</sub>/B<sub>2</sub>O<sub>3</sub> catalysts, *Chemical Papers*, 63 (2009) 226-232.
- [83] E. Vonghia, D.G.B. Boocock, S.K. Konar, A. Leung, Pathways for the deoxygenation of triglycerides to aliphatic-hydrocarbons over activated alumina, *Energy & Fuels*, 9 (1995) 1090-1096.
- [84] R.O. Idem, S.P.R. Katikaneni, N.N. Bakhshi, Catalytic conversion of canola oil to fuels and chemicals: Roles of catalyst acidity, basicity and shape selectivity on product distribution, *Fuel Processing Technology*, 51 (1997) 101-125.
- [85] K. Smets, A. Roukaerts, J. Czech, G. Reggers, S. Schreurs, R. Carleer, J. Yperman, Slow catalytic pyrolysis of rapeseed cake: Product yield and characterization of the pyrolysis liquid, *Biomass & Bioenergy*, 57 (2013) 180-190.
- [86] J.M. Xu, J.C. Jiang, Y.J. Lu, J. Chen, Liquid hydrocarbon fuels obtained by the pyrolysis of soybean oils, *Bioresource Technology*, 100 (2009) 4867-4870.
- [87] J. Xu, J. Jiang, J. Chen, Y. Sun, Biofuel production from catalytic cracking of woody oils, *Bioresource Technology*, 101 (2010) 5586-5591.
- [88] J. Xu, J. Jiang, Y. Sun, J. Chen, Production of hydrocarbon fuels from pyrolysis of soybean oils using a basic catalyst, *Bioresource Technology*, 101 (2010) 9803-9806.
- [89] S.P.R. Katikaneni, J.D. Adjaye, N.N. Bakhshi, Studies on the catalytic conversion of canola oil to hydrocarbons-influence of hybrid catalysts and steam, *Energy & Fuels*, 9 (1995) 599-609.

- [90] F.A.A. Twaiq, A.R. Mohamad, S. Bhatia, Performance of composite catalysts in palm oil cracking for the production of liquid fuels and chemicals, *Fuel Processing Technology*, 85 (2004) 1283-1300.
- [91] Y.S. Ooi, R. Zakaria, A.R. Mohamed, S. Bhatia, Catalytic conversion of fatty acids mixture to liquid fuel and chemicals over composite microporous/mesoporous catalysts, *Energy & Fuels*, 19 (2005) 736-743.
- [92] D. Kubicka, I. Kubickova, J. Cejka, Application of molecular sieves in transformations of biomass and biomass-derived feedstocks, *Catalysis Reviews-Science and Engineering*, 55 (2013) 1-78.
- [93] H. Insley, R.H. Ewell, Thermal behavior of the kaolin minerals, *National bureau of standards*, 14 (1935) 615-627.
- [94] S.H. Sun, S.Q. Zheng, Z.F. Wang, Y.H. Zhang, J.T. Ma, Sulphur reduction additive prepared from caustic-modified kaolin, *Clay Minerals*, 40 (2005) 311-316.
- [95] C.H. Liu, Y.Q. Deng, Y.Q. Pan, S.G. Zheng, X.H. Gao, Interactions between heavy metals and clay matrix in fluid catalytic cracking catalysts, *Applied Catalysis a-General*, 257 (2004) 145-150.
- [96] H.H. Liu, J.T. Ma, X.H. Gao, Synthesis, characterization and evaluation of a novel resid FCC catalyst based on in situ synthesis on kaolin microspheres, *Catalysis Letters*, 110 (2006) 229-234.
- [97] P. Simacek, D. Kubicka, G. Sebor, M. Pospisil, Hydroprocessed rapeseed oil as a source of hydrocarbon-based biodiesel, *Fuel*, 88 (2009) 456-460.
- [98] X.X. Ma, Y. Xia, Pinpointing double bonds in lipids by Paterno-Buchi reactions and mass spectrometry, *Angewandte Chemie-International Edition*, 53 (2014) 2592-2596.
- [99] Y. Hu, Study on direct catalytic cracking of high TAN crude oil. PhD thesis. , in, China University of petroleum (East China), 2011.

- [100] R. Costa, B.D. Zellner, M.L. Crupi, M.R. De Fina, M.R. Valentino, P. Dugo, G. Dugo, L. Mondello, GC-MS, GC-O and enantio-GC investigation of the essential oil of *Tarchonanthus camphoratus* L, *Flavour and Fragrance Journal*, 23 (2008) 40-48.
- [101] J.W. Ward, Nature of active sites on zeolite. Rare earth Y zeolite, *Journal of Catalysis*, 13 (1969) 321-327.
- [102] X. Wu, Acidity and catalytic activity of zeolite catalysts bound with silica and alumina, in, Texas A&M University, 2003.
- [103] Y.Z. Liang, K.T. Fang, Q.S. Xu, Uniform design and its applications in chemistry and chemical engineering, *Chemometrics and Intelligent Laboratory Systems*, 58 (2001) 43-57.
- [104] K.T. Fang, D.K.J. Lin, P. Winker, Y. Zhang, Uniform design: Theory and application, *Technometrics*, 42 (2008) 237-248.
- [105] M. Krar, S. Kovacs, D. Kallo, J. Hancsok, Fuel purpose hydrotreating of sunflower oil on CoMo/Al<sub>2</sub>O<sub>3</sub> catalyst, *Bioresource Technology*, 101 (2010) 9287-9293.
- [106] wikipedia, diesel fuel, in.
- [107] [orgchem.colorado.edu](http://orgchem.colorado.edu),  
<http://orgchem.colorado.edu/Spectroscopy/irtutor/alkanesir.html>.
- [108] M. Snare, I. Kubickova, P. Maki-Arvela, K. Eranen, D.Y. Murzin, Heterogeneous catalytic deoxygenation of stearic acid for production of biodiesel, *Industrial & Engineering Chemistry Research*, 45 (2006) 5708-5715.
- [109] B. Donnis, R.G. Egeberg, P. Blom, K.G. Knudsen, Hydroprocessing of bio-oils and oxygenates to hydrocarbons. Understanding the reaction routes, *Topics in Catalysis*, 52 (2009) 229-240.

- [110] G.W. Huber, P. O'Connor, A. Corma, Processing biomass in conventional oil refineries: Production of high quality diesel by hydrotreating vegetable oils in heavy vacuum oil mixtures, *Applied Catalysis a-General*, 329 (2007) 120-129.
- [111] R.J. French, J. Stunkel, R.M. Baldwin, Mild Hydrotreating of Bio-Oil: Effect of Reaction Severity and Fate of Oxygenated Species, *Energy & Fuels*, 25 (2011) 3266-3274.
- [112] S. Kovacs, T. Kasza, A. Thernesz, I.W. Horvath, J. Hancsok, Fuel production by hydrotreating of triglycerides on NiMo/Al<sub>2</sub>O<sub>3</sub>/F catalyst, *Chemical Engineering Journal*, 176 (2011) 237-243.
- [113] C. Calais, N. Matsubayashi, C. Geantet, Y. Yoshimura, H. Shimada, A. Nishijima, M. Lacroix, M. Breysse, Crystallite size determination of highly dispersed unsupported MoS<sub>2</sub> catalysts, *Journal of Catalysis*, 174 (1998) 130-141.
- [114] H.P. Zhang, H.F. Lin, W.Z. Wang, Y. Zheng, P.J. Hu, Hydroprocessing of waste cooking oil over a dispersed nano catalyst: Kinetics study and temperature effect, *Applied Catalysis B-Environmental*, 150 (2014) 238-248.
- [115] J. Gusmão, D. Brodzki, G. Djéga-Mariadassou, R. Frety, Utilization of vegetable oils as an alternative source for diesel-type fuel: hydrocracking on reduced Ni/SiO<sub>2</sub> and sulphided Ni-Mo/  $\gamma$ -Al<sub>2</sub>O<sub>3</sub>, *Catalysis Today*, 5 (1989) 533-544.
- [116] S. Brunet, D. Mey, G. Perot, C. Bouchy, F. Diehl, On the hydrodesulfurization of FCC gasoline: a review, *Applied Catalysis A: General*, 278 (2005) 143-172.
- [117] O.I. Senol, E.M. Ryymin, T.R. Viljava, A.O.I. Krause, Reactions of methyl heptanoate hydrodeoxygenation on sulphided catalysts, *Journal of Molecular Catalysis A: Chemical*, 268 (2007) 1-8.
- [118] D. Kubicka, L. Kaluza, Deoxygenation of vegetable oils over sulfided Ni, Mo and NiMo catalysts, *Applied Catalysis A: General*, 372 (2010) 199-208.

- [119] L. Boda, O. Gyorgy, H. Solt, L. Ferenc, J. Valyon, A. Thernesz, Catalytic hydroconversion of tricaprylin and caprylic acid as model reaction for biofuel production from triglycerides, *Applied Catalysis A: General*, 374 (2010) 158-169.
- [120] G.W. Huber, P. O'Connor, A. Corma, Processing biomass in conventional oil refineries: Production of high quality diesel by hydrotreating vegetable oils in heavy vacuum oil mixtures, *Applied Catalysis A: General*, 329 (2007) 120-129.
- [121] B. Delmon, New technical challenges and recent advances in hydrotreatment catalysis. A critical updating review, *Catalysis Letters*, 22 (1993) 1-32.
- [122] A.Y. Bunch, U.S. Ozkan, Investigation of the Reaction Network of Benzofuran Hydrodeoxygenation over Sulfided and Reduced Ni-Mo/Al<sub>2</sub>O<sub>3</sub> Catalysts, *Journal of Catalysis*, 206 (2002) 177-187.
- [123] J.A. Moulijn, A.E. van Diepen, F. Kapteijn, Catalyst deactivation: is it predictable? What to do?, *Applied Catalysis a-General*, 212 (2001) 3-16.
- [124] E. Furimsky, F.E. Massoth, Deactivation of hydroprocessing catalysts, *Catalysis Today*, 52 (1999) 381-495.
- [125] Y. Yoshimura, H. Shimada, T. Sato, M. Kubota, A. Nishijima, Initial catalyst deactivation in the hydrotreatment of coal liquid over Ni-Mo and Co-Mo-gamma-Al<sub>2</sub>O<sub>3</sub> catalysts, *Applied Catalysis*, 29 (1987) 125-140.
- [126] Ratnasam.P, D.K. Sharma, L.D. Sharma, Surface acidity of Co-Mo-Al<sub>2</sub>O<sub>3</sub> catalysts, *Journal of Physical Chemistry*, 78 (1974) 2069-2070.
- [127] Z. Biying, L. Huizhu, G. Linlin, T. Qi, Surface acidity and surface structure of molybdenum trioxide-Titanium dioxide, *Chinese journal of catalysis*, 8 (1987) 413-417.
- [128] Z. Biying, K. Zhijun, L. Chao, X. Youchang, T. Youqi, Study of the surface acidity of systems MoO<sub>3</sub>/Al<sub>2</sub>O<sub>3</sub> and MoO<sub>3</sub>/SiO<sub>2</sub>, *Chinese journal of catalysis*, 6 (1985) 219-224.

- [129] L. Jianyu, S. Wanfu, Study on deactivated commercial hydrocracking catalysts, *Industrial Catalysis*, 11 (2003) 12-17.
- [130] X.Y. Lin, Y. Fan, G. Shi, H.Y. Liu, X.J. Bao, Coking and deactivation Behavior of HZSM-5 zeolite-based FCC gasoline hydro-upgrading catalyst, *Energy & Fuels*, 21 (2007) 2517-2524.
- [131] C.L. Pieck, E.L. Jablonski, J.M. Parera, R. Frety, F. Lefebvre, Characterization of residual coke during burning, *Industrial & Engineering Chemistry Research*, 31 (1992) 1017-1021.
- [132] Y. Yoshimura, E. Furimsky, Oxidative regeneration of hydrotreating catalysts, *Applied Catalysis*, 23 (1986) 157-171.
- [133] S. Eijsbouts, L.C.A. van den Oetelaar, J.N. Louwen, R.R. van Puijenbroek, K.G.C. van Leerdam, Changes of MoS<sub>2</sub> morphology and the degree of Co segregation during the sulfidation and deactivation of commercial Co-Mo/Al<sub>2</sub>O<sub>3</sub> hydroprocessing catalysts, *Industrial & Engineering Chemistry Research*, 46 (2007) 3945-3954.
- [134] F.V. Stohl, H.P. Stephens, A comparative study of catalyst deactivation in integrated two-stage direct coal liquiefaction processes, *Industrial & Engineering Chemistry Research*, 26 (1987) 2466-2473.
- [135] H. Topsoe, B.S. Clausen, R. Candia, C. Wivel, S. Morup, In Situ Mossbauer Emission Spectroscopy studies of unsupported and supported sulfided Co-Mo hydrodesulfurization catalysts: evidence for and nature of a Co-Mo-S phase, *Journal of Catalysis*, 68 (1981) 433-452.
- [136] E. Furimsky, F.E. Massoth, Regeneration of hydroprocessing catalysts, *Catalysis Today*, 17 (1993) 537-659.
- [137] P. Forzatti, L. Lietti, Catalyst deactivation, *Catalysis Today*, 52 (1999) 165-181.

- [138] Y. Yoshimura, T. Sato, H. Shimada, N. Matsubayashi, A. Nishijima, Influences of oxygen-containing substances on deactivation of sulfided molybdate catalysts, *Applied Catalysis*, 73 (1991) 55-63.
- [139] S. Bouwens, F.B.M. Vanzon, M.P. Vandijk, A.M. Vanderkraan, V.H.J. Debeer, J.A.R. Vanveen, D.C. Koningsberger, On the structural differences between alumina-supported CoMoS type I and alumina-, silica-, and carbon-supported CoMoS type-II phases studied by XAFS, MES, and XPS, *Journal of Catalysis*, 146 (1994) 375-393.
- [140] W.H. Qian, A. Ishihara, G.D. Wang, T. Tsuzuki, M. Godo, T. Kabe, Elucidation of behavior of sulfur on sulfided Co-Mo/Al<sub>2</sub>O<sub>3</sub> catalyst using a S-35 radioisotope pulse tracer method, *Journal of Catalysis*, 170 (1997) 286-294.
- [141] O.I. Senol, E.M. Ryymin, T.R. Viljava, A.O.I. Krause, Reactions of methyl heptanoate hydrodeoxygenation on sulphided catalysts, *Journal of Molecular Catalysis a-Chemical*, 268 (2007) 1-8.
- [142] C. Dupont, R. Lemeur, A. Daudin, P. Raybaud, Hydrodeoxygenation pathways catalyzed by MoS<sub>2</sub> and NiMoS active phases: A DFT study, *Journal of Catalysis*, 279 (2011) 276-286.
- [143] C.L. Yaws, *The Yaws handbook of thermodynamic properties for hydrocarbons and chemicals*, Gulf Pub., Houston, Tex., 2006.
- [144] B. Peng, C. Zhao, S. Kasakov, S. Foraita, J.A. Lercher, Manipulating Catalytic Pathways: Deoxygenation of Palmitic Acid on Multifunctional Catalysts, *Chemistry-a European Journal*, 19 (2013) 4732-4741.
- [145] R. Cerny, M. Kubu, D. Kubicka, The effect of oxygenates structure on their deoxygenation over USY zeolite, *Catalysis Today*, 204 (2013) 46-53.
- [146] D.P. Serrano, J. Dufour, D. Iribarren, On the feasibility of producing hydrogen with net carbon fixation by the decomposition of vegetable and microalgal oils, *Energy & Environmental Science*, 5 (2012) 6126-6135.

- [147] R.W. Gosselink, S.A.W. Hollak, S.W. Chang, J. van Haveren, K.P. de Jong, J.H. Bitter, D.S. van Es, Reaction Pathways for the Deoxygenation of Vegetable Oils and Related Model Compounds, *Chemsuschem*, 6 (2013) 1576-1594.
- [148] B. Rozmyslowicz, P. Maki-Arvela, A. Tokarev, A.R. Leino, K. Eranen, D.Y. Murzin, Influence of Hydrogen in Catalytic Deoxygenation of Fatty Acids and Their Derivatives over Pd/C, *Industrial & Engineering Chemistry Research*, 51 (2012) 8922-8927.
- [149] J.G. Immer, M.J. Kelly, H.H. Lamb, Catalytic reaction pathways in liquid-phase deoxygenation of C18 free fatty acids, *Applied Catalysis a-General*, 375 (2010) 134-139.
- [150] A. Demirbas, H. Kara, New options for conversion of vegetable oils to alternative fuels, *Energy Sources Part a-Recovery Utilization and Environmental Effects*, 28 (2006) 619-626.
- [151] J. Asomaning, P. Mussone, D.C. Bressler, Thermal deoxygenation and pyrolysis of oleic acid, *Journal of Analytical and Applied Pyrolysis*, 105 (2014) 1-7.
- [152] F. Billaud, A.K.T. Minh, P. Lozano, D. Pioch, Catalytic cracking of octanoic acid, *Journal of Analytical and Applied Pyrolysis*, 58 (2001) 605-616.
- [153] R. Omar, J.P. Robinson, resultsConventional and microwave-assisted pyrolysis of rapeseed oil for bio-fuel production-reaction pathways analysis by GCMS results, *Journal of Analytical and Applied Pyrolysis*, 105 (2014) 131-142.
- [154] T. Yoshioka, T. Handa, G. Grause, Z.G. Lei, H. Inomata, T. Mizoguchi, Effects of metal oxides on the pyrolysis of poly(ethylene terephthalate), *Journal of Analytical and Applied Pyrolysis*, 73 (2005) 139-144.
- [155] R. Frety, M.d.G.C. da Rocha, S.T. Brandao, L.A.M. Pontes, J.F. Padilha, L.E.P. Borges, W.A. Gonzalez, Cracking and hydrocracking of triglycerides for renewable liquid fuels: Alternative processes to transesterification, *Journal of the Brazilian Chemical Society*, 22 (2011) 1206-1220.

- [156] H. Li, P.H. Yu, B.X. Shen, Biofuel potential production from cottonseed oil: A comparison of non-catalytic and catalytic pyrolysis on fixed-fluidized bed reactor, *Fuel Processing Technology*, 90 (2009) 1087-1092.
- [157] K.V. Padmaja, N. Atheya, A. Bhatnagar, K.K. Singh, Conversion of Calotropis procera biocrude to liquid fuels using thermal and catalytic cracking, *Fuel*, 88 (2009) 780-785.
- [158] Y.K. Luo, Z. Ma, J. Wu, X.Z. Qi, Effect of different calcination temperature on structure and extraction ratio of alumina from kaolinite, *Chemical Industry and Engineering*, 22 (2005) 263-266.
- [159] W.Z. Wang, Y. Zheng, K. Lee, Role of the hydrophobicity of mineral fines in the formation of oil-mineral aggregates, *Canadian Journal of Chemical Engineering*, 91 (2013) 698-703.
- [160] A. Corma, G.W. Huber, L. Sauvanauda, P. O'Connor, Biomass to chemicals: Catalytic conversion of glycerol/water mixtures into acrolein, reaction network, *Journal of Catalysis*, 257 (2008) 163-171.
- [161] Y. Luo, handbook of bond dissociation energies in organic compounds, CRC press LLC, 2003.
- [162] S.X. Lin, Petroleum refining engineering (The third edition), Petroleum Industry Press, 2000.
- [163] [http://en.wikipedia.org/wiki/Diesel\\_fuel](http://en.wikipedia.org/wiki/Diesel_fuel), in.
- [164] A. Osmont, L. Catoire, I. Goekalp, M.T. Swihart, Thermochemistry of C-C and C-H bond breaking in fatty acid methyl esters, *Energy & Fuels*, 21 (2007) 2027-2032.
- [165] H.J. Lu, The functions of B and L acids on FCC catalysts, *Catalytic cracking*, 17 (1998) 13-14, 23.

[166] C.A. Fisk, T. Morgan, Y.Y. Ji, M. Crocker, C. Crofcheck, S.A. Lewis, Bio-oil upgrading over platinum catalysts using in situ generated hydrogen, *Applied Catalysis a-General*, 358 (2009) 150-156.

[167] T.J. Benson, P.R. Daggolu, R.A. Hernandez, S.T. Liu, M.G. White, Catalytic deoxygenation chemistry: Upgrading of liquids derived from biomass processing, in: B.C. Gates, F.C. Jentoft (Eds.) *Advances in Catalysis*, Vol 56, 2013, pp. 187-353.

## Curriculum Vitae

Candidate's full name: Hui Wang

Universities attended:

Ph.D in Chemical Technology, East China University of Science and Technology,  
Shanghai, P. R. China, 2011.3

Master's of Science in Chemical Engineering, Liaoning University of Petroleum and  
Chemical Technology, Fushun, P. R. China, 2007.1

Bachelor's of Science in Environmental Engineering, Liaoning University of Petroleum  
and Chemical Technology, Fushun, P. R. China, 2004.7

Publications:

1. Wang, Hui; Lin, Hongfei; Zheng, Ying; Ng, Siau; Brown, Hilary; Xia, Yu. High Deoxygenation and Low Aromatization Performance of Kaolin-based Catalytic Cracking Catalysts for Waste Cooking Oil (WCO) Upgrading. Submitted to Catalysis Science and Technology.
2. Wang, Hui; Rogers, Kyle; Zhang, Lin; Li, Guoliang; Lin, Hongfei; Zheng, Ying. Hydrotreating of Triglycerides - Operational parameters optimization. To be submitted.
3. Wang, Hui; Zhang, Haiping; Li, Guoliang; Rogers, Kyle; Lin, Hongfei; Zheng, Ying. Hydrotreating of Waste Cooking Oil over CoMo Sulfided Catalysts: Effect of Catalyst Support and Temperature on Reaction Pathways. To be submitted.

4. Wang, Hui; Li, Guoliang; Rogers, Kyle; Lin, Hongfei; Zheng, Ying. Deactivation of Sulfided CoMo Hydrodesulfurization Catalyst in Hydrotreating of Waste Cooking Oil. To be submitted.
5. Wang, Hui; Lin, Hongfei; Zheng, Ying. Catalytic decomposition of oleic acid to fuels and chemicals: roles of catalyst acidity and basicity on product distribution and reaction pathways. In preparation.
6. Wang, Hui; Lin, Hongfei; Feng, Peng; Zheng, Ying. Novel Deoxygenation Technology for Triglyceride Upgrading: Integration of Catalytic Cracking and Hydrotreating. In preparation.
7. Wang, Yun; Wang, Hui; Lin, Hongfei; Zheng, Ying, et al. Current organic chemistry. 2013, 17(15): 1596-1603.
8. Wang, Yun; Wang, Hui; Lin, Hongfei; Zheng, Ying, et al. Biomass and bioenergy. 2013, 59: 158-167.
9. Wang, Hui; Zou, Ying; Yu, Feng; Weng, Huixin. Energy sources. Part A. Accepted. Sept. 2010
10. Wang, Hui; Zou, Ying; Yu, Feng; Weng, Huixin. Energy sources. Part A. Accepted. June 2009.
11. Wang, Hui; Zou, Ying; Weng, Huixin. Chemical industry and engineering progress. 2011, 30(3): 656-661.
12. Wang, Hui; Zou, Ying; Weng, Huixin. Chemical industry and engineering progress. 2008, 27: 598-601.

13. Yu, Feng; Zou, Ying; Wang, Hui; Weng, Huixin. Journal of East China University of Science and Technology (natural science edition). 2011, 37(2): 145-150.
14. Sun, Dongxue; Zou, Ying; Wang, Hui; Weng, Huixin. Journal of Fuel Chemistry and Technology. 2011, 39(5): 396-400.
15. Sun, Dongxue; Zou, Ying; Wang, Hui; Weng, Huixin. Energy sources. Part A. 2011, 33(19): 1822-1831.
16. Sun, Dongxue; Zou, Ying; Wang, Hui; Weng, Huixin. Speciality petrochemicals. 2009, 26(4): 59-63.
17. Wang, Hui; Li, Xiaoou; Li, Dongsheng; et al. Journal of Liaoning University of Petroleum and Chemical Technology. 2006, 26(3): 19-22.
18. Zhang, Shibo; Wang, Hui; Li, Dongsheng, et al. Contemporary chemical industry. 2006, 35(5): 297-299, 302.
19. Sun, Lingling; Li, Xiaoou; Li, Dongsheng; Liu, Jie; Wang, Hui. Journal of Liaoning University of Petroleum and Chemical Technology. 2008, 28(4): 16-19.

Conference Presentations:

Oral:

1. Wang, Hui; Zheng, Ying. Catalytic hydrodeoxygenation of Triglycerides: Effect of catalyst support. 1st Chemistry in Energy Conference (1st CEC). Edinburgh Conference Centre, Heriot-Watt University, Edinburgh, UK. July 20<sup>th</sup> -22<sup>nd</sup>, 2015.

2. Wang, Hui; Zhang, Haiping; Zheng, Ying. Catalytic Hydrodeoxygenation of Triglycerides: Reaction Pathway and Catalyst Deactivation. 64<sup>th</sup> Canadian Chemical Engineering Conference. Niagara Falls, Ontario. 2014.
3. Wang, Hui; Lin, Hongfei; Zheng, Ying; Ng, Siau. New kaolin-based fluid catalytic cracking (FCC) catalysts for upgrading waste cooking oil. 23rd Canadian Symposium on Catalysis. Edmonton, Alberta. 2014.
4. Wang, Hui; Li, Guoliang; Rogers, Kyle; Zheng, Ying. Hydrotreating of triglycerides-operational parameters optimization and pathways discussion. 63<sup>rd</sup> Canadian Chemical Engineering Conference. Fredericton, New Brunswick. 2013.
5. Wang, Hui; Rogers, Kyle; Li, Guoliang; Lin, Hongfei; Zheng, Ying. Hydrotreating of triglycerides-reaction routines exploitation using uniform design method. 63<sup>rd</sup> Canadian Chemical Engineering Conference. Fredericton, New Brunswick. 2013.

Poster:

1. Wang, Hui; Lin, Hongfei; Zheng, Ying. An Improved Integrated Process for Transformation of Plant Oils to Renewable Diesels: Development of Deoxygenation Catalyst. The First Commonwealth Science Conference. Bengaluru, India. 2014.
2. Wang, Hui; Zheng, Ying. Deactivation of CoMo catalysts in hydrotreating of triglycerides. 23rd Canadian Symposium on Catalysis. Edmonton, Alberta. 2014.